Received: 14 March 2024 | Revised: 11 April 2024 | Accepted: 30 April 2024

DOI: 10.1002/inf2.12559

REVIEW ARTICLE

WILEY

Stabilization of halide perovskites with silicon compounds for optoelectronic, catalytic, and bioimaging applications

Atanu Jana[1] | **Sangeun Cho**[1] | **Abhishek Meena**[1] | **Abu Talha Aqueel Ahmed**[1] | **Vijaya Gopalan Sree**[2] | **Youngsin Park**[3] | **Hyungsang Kim**[2] | **Hyunsik Im**[1] | **Robert A. Taylor**[4]

[1]Division of System Semiconductor, College of AI Convergence, Dongguk University, Seoul, Republic of Korea

[2]Department of Physics, Dongguk University, Seoul, Republic of Korea

[3]Department of Chemistry, School of Natural Science, Ulsan National Institute of Science and Technology (UNIST), Ulsan, Republic of Korea

[4]Clarendon Laboratory, Department of Physics, University of Oxford, Oxford, UK

Correspondence
Hyunsik Im, Division of System Semiconductor, College of AI Convergence, Dongguk University, Seoul 04620, Republic of Korea.
Email: hyunsik7@dongguk.edu

Funding information
National Research Foundation of Korea, Grant/Award Numbers: 2021R1F1A1062528, 2021R1A4A5031805, 2021R1A2C1006113, BrainLink RS-2023-00236798

Abstract

Silicon belongs to group 14 elements along with carbon, germanium, tin, and lead in the periodic table. Similar to carbon, silicon is capable of forming a wide range of stable compounds, including silicon hydrides, organosilicons, silicic acids, silicon oxides, and silicone polymers. These materials have been used extensively in optoelectronic devices, sensing, catalysis, and biomedical applications. In recent years, silicon compounds have also been shown to be suitable for stabilizing delicate halide perovskite structures. These composite materials are now receiving a lot of interest for their potential use in various real-world applications. Despite exhibiting outstanding performance in various optoelectronic devices, halide perovskites are susceptible to breakdown in the presence of moisture, oxygen, heat, and UV light. Silicon compounds are thought to be excellent materials for improving both halide perovskite stability and the performance of perovskite-based optoelectronic devices. In this work, a wide range of silicon compounds that have been used in halide perovskite research and their applications in various fields are discussed. The interfacial stability, structure–property correlations, and various application aspects of perovskite and silicon compounds are also analyzed at the molecular level. This study also explores the developments, difficulties, and potential future directions associated with the synthesis and application of perovskite-silicon compounds.

KEYWORDS

biomedical, halide perovskite, optoelectronics, photocatalysis, silicon compounds, water stability

1 | INTRODUCTION

Halide perovskites (HPs) are used extensively in various research areas, for example, solar cells,[1–10] light-emitting diodes (LEDs),[11–17] photodetectors,[12] transistors,[18,19] high-energy-resolution scintillators and detectors,[20] bioimaging,[21–30] catalysis,[31] and other optoelectronic devices.[32,33] However, these materials become less stable

when exposed to moisture, heat, or light.[34] There are intrinsic stability issues associated with the bulk form of HPs, that is, single crystals and powder, due to their inherent ionic nature and low formation energy. There are also additional stability issues associated with perovskite nanocrystals (NCs); perovskite NCs may aggregate and decompose as a result of the dynamic binding of surface ligands.[35] Various materials have been used to stabilize these NCs, such as metal oxides,[36] phosphate,[37] hydroxides,[38] sulfates,[39–41] polymers,[42,43] clay,[44,45] and zwitterions.[46–48] Additionally, various silicon compounds play a crucial role in stabilizing and enhancing the optoelectronic and catalytic performance of HP compounds. Perovskite NCs are enclosed in a variety of materials, including metal–organic frameworks (MOFs),[49] mesoporous alumina,[50] mesoporous titania,[51] and zeolitic imidazolate frameworks.[52] Silicon compounds are important for the synthesis, stabilization, and surface modification of various HP NCs; they are used in several ways to allow for HP NCs to be employed in optoelectronic applications. HP NCs can be synthesized using silicon compounds as precursors or templates. For example, silicon alkoxides can be used as a precursor in the synthesis of lead HP NCs.[53,54] Furthermore, silicon compounds can be used to synthesize organosilica hybrid materials, which can subsequently be used to encase HP NCs. These hybrid materials have been found to significantly increase the stability of the material because they protect HP NCs from being exposed to moisture and other environmental conditions. To stop the growth or agglomeration of HP NCs, silicon compounds can also be used as stabilizers. HP NC surfaces can be stabilized using silicon-based ligands, such as alkylsilanes, to prevent degradation.[55,56] The surface characteristics of HP NCs can also be modified with silicon compounds; for example, silicon-based ligands can be used to functionalize the surface of HP NCs with various chemical groups, enabling a wide range of applications.[57] The optoelectronic characteristics of HP NCs can also be modified by silicon compounds, such that doping or alloying silicon into the HP crystal structure can change the bandgap and enhance the electrical and optical characteristics of the material.[58–61] Notably, it has been shown that silicon-doped perovskite films exhibited increased carrier mobility and decreased trap density, resulting in improved device performance.

Here, we discuss the advantages and disadvantages of several silicon compounds widely used in HP research, which include silane, silicon dioxide, silica gel, silicate, silanol, polysilsesquioxanes, silicone resin, siloxane, and polysilazanes. We shed light on the applications of silicon compounds and HP NCs in various fields such as LEDs, solar cells, catalysis, and biomedical applications. We also explore the future implications of HP research based on these silicon compounds.

2 | IONIC NATURE AND STABILITY OF HALIDE PEROVSKITES

HPs are structurally unstable for a number of reasons, one of which is the decreased lattice energy compared to perovskite oxides.[62] The energy needed to separate ions in a crystal lattice by an infinite distance is known as the lattice energy, and it depends on the size, charge, and separation between the ions. The lattice energy of HPs is lower than that of perovskite oxides, which suggests that the forces keeping the crystal lattice together are weaker. This increases the tendency for the crystal structure to deform or break, which can lead to stability issues. The structural instability of HPs can also be attributed to the low formation energies of the vacancies or surface trap-states. These imperfections are a result of defects in the crystal lattice such as excess or missing atoms, which can lead to localized alterations in the electronic properties and stability of the material. Researchers are working on various methods of addressing these issues, for example, by introducing dopants or stabilizing agents to improve the structural stability of HPs.[63]

Van der Waals interactions, hydrogen bonding, and electrostatic forces are examples of non-covalent interactions that frequently drive the binding of the ligands to the HP surface.[64] These interactions are dynamic and can change depending on the surrounding environment. This highly dynamic ligand-HP NC binding can also contribute to ligand loss and instability of HPs. Because of the dynamic nature of the binding, the ligands are always in motion and may interact with other molecules or particles in the environment, modifying the optoelectronic and colloidal properties of the HP NCs.[35] Solubility equilibrium and the highly dynamic nature of ligands at the HP surface can also affect how hydrophobic ligands bind to the surface of HP NCs. The hydrophobic ligands attach to HP NCs via van der Waals interactions and hydrophobic forces, which are weak and reversible. Because of this, hydrophobic ligands have a tendency to be lost when HP NCs are exposed to polar solvents during isolation and purification. The hydrophobic ligands are unstable in polar solvents and can dissolve in the solvent, leading to ligand loss and damage to the optical and colloidal stability of the HP NCs. To address this, researchers are seeking to develop new ligands and surface functionalization strategies for ameliorating the stability and reproducibility of HP NC-based devices. For example, the functionalization of HP NCs with more stable ligands or surface

coatings can improve stability and reduce ligand loss during isolation and purification. Additionally, controlling the synthetic parameters of HP NCs such as temperature and reaction time can also impact the stability and reproducibility of the resulting HP NCs.

The crystal energy and entropy of mixing play significant roles in the production of solid solutions in the fast halide-exchange reaction of HPs.[65] The crystal energy refers to the energy required to break the bonds between the ions in a crystal lattice, while the entropy of mixing refers to the increase in disorder that occurs when two substances are mixed together. The stability of the resulting solid solution is influenced by the size disparity between the two halides being exchanged, which can also have an impact on the crystal energy and entropy of mixing. In general, a higher deformation of the crystal lattice may encourage the formation of a solid solution when the ionic radius variations between the halides are greater. However, solid solutions are not always more stable than single-halide crystals. The stability of a perovskite material depends on a variety of factors, which include the identity of metal cations and halide anions, composition of the material, and the processing conditions under which it was synthesized.[66] In some cases, solid solutions may be more stable than single-halide crystals, particularly if the crystal lattice can better accommodate the different-sized ions in the solid solution. Phase stability of halide perovskites poses a significant challenge, which reduces the stability of the perovskite material and device performance. For example, α-$FAPbI_3$ transitions to the non-perovskite δ-$FAPbI_3$ phase, typically induced by high strain localized in specific crystal planes, notably the (111) plane.[67] The strain in the crystal lattice serves as a catalyst for the phase transition from the stable α-phase to the metastable δ-phase. To address this, alloying $FAPbI_3$ with MABr mitigates lattice strain by substituting larger iodide ions with smaller bromide ions, effectively reducing the lattice size and stabilizing the perovskite structure, thereby reducing susceptibility to phase transitions.[67] Incorporating chloride-based additives in $FAPbI_3$ precursor solutions also stabilizes the pseudocubic phase, mitigating defects by altering crystal growth kinetics and promoting the formation of a stable, defect-free perovskite film.[68] Manipulating strain at the atomic scale extends beyond the alloying of A-site cations in perovskite materials. The presence of chloride within the $[PbX_6]$ framework in mixed bromide/iodide compositions suppresses phase segregation by increasing the activation energy and intensity threshold for segregation, even at low concentrations. This suppression is attributed to enhanced lattice rigidity and increased formation energy of the inorganic framework bonds. These strategies enhance perovskite material stability, which is crucial for optoelectronic applications.

The stability of the ABX_3 perovskite structure is determined by Goldschmidt's tolerance factor (τ), which usually ranges from 0.7 to 1.0.[69,70] When a cation such as Cs^+ is too small, it results in the formation of a non-photoactive yellow delta phase (δ-phase) even at room temperature (Figure 1A). Conversely, FA^+ being too large struggles to fit within the perovskite structure, resulting in the room temperature freezing of pure $FAPbI_3$, posing an additional challenge (Figure 1B). HPs are fragile and prone to degradation because of their ionic composition, which renders them vulnerable to moisture, oxygen, light, and heat, among other environmental conditions. As HPs degrade, the following reactions could take place:

2.1 | Hydrolysis reaction

HPs are known to undergo hydrolysis reactions when exposed to water or moisture.[73] The hydrolysis reaction involves the halide ions in the perovskite lattice reacting with water molecules, forming metal hydroxide and hydrogen halide.[74] For example, in the case of methylammonium lead iodide ($MAPbI_3$), the hydrolysis reaction can be represented as follows:

$$MAPbI_3 + 2H_2O = Pb(OH)_2 + MAI + 2HI$$

The hydrolysis reaction can be catalyzed by the presence of certain impurities or defects in the perovskite material, such as residual solvents or moisture in the precursor solution or on the substrate. The hydrolysis reaction leads to a loss of crystallinity and structural integrity in the perovskite material, which can negatively impact the optoelectronic properties and stability of the material. Therefore, it is essential to minimize the exposure of HP materials to moisture or water and develop strategies to improve their resistance to hydrolysis. Water molecules can hydrate the perovskite to form monohydrate or dihydrate phases,[75,76] which can be expressed as follows:

$$MAPbI_3(s) + H_2O(g) \rightleftharpoons MAPbI_3 \cdot H_2O$$

$$4[MAPbI_3 \cdot H_2O] \rightleftharpoons (MA)_4PbI_6 \cdot 2H_2O + 3PbI_2 + 2H_2O$$

2.2 | Reductive degradation

The reductive degradation of HPs refers to a degradation process in which the perovskite material is exposed

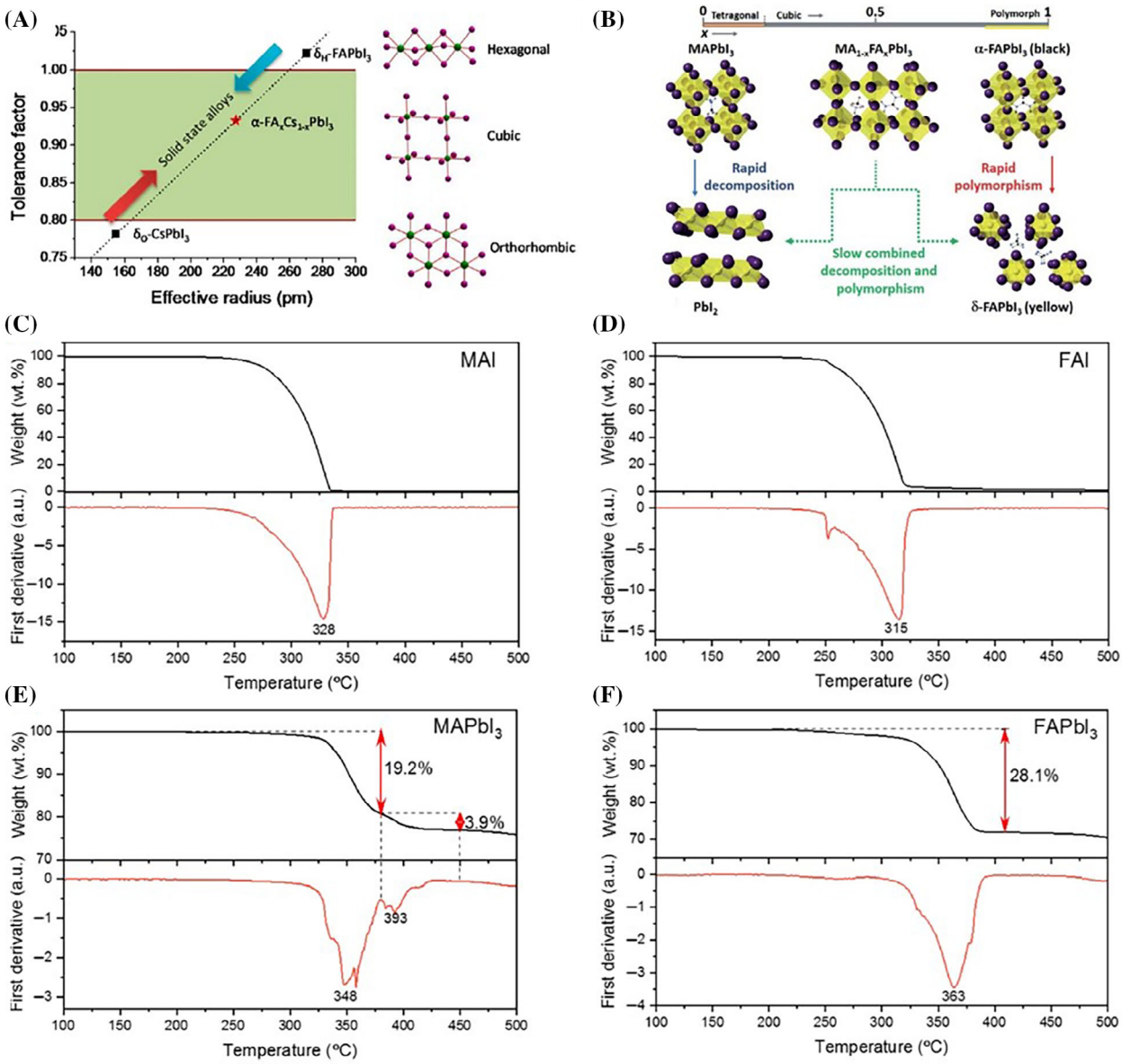

FIGURE 1 (A) The tolerance factor versus radius profile is employed to elucidate the crystal structure of the perovskites. Reprinted with permission.[69] Copyright 2016, American Chemical Society. (B) Reprinted with permission.[71] Copyright 2017, Royal Society of Chemistry. Thermogravimetric analysis spectra and the first derivative graphs of (C) MAI, (D) $MAPbI_3$, (E) FAI, and (F) $FAPbI_3$. Reprinted with permission.[72] Copyright 2019, American Chemical Society.

to reducing agents, such as moisture, oxygen, and organic impurities, resulting in the reduction of metal cations in the perovskite lattice and the formation of metallic species or metal halides.[77] This can occur in the presence of light, heat, or other environmental factors. The exact mechanism of the reductive degradation of HPs is not yet known, but several ideas have been posited. One proposed mechanism involves the reduction of lead (Pb) cations in the perovskite lattice, which can lead to the formation of metallic lead and halogen gas. Another proposed mechanism involves the formation of lead iodide (PbI_2) as a result of the reduction of lead iodide perovskites, which can lead to the degradation of the perovskite and affect its optoelectronic properties. The reductive degradation of HPs can have significant implications on the stability and performance of HP-based devices such as solar cells or LEDs. To mitigate the effects of reductive degradation, researchers are exploring ways to enhance the stability of HPs in a reducing environment. This can include the use of protective layers or encapsulation techniques to prevent exposure to reducing agents, as well as the development of more stable and resilient perovskite materials.

2.3 | Redox reactions

Redox chemistry, which involves the exchange of electrons between molecular species, is an important consideration because it drives critical reactions responsible for the deterioration of these devices over time.[78] In metal halide perovskite optoelectronics, these redox reactions can lead to changes in the oxidation states of elements within the perovskite materials and at their interface, ultimately leading to performance degradation and material decomposition. Despite the promising optoelectronic properties of metal HP, their susceptibility to redox-driven degradation highlights a key challenge that researchers must address to enhance the stability and reliability of these devices for practical applications in solar cells, LEDs, and photodetectors.

Oxygen or other oxidizing substances can cause the oxidation of HPs, resulting in the formation of various products such as metal oxides, metals, and gases.[79,80] In perovskite solar cells (PSCs), the oxidation of iodide ions (I^-) to form iodine vapor (I_2) is a chemical reaction of concern, especially when PSCs are exposed to light,[81] because it can lead to the deterioration of critical components within the PSCs, ultimately affecting their performance and longevity. Of the ions involved in these redox reactions, the most vulnerable are lead (Pb^{2+}), tin (Sn^{2+}), and iodine (I^-) ions, which play an essential role in the composition and function of PSC materials. It is also important to note that these redox reactions are not confined solely to the perovskite layer of the PSC. They can also occur within other integral components of the device, including the electrodes, the electron transport layer (ETL), the hole transport layer (HTL), and the interfaces between these various layers. Consequently, these redox reactions have the potential to affect the entire PSC system, impacting its overall efficiency and stability. Given these challenges, it is important to effectively manage and mitigate these redox reactions to ensure the stability and long-term performance of PSCs.

2.4 | Photodegradation

Photochemical degradation is one of the main mechanisms that can lead to the degradation of HPs.[82] The perovskite material absorbs photons during the photochemical degradation process, which can result in the creation of excitons and free charge carriers. These excited particles then undergo a series of reactions that result in the degradation of the perovskite material. Several mechanisms have been proposed for the photochemical degradation of HPs, which include:

i. Photo-oxidation: Excited charge carriers in the perovskite material react with oxygen or other oxidizing agents to form reactive oxygen species (ROS) like superoxide radicals ($\cdot O^{2-}$) or singlet molecular oxygen ($^1O_2$). The ROS reacts with the perovskite material and degrades the material.
ii. Ion migration: Excited charge carriers formed in the perovskite material can cause the migration of metal ions, such as Pb^{2+}[83] or Sn^{2+},[84] within the perovskite lattice. This may cause the generation of defects or disordered regions, which can influence the electronic and optical properties of HPs.
iii. Recombination-induced degradation: Excited charge carriers formed in the perovskite material can recombine with defects or trap states in the material, which act as non-radiative recombination centers, lowering the performance of perovskite-based optoelectronic devices.

2.5 | Thermal degradation

The thermal stability of PSCs remains a significant challenge that needs to be addressed for their successful commercialization. PSCs have shown remarkable efficiency and promise as a renewable energy technology. However, their vulnerability to high temperatures poses a barrier to widespread adoption and long-term reliability. As temperatures rise, perovskite materials can degrade, leading to reduced performance, shorter lifespans, and potential safety concerns. Therefore, developing strategies to enhance the thermal stability of halide PSCs is crucial to ensure their commercial viability and competitiveness in the solar energy market.[85] Exposure to high temperatures can cause $MAPbX_3$ or $FAPbX_3$ (Figure 1C–F) to decompose into a variety of degradation products including PbX_2, MAX, and CH_3NH_2.[86] Two significant studies by Ning et al.[87] and Kumar et al.[88] have advanced the understanding of the thermal stability and degradation mechanisms of halide PSCs. Ning et al. demonstrated that inverted PSCs exhibit superior thermal stability due to the improved crystalline order and larger domain sizes in the perovskite film. Their observations of lower film absorption during heating revealed structural changes under thermal stress, while transient photoconductivity analysis highlighted the role of charge-carrier dynamics in thermal degradation. Kumar et al. found that PSCs exhibited higher thermal stability up to 70°C, with irreversible degradation occurring at temperatures higher than 80°C. They also demonstrated the use of low-frequency noise analysis as a sensitive, non-invasive tool for assessing PSC degradation mechanisms. These studies have collectively contributed to enhancing the

understanding of PSC thermal stability, which is vital for the development of more resilient and long-lasting PSCs for renewable energy applications.

Fang et al. conducted a study on inverted $MAPbI_3$ PSC and observed that, when these devices were not enclosed in a protective layer, they retained only 30% of their initial power conversion efficiency (PCE) at 85°C after 30 days.[89] This decline in efficiency was due to the degradation of $MAPbI_3$ due to the high temperature. However, when the devices were encapsulated, they maintained about 95% of their initial PCE, which was attributed to the dual function of the [6,6]-phenyl-C_{61}-butyric acid methylester (PCBM)/CeOx bilayer ETL, which acted as a chemical barrier and effectively extracted electrons. Mixed-cation perovskite materials have the potential to be used to produce films with a lower trap state density and higher thermal stability.[90–93]

2.6 | Stability under electric fields

The stability of perovskite devices under electric fields is a crucial consideration in the advancement of efficient and reliable electronic devices, particularly within the realm of perovskite solar cells. Perovskite materials, distinguished by their unique crystal structure, exhibit outstanding optoelectronic properties. Despite these merits, their susceptibility to degradation under external stimuli, such as electric fields, presents a notable challenge for practical applications.[94–97] When exposed to an electric field, perovskite materials can experience ionic migration within the crystal lattice, potentially inducing structural changes and affecting the overall device performance. Electric field-induced polarization effects can alter the charge distribution and potential barriers within the perovskite layers, thereby influencing device efficiency and stability.[98] Furthermore, defects and grain boundaries in perovskite films, exacerbated by electric fields, can trap charges, leading to non-radiative recombination and reducing the overall device efficiency. Interfaces between different layers in a perovskite device are also sensitive to electric fields, necessitating precise engineering for stability. The observed hysteresis phenomena in perovskite solar cells, which are influenced by electric fields, pose an additional challenge that requires understanding and control for stable and reproducible device performance. External environmental factors, including temperature and humidity, interacting with electric fields further complicate stability assessments. Ongoing research focuses on material and device engineering strategies, such as the development of more robust perovskite compositions, interface optimization, and the incorporation of additives to enhance stability. Through testing and monitoring, employing advanced characterization techniques is essential for gaining insights into degradation mechanisms and developing strategies to mitigate the impact of electric fields on perovskite devices. Addressing these challenges is imperative for advancing the commercial viability of perovskite technologies and ensuring their resilience and reliability in real-world applications.

3 | SILICON COMPOUNDS FOR THE STABILIZATION OF PEROVSKITE NANOCRYSTALS

Silicon compounds have been shown to improve the stability of HP NCs. By forming a dense network around the NCs, silicon-containing organic ligands prevent moisture, light, and other environmental factors from affecting the crystal structure, which can significantly improve the stability and long-term performance of HP NCs. Furthermore, silicon compounds can be used to modify the surface of HP NCs, reducing defects, preventing ion migration, and reducing the degradation rate. The use of silicon-based compounds has been found to enhance the photoluminescence (PL) properties of perovskite NCs, resulting in brighter and more efficient emissions. Many silicon-based ligands are biocompatible, which makes them suitable for biomedical applications. Silicon-based ligands are relatively easy to synthesize and can be produced in large quantities, making them suitable to be used in the mass production of HP NCs. Overall, silicon compounds have been shown to be effective for stabilizing HP NCs and may also have the potential to enhance the optoelectronic performance and stability of HP-based devices. Nevertheless, further research is necessary to fully understand the mechanisms that describe the stabilization of HP NCs using silicon compounds. Perovskite@silicon compounds represent a transformative innovation with far-reaching implications across diverse scientific domains. This review highlights the profound advancements and significance of these compounds in various applications, with a focus on their influence on solar cells, LEDs, photocatalysis, biomedical applications, and memresistors. In the realm of solar cells, the integration of perovskite and silicon has led to a paradigm shift in photovoltaic technology. The unique properties of perovskite, such as its exceptional light-absorption capabilities and tuneability, complement the stability and conductivity of silicon. This synergistic combination has resulted in unprecedented advancements in solar cell efficiency. The perovskite@silicon compounds not only optimize charge carrier transport, minimizing losses, but also enhance the stability and reliability of solar cells, paving

the way for their extensive adoption in clean energy solutions. Expanding their applications beyond solar cells, perovskite@silicon compounds have demonstrated their capabilities in LEDs. The precise tuning of the optical properties of perovskite enables the development of efficient and vibrant LEDs. The integration of silicon contributes stability and reliability to LED devices, making them promising candidates for next-generation lighting technologies with enhanced energy efficiency and color purity. Perovskite@silicon compounds exhibit significant promise in the field of photocatalysis. Because of their unique electronic structure and efficient charge separation, these compounds serve as effective catalysts for light-driven chemical reactions. Their potential applications extend to harnessing solar energy for processes such as water splitting and pollutant degradation, thus contributing to the development of sustainable and environmentally friendly technologies. In addition, the biomedical applications of perovskite@silicon compounds represent an emerging frontier with exciting prospects. Their biocompatibility, tuneable optical properties, and potential for controlled drug release position them as compelling candidates for imaging, sensing, and therapeutic applications. The integration of these compounds into biomedical devices introduces opportunities for the development of cutting-edge diagnostic tools and targeted therapies with minimal side effects. In the field of memresistors, perovskite@silicon compounds demonstrate their utility in non-volatile memory devices. Their unique resistive switching behavior, which is influenced by the interplay between perovskite and silicon, holds promise for the development of high-density, low-energy-consuming memory technologies. This not only contributes to the advancement of information storage but also aligns with the growing demand for efficient and sustainable electronic devices.

3.1 | Silane

Silane (SiH_4) compounds, particularly organosilanes, ae widely used to stabilize halide perovskite materials, especially for perovskite solar cells (PSCs) and optoelectronic devices.[99–101] They induce surface passivation by forming chemical bonds with the perovskite surface, reducing defects and improving charge-carrier dynamics. Their hydrophobic properties act as a moisture-resistant barrier, safeguarding against degradation. Silane coatings are customizable, enhancing adhesion between layers, are compatible with fabrication processes, and protect against contaminants. These attributes collectively enhance the stability and reliability of halide perovskite-based devices, making them more suitable for practical renewable energy and optoelectronics applications.

Silane is a simple chemical compound that consists of one silicon atom and four hydrogen atoms; it has a similar structure to methane (CH_4). All the H-atoms in the compound can be replaced by halide, alkyl, or alkoxy groups. Scheme 1 details the SiH_4 derivatives that are often used in the stabilization of HP NCs. Silane is also a crucial building block for a variety of silicon-containing compounds such as silicones, silicates, and so forth. Alkylsilanes, ethoxysilanes, or aminosilanes can be formed by substituting one or more hydrogen atoms in SiH_4 with alkyl, ethoxy, or aminoalkyl groups, respectively.[102,103] Typically, this procedure is carried out using a chemical reaction known as hydrosilylation or SiH_4 coupling. For example, ethylene can react with trimethylsilane in the existence of a catalyst (such as platinum compounds) to form methylpropylsilane. Similarly, an alkene or alkyne with an ethoxy group can react with a silane like silicon tetrahydride in the presence of a catalyst when it comes to ethoxysilanes. An ethoxy group is substituted for one or more hydrogen atoms in the SiH_4 as a result of the reaction, creating a compound like ethyltriethoxysilane. When it comes to aminosilanes, the reaction entails the presence of a catalyst and the reaction of a SiH_4 with either an aminoalkene or an aminoalkyne. A compound for example, 3-aminopropyltriethoxysilane (APTES) is produced via the reaction, which involves the replacement of one or more hydrogen atoms in the SiH_4 with an aminoalkyl group. Depending on the specific alkyl, ethoxy, or aminoalkyl group involved and the quantity of hydrogen atoms substituted, the resulting alkylsilanes, ethoxysilanes, and aminosilanes will have varying properties and applications. These compounds are widely utilized in a number of industrial applications, including the development of composites, coatings, electronic devices, coupling agents, adhesion boosters, and surface modifiers.

Wang et al. reported a simple method for the efficient and concurrent passivation of defects as well as the optimization of the interfacial energy-level alignment at the perovskite/hole transport layer (HTL) interface by strategically inserting chlorosilane which is highly polar molecules.[104] Chloropropyltrimethoxysilane (CPS, Cl-$(CH_2)_3$-Si-$(OCH_3)_3$) and chloromethyltrimethoxysilane (CMS, Cl-CH_2-Si-$(OCH_3)_3$) are chosen as the surface-passivating molecules and are deposited to the surface of the HP film. The polar chlorine-terminated silane molecule reduces the energy gap between HP and HTL and allows for the passivation of defects. Dai et al. used the mixed-composition metal halide perovskite with excess PbI_2 (4 mol %), optimized for high power conversion

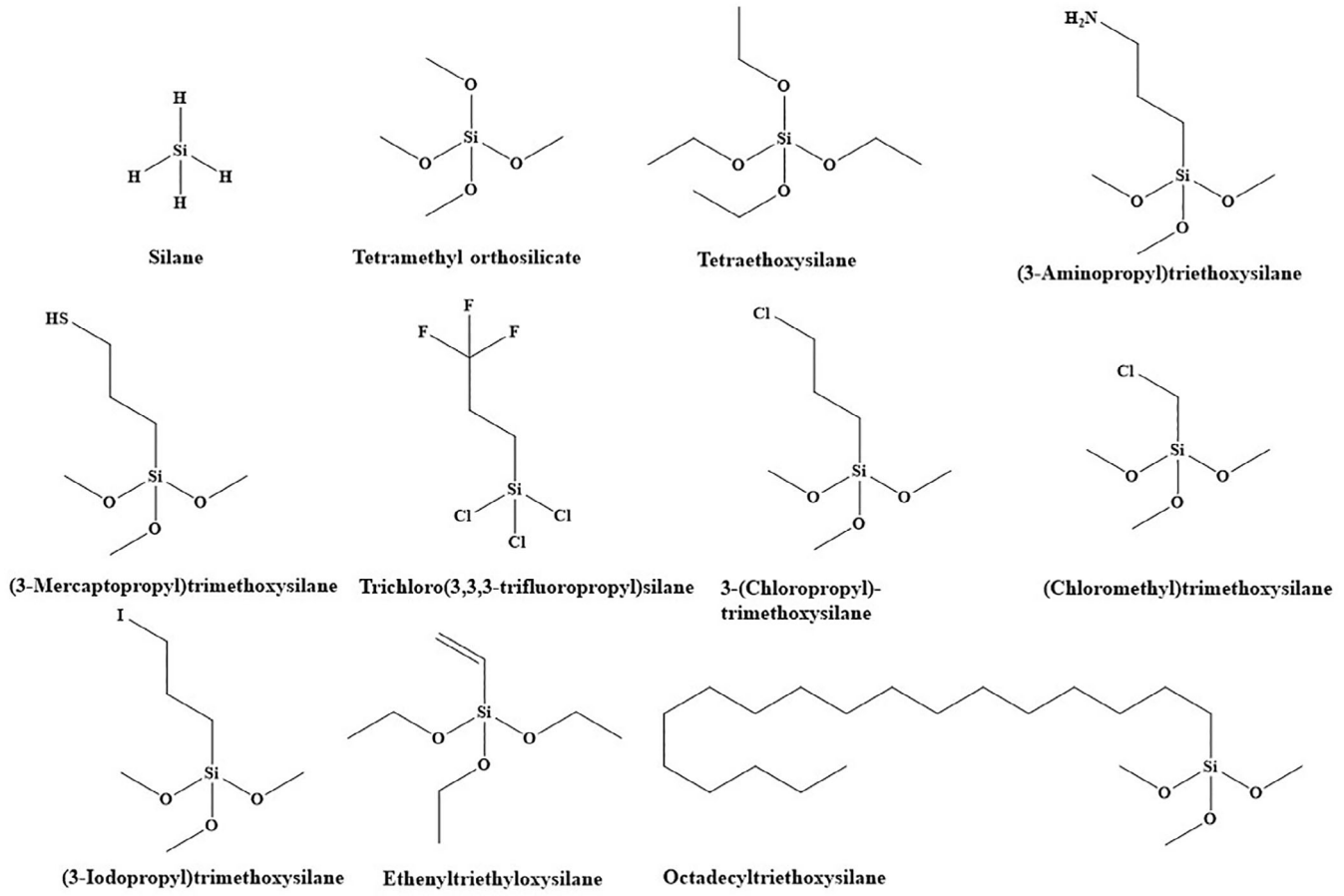

SCHEME 1 Structural representation of silane and its derivatives.

efficiency (PCE) and stability.[105] Instead of TiO_2, SnO_2 was chosen as the electron transport layer (ETL) due to its better energy-level alignment with the perovskite, which reduces the subsequent photocatalytic degradation of the perovskite. In order to improve the mechanical stability of the PSCs, an iodine-terminated 3-iodopropyl trimethoxysilane [$Si(OCH_3)_3(CH_2)_3I$, I-SAM] was used. Dai et al. showed that the I-SAM increased the adhesion hardness between the ETL and the halide perovskite thin-film at the interface by 50%. There are many advantages associated with using I-SAM as a linker.

An SnO_2 ETL layer is used in most other oxides, which can be covered in adsorbed hydroxyl groups that interfere with the performance of the PSCs when the HP thin-film is deposited on top. On these oxide surfaces, I-SAMs are self-assembled and crosslinked easily by silanization; I-SAMs also dramatically reduce the number of surface hydroxyl groups by forming O—Si bonds. Furthermore, Dai et al. utilized SAMs with short alkyl chains, the I-terminal group of which was expected to create electrostatic bonds with the HP thin layer on top. The SAM-coated surface is also suitably lyophilic for the solution deposition of thin HP films due to the short length of the $n = 3$ alkyl chain. Finally, Dai et al. also showed that the perovskite and ETL interfaces of the PSCs without SAMs experienced irreversible morphological degradation, including the formation of voids and delamination, while the PSCs with I-SAM experienced minimal damage. Similarly, Shi et al. synthesized a fully air-processed PSC by using an interlayer consisting of a 3-mercaptopropyltrimethoxysilane (MPTMS) SAM.[106] The MPTMS SAM sulfhydryl groups may interact with PbI_2, resulting in worse crystallization and larger crystals in the HP film. Moreover, the utilization of the MPTMS SAM allows for the smoothening of the ETL surface on SnO_2, which can enhance the film quality of the perovskite absorber. The photogenerated electron extraction can be improved by anchoring the Pb atoms onto the MPTMS SAM with the help of the S atoms. The hydrolyzed methoxy groups on MPTMS can strengthen the perovskite structure by reacting with SnO_2. Their fabricated air-processed exhibited an average PCE of 18.75% and long-term stabilities in the ambient atmosphere. Liu et al. used a SiH_4 coupling agent for efficient perovskite solar cells to modify the surface of cuprous oxide (Cu_2O) quantum dots (QDs).[107] The functional group of the SiH_4

coupling agent dramatically affects the properties of the modified Cu_2O QDs. Ethenyltriethyloxysilane was used to modify the surface of the QDs to synthesize Cu_2O QD-based PSCs, which led to the improved dispersion of Cu_2O in a non-polar solvent. Adding a hydrophobic functional group by the ethenyltriethoxysilane to the Cu_2O surface further strengthen PSCs under humid conditions. In comparison to PSCs employing unmodified Cu_2O as the HTL, which had an efficiency of 11.9%, surface-modified Cu_2O had a higher efficiency of 18.9%. In order to increase the moisture stability of p-i-n planar PSCs, Bai et al. reported on a trichloro(3,3,3-trifluoropropyl) SiH_4 functionalized fullerene ETL that is water-resistant and cross-linkable.[108] A specific cross-linked C_{60}-SAM ETL is synthesized by coupling a hydrophobic SiH_4 coupling agent to a C_{60}-substituted benzoic acid self-assembled monolayer. The cross-linked SiH_4 agent quickly hydrolyzes to generate three hydroxyl groups after forming hydrogen bonds with C_{60}-SAM. The carboxyl group formed the silicon-oxygen (Si—O) bonds within the C_{60}-SAM, quickly forming strong hydrogen bonds with the hydroxyl (—OH) groups of SiH_4. Trifluoromethyl groups (—CF_3) from the SiH_4 compounds further increased the hydrophobicity of the cross-linked C_{60}-SAM layer, protecting perovskite layer under humid conditions. The fabricated devices have a high fill factor of 80.6% and an efficiency of 19.5% without photocurrent-hysteresis.

3.2 | Silicon dioxide

In PSCs, silicon dioxide provides multiple critical functions, including surface passivation, moisture resistance, thermal stability, compatibility with fabrication processes, tuneable optical properties, and protection from external factors. It forms a protective layer on perovskite surfaces, reducing trap states and enhancing charge carrier dynamics, while also acting as a hydrophobic moisture barrier to safeguard against degradation. The high thermal stability of SiO_2 ensures consistent device performance, and its compatibility with various deposition methods simplifies integration. Further, the customizable optical properties aid in optimizing light management, and provides a physical shield against environmental elements and mechanical stress.

Silica (SiO_2) is a widely used material for passivating QDs due to its excellent transparency, chemical stability, and biocompatibility.[109–111] Recently, SiO_2-coated QDs have been the subject of investigation for a variety of uses in optoelectronic devices, photocatalysis, biological imaging, and sensing. Table 1 summarizes the various synthetic procedures, Si precursors, optical properties, stability, and applications of SiO_2-coated HPs. One of the main advantages of SiO_2-coated QDs is their improved photostability, such that the coating serves as a barrier to stop the QDs from degrading from light or moisture exposure. Therefore, SiO_2-coated QDs are better suited to long-term imaging applications due to their higher photobleach-resistance. The properties of various types of SiO_2-coated QDs, such as CdSe/CdS,[143] CdSe/ZnS,[144] CdSe/CdS/ZnS,[145] and ZnSe/ZnS[146] have been analyzed extensively. The thickness of the SiO_2 coating can be varied to optimize the properties of the QDs for specific applications. Notably, the use of tetraethyl orthosilicate (TEOS) in SiO_2 synthesis is preferred over other precursors because it is reasonably priced, easily accessible, easily hydrolyzed into silica particles in the presence of water, and produces high-quality SiO_2 with superior mechanical and optical properties. TEOS can be used to synthesize SiO_2 in a controlled mixture with (3-mercaptopropyl)-trimethoxysilane (MPS), water, and ethanol. To slow down the reaction and stop the aggregation of the silica particles, ethanol is repeatedly added to the mixture to act as a solvent. MPS and ammonia are also added to stabilize the mixture and regulate the morphology of the SiO_2 particles.

The development of an SiO_2 coating technique on perovskite QDs is challenging due to the possibility that the SiO_2 deposition procedure could negatively affect the perovskite QDs, causing them to lose their PL properties. The main challenge of this is identifying a suitable solvent that can be applied during the SiO_2 coating process without harming the perovskite QDs. The perovskite QDs tend to degrade when reacted with water; therefore, solvents such toluene or hexane (which cannot be aqueous) must be used in place of water. To avoid causing any structural or chemical damage to the perovskite QDs, the coating procedure must also be optimized to ensure that the SiO_2 layer is deposited uniformly.

The SiO_2 encapsulation process for perovskite QDs involves the following steps:

i. *Synthesis of perovskite QDs*: Perovskite QDs are typically synthesized by hot-injection via the heating of precursor materials in an inert gas environment in a high-boiling solvent, which is then followed by the coating of the ligand layer.[11]
ii. *Preparation of SiO_2 precursor solution*: The SiO_2 solution is prepared by dissolving TEOS or tetramethyl orthosilicate (TMOS) in ethanol or methanol or water.[147]
iii. *Encapsulation of perovskite QDs*: The SiO_2 precursor solution is added dropwise to the perovskite QDs dispersed in ethanol or methanol. The mixture is then stirred and left to react to form a SiO_2 shell around

TABLE 1 Various synthetic methods, Si precursors, properties, and applications of HPs@SiO_2.

S. No.	HP/SiO_2	Synthetic protocol	Various Si precursors	PL peak and PLQY	Stability	Various applications	References
1	$CsPbBr_3$@Cs_4PbBr_6/SiO_2	LARP	APTES	520 nm, 48%	There is no change after 10 cycles of heating and cooling between 30 and 150°C with 50% relative humidity	Anti-counterfeiting	[60]
2	$CsPb(Br/I)_3/SiO_2$	Hot-injection	APTES	624 nm, 88%	Only 5% of the PLQY value is lost after 3 months in the air	LEDs	[15]
3	$CsPbBr_3$@SiO_2/Al_2O_3	Hot-injection	DBATES (di-sec-butoxyaluminoxytriethoxysilane)	519 nm, 90%	There is no change at 50°C after 1 h in vacuum	LEDs	[112]
4	$CsPbBr_3$@SiO_2	LARP	APTES	518 nm	Under visible lighting and oxygen environment, only 2% of initial PL intensity is reduced after 1 h	Photocatalysis	[113]
5	$MAPbBr_3/SiO_2$	LARP	APTES	452–524 nm, 15–55%	After 2.5 h, ~30% of the PL intensity is reduced in isopropanol.	–	[114]
6	$CsPbBr_3/SiO_2$	Hot-injection	APTES and TEOS	514 nm, 61.9%	37.9% of the initial PL intensity of the solution remains after 34 days After 30 days, 82.8% of the original PL intensity of the film is still present	LEDs	[115]
7	$CsPbBr_3/SiO_2$	Hot-injection	APTES	522 nm, 85%	PLQY remains almost the same after 3 months	LEDs	[15]
8	$CsPbBr_3/SiO_2$	Hot-injection	$(NH_4)_2SiF_6$	500 nm, 84%	At 353 K, its emission intensity drops to 90% of its initial value	LEDs	[116]
9	$CsPbBr_3/SiO_2$	Hot-injection	TMOS	517 nm, 80%	After 7 days of water treatment, over 80% of the PL stability is still present	LEDs	[117]
10	Cs_4PbBr_6:Sn@SiO_2	LARP	TMOS	–	In water and toluene, after 24 h, 40.4% of the original PL intensity is lost	–	[118]
11	$CsPbBr_3/SiO_2$	Hot-injection	APTES	519 nm, 80%	After 2 months, 77% of the initial PLQYs is still present	–	[119]
12	$MAPbBr_3/SiO_2$	LARP	TMOS	505 nm, 89%	After 49 h of exposure to 450 nm LED light (with 175 mW cm^{-2}), 38.99% of the PL intensity is reduced	LEDs	[54]

TABLE 1 (Continued)

S. No.	HP/SiO_2	Synthetic protocol	Various Si precursors	PL peak and PLQY	Stability	Various applications	References
13	$MAPbBr_3$@SiO_2	LARP	TEOS, APTES	523 nm, 60.3%	When exposed to 60 mW cm^{-2}, 450 nm light, the emission remains nearly constant for 350 h	LEDs	[120]
14	($CsPbBr_3$/Fe_3O_4) @MPSs@SiO_2	Hot-injection	TMOS	508 nm	–	Capturing circulating tumor cells	[121]
15	$CsPbBr_3$ QDs/SiO_2	Hot-injection	APTES	537 nm	After 16 days of storage in the air, PL intensity drops to around 70%	LEDs	[122]
16	$CsPbBr_3$@SiO_2	Hot-injection	APTES	519 nm, 90%	The fluorescence remains in various alcohols, esters and octane after 3000 h., esters, and octane, after 3000 h	LEDs	[123]
17	CsPb ($Br_{0.3}I_{0.7}$)$_3$@SiO_2	Hot-injection	APTES	663 nm	–	LEDs	[123]
18	$CsPbBr_3$/SiO_2	LARP	TMOS	501 nm, 90%	In water, the PL intensity of the sample is approximately 112 and 63% at the start ($t = 1$ min) and maximum ($t = 16$ min) ultrasonication times, respectively	–	[55]
19	$CsPb_2Br_5$@SiO_2	Hot-injection	TEOS	432 nm, ~5%	Blue emission still persists in water after 3 days	Biosensing	[124]
20	$CsPbBr_3$ QDs/$FSiO_2$	Hot-injection	FPEOS (perfluorodecyltriethoxysilane)	519 nm, 75%	The PL intensity remains 29.8% between 30 and 90°C	LEDs	[125]
21	$CsPbBr_3$@SiO_2	LARP	TMOS	520 nm, 72%	28% of the initial PL is reduced under UV light for 5 h	LEDs	[59]
22	$CsPbBr_3$@SiO_2	Hot-injection	TEOS	533 nm	Strong emission is observed even after 12 h	Lasing	[61]
23	$CsPbBr_3$@SiO_2	Hot-injection	APTES	~500 nm, ~90%	–	–	[57]
24	$CsPbBr_3$/$CsPb_2Br_5$ @SiO_2	Hot-injection	TEOS	42%	–	LEDs	[126]
25	$CsPbBr_3$-coreactant@SiO_2	Hot-injection	TMOS	518 nm, 65%	After 48 h of storage at 100% relative humidity, only 55% of the ECL value is left	ECL (electrochemiluminescence)	[127]
26	$CsPbI_3$@SiO_2	Hot-injection	APTES	84%	In water, it takes 1 h for the florescence to disappear	–	[128]
27	$CsPbBr_3$@SiO_2	Hot-injection	MPTMS [(3-mercaptopropyl) trimethoxysilane]	527 nm, 78%	After over 20 days of storage in water, 50% of the original PL intensity is reduced	Lasing	[32]

(Continues)

TABLE 1 (Continued)

S. No.	HP/SiO_2	Synthetic protocol	Various Si precursors	PL peak and PLQY	Stability	Various applications	References
28	$CsPbX_3$@SiO_2; (X = Cl, Br, I)	Hot-injection	TEOS	523 nm and 11.2% ($CsPbCl_3/SiO_2$), 523 nm and 82% ($CsPbBr_3/SiO_2$), 634 nm, 73% ($CsPb(Br_{0.3}I_{0.7})_3/SiO_2$	40% of its emission remains after being kept in water for 4 h	LEDs	[13]
29	$CsPbMnX_3$@SiO_2	LARP	TEOS	446 nm and 607 nm, 50.5%	Only 10% of the initial PLQY value is reduced after 6 days	LEDs	[58]
30	DDAB-$CsPbBr_3$@SiO_2	Hot-injection	TMOS	519 nm, 80.45%	Strong fluorescence remains even after 40 min ultrasonication in water	LEDs	[56]
31	$CsPbBr_3$@SiO_2	Hot-injection	TEOS	64%	60% of the PL intensity remains after 10 h under 365 nm UV light	PEC (photoelectrochemical)	[129]
32	$CsPbBr_3$@SiO_2	Hot-injection	PHPS (perhydropolysilazane)	510 nm, 74%	In water, a bright emission occurs after 4 h	LEDs	[130]
33	$CsPbBr_3$@SiO_2	Hot-injection	TEOS	525 nm	After 96 h in water, PL intensity is reduced by 15%	LEDs	[131]
34	$CsPbBr_{1.2}I_{1.8}$@SiO_2	Hot-injection	PHPS	616 nm, 79%	–	LEDs	[130]
35	$CsPbBr_3$@SiO_2	Hot-injection	APTES	514 nm	In water, 41%, 50.5%, 58.9%, 64.2% of the initial PL intensity remain after 6 h, 12 h, 24 h, 48 h, respectively	Cell imaging	[23]
36	$CsPbBr_3$@SiO_2	Hot-injection	APTES, TEOS, and TMOS	515 nm, 82%	After 84 h at 60°C, the peak of the PL remains unchanged	–	[132]
37	$CsPbBr_3$@SiO_2	LARP	TMOS	515 nm, 10.2%	In water, 80% of the initial PL intensity remains after 24 h	Bioimaging and Drug Delivery	[22]
38	$CsPbBr_3$@SiO_2	Hot-injection	TEOS	530 nm	–	Lasing	[133]
39	$CsPbBr_3$@SiO_2	Hot-injection	TEOS	~87%, 519 nm	At 120°C, ~15% of the initial PL intensity drops	LEDs	[134]
40	$CsPbBr_3$@SiO_2	Hot-injection	APTES and TMOS	530 nm	After more than 250 days in air, there is no significant degradation	LEDs	[135]
41	$CsPbBr_3$/mesoporous-SiO_2	Low-temperature molten salts	Commercial MCM-41 Mesoporous SiO_2	90%	After 30 days in the air, 95% of the PL intensity is still present	LEDs	[136]

TABLE 1 (Continued)

S. No.	HP/SiO_2	Synthetic protocol	Various Si precursors	PL peak and PLQY	Stability	Various applications	References
42	$CsPbBr_3$@SiO_2	Hot-injection	APTES	516 nm, 98.56%	–	Daytime Radiative Cooling	[137]
43	$CsPbBr_3$@SiO_2	Hot-injection	Commercial SBA-15	519 nm	20% of the PL intensity is reduced under UV-light irradiation (365 nm, 6 W)	LEDs	[132]
44	$CsPbBr_3$@SiO_2	Hot-injection	SiO_2 spheres	517 nm, 96%	The PL intensity is reduced by 68% after annealing at 70°C for 10 h	Lasing	[138]
45	$Cs_2AgInCl_6$/SiO_2	LARP	TEOS	505 nm and 580 nm	The fluorescence is reduced by 67.04% after six air plasma bombardments	LEDs	[139]
46	$CsPbBr_3$@SiO_2	Impregnation	TEOS	524 nm, 32.5%	–	Anti-counterfeiting	[140]
47	$MAPbBr_xI_{3-x}$@SiO_2	Impregnation	TEOS, TMOS, TPOS	520 nm, 5.5 ± 1.1% ($MAPbBr_3$@SiO_2)	–		[141]
48	$CsPbBr_3$/SiO_2	Hot-injection	TEOS	515 nm	–	LEDs	[142]

the perovskite QDs. The thickness of the SiO_2 shell can be tuned by adjusting the concentration of the SiO_2 solution and the reaction time.

iv. *Purification and drying*: To remove unreacted precursor materials and by-products, the SiO_2-encapsulated perovskite QDs are purified by centrifugation or filtration. They are then dried in a vacuum or nitrogen atmosphere to remove any residual solvent.

In recent years, $MAPbBr_3$ QDs have received a lot of attention due to their promising optoelectronic applications. However, the QDs have a tendency to degrade when exposed to air and moisture. Huang et al. were able to synthesize highly stable $MAPbBr_3$ QDs by implementing an SiO_2 layer and using the modified ligand-assisted reprecipitation method[54]; TEOS/TMOS was mixed with $MAPbBr_3$ QDs dissolved in toluene, which contains a small amount of catalytic water that provides H^+ for the hydrolysis reaction. The catalytic water was consumed at a faster rate when TMOS was used due to the decreased inductive effect of the methyl group compared to the ethyl group. It was concluded that TMOS was more effective in improving the stability of $MAPbBr_3$ QDs compared to TEOS. During the hydrolysis reaction of TMOS, the thickness of the spherical SiO_2 layer became larger from several nanometers to ~470 nm within 36 h (Figure 2). The SiO_2-coated $MAPbBr_3$ QDs exhibited a PL emission of 94.10% after illumination (470 nm LED light and power 21 mW/cm^2) for 7 h; it was found to have decreased to 38.36% when using bare QDs. A main disadvantage of acid-catalyzed SiO_2 growth is that the acid can dissolve the $CsPbBr_3$ NCs during the synthesis process. To combat this, Cs_4PbX_6 (X = Cl, Br, I), which produces emissive $CsPbBr_3$ NCs under acidic reaction conditions, can be used. Park et al. posited a method in which Cs_4PbBr_6 NCs were treated with HNO_3 and TEOS and converted into $CsPbBr_3$ NCs under acidic conditions as shown in reaction (i) below.[148]

The TEOS is then hydrolyzed to form silicic acid, which condenses around the newly formed $CsPbBr_3$ NCs to form a SiO_2 matrix (reaction(ii)) that stabilizes the NCs and prevents aggregation. The following two step reaction occurs during the synthesis:

i. $Cs_4PbX_6 = CsPbX_3 + 3CsX$

ii. $Si(OC_2H_5)_4 + 4H_2O = Si(OH)_4 + 4C_2H_5OH$

$$x\,Si(OC_2H_5)_4 + x\,Si(OH)_4 = (-SiO_2-)_x + 4x\,C_2H_5OH$$

$$x\,Si(OH)_4 + x\,Si(OH)_4 = (-SiO_2-)_x + 4x\,H_2O$$

However, acidic conditions will affect the stability of HP NCs, which makes milder reaction conditions more suitable for the Cs_4PbBr_6 to $CsPbBr_3$ NCs transformation. Maleic anhydride (MANH) is able to initialize the transformation of Cs_4PbBr_6 NCs into $CsPbBr_3$ NCs and catalyze the growth of a SiO_2 shell around the NCs. In this process, MANH reacts with the long chain surfactant amines present on the surface of the NCs, resulting

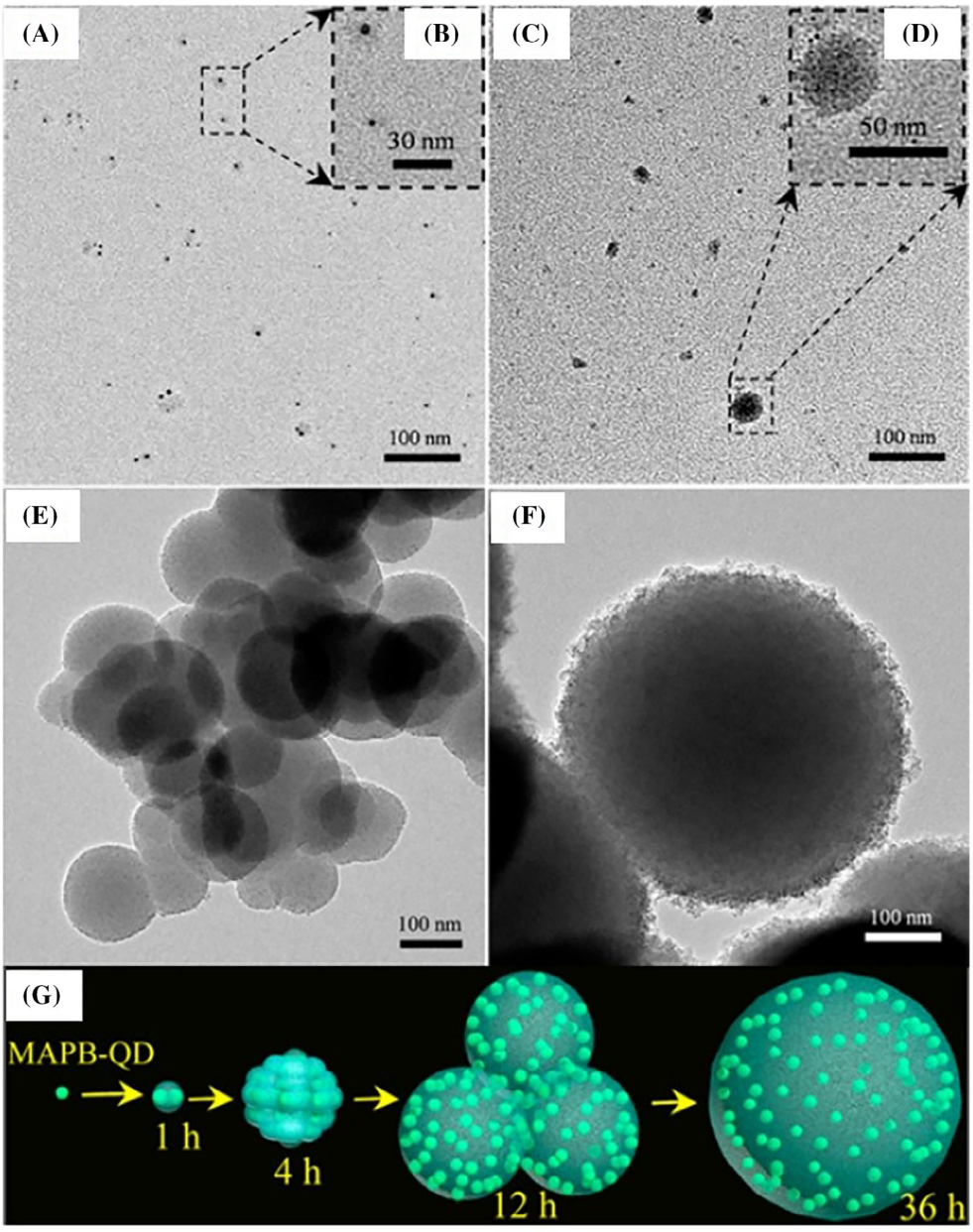

FIGURE 2 Size evolution of $MAPbBr_3$-QDs/SiO_2 under different reaction conditions: (A and B) 1 h, (C and D) 4 h, (E) 12 h, and (F) 36 h. (G) Illustration of the growth mechanism of SiO_2 with time. Reprinted with permission.[54] Copyright 2016, American Chemical Society.

in acidification of the reaction medium. This helps catalyze the SiO_2 growth by facilitating the hydrolysis and condensation reactions required for silica shell formation.[149]

He et al. described an innovative approach toward synthesizing dual-shelled perovskite NCs, which contain perovskite/SiO_2 core/shell NCs which is passivated with polymer ligands.[150] They used a unique method for controlling the size, surface passivation, and stability of the resulting perovskite NCs. Figure 3 illustrates the process of synthesizing core/shell NCs of $MAPbBr_3$/SiO_2 with different polymer ligands. This process uses multi-arm star-like triblock copolymers as nanoreactors for the formation of NCs. The polymer ligands used to cap the NCs are polyethylene oxide (PEO) and polystyrene (PS), which are attached to the P4VP-b-PtBA-b-PEO and P4VP-b-PtBA-b-PS copolymers, respectively. The resulting NCs exhibited improved stability, including photostability, chemical composition stability, colloidal stability, water stability, and solution processability.

Perovskite QDs can be attached to the surfaces of monodisperse SiO_2 particles via amino-mediated coupling[151]; this involves using a coupling agent that

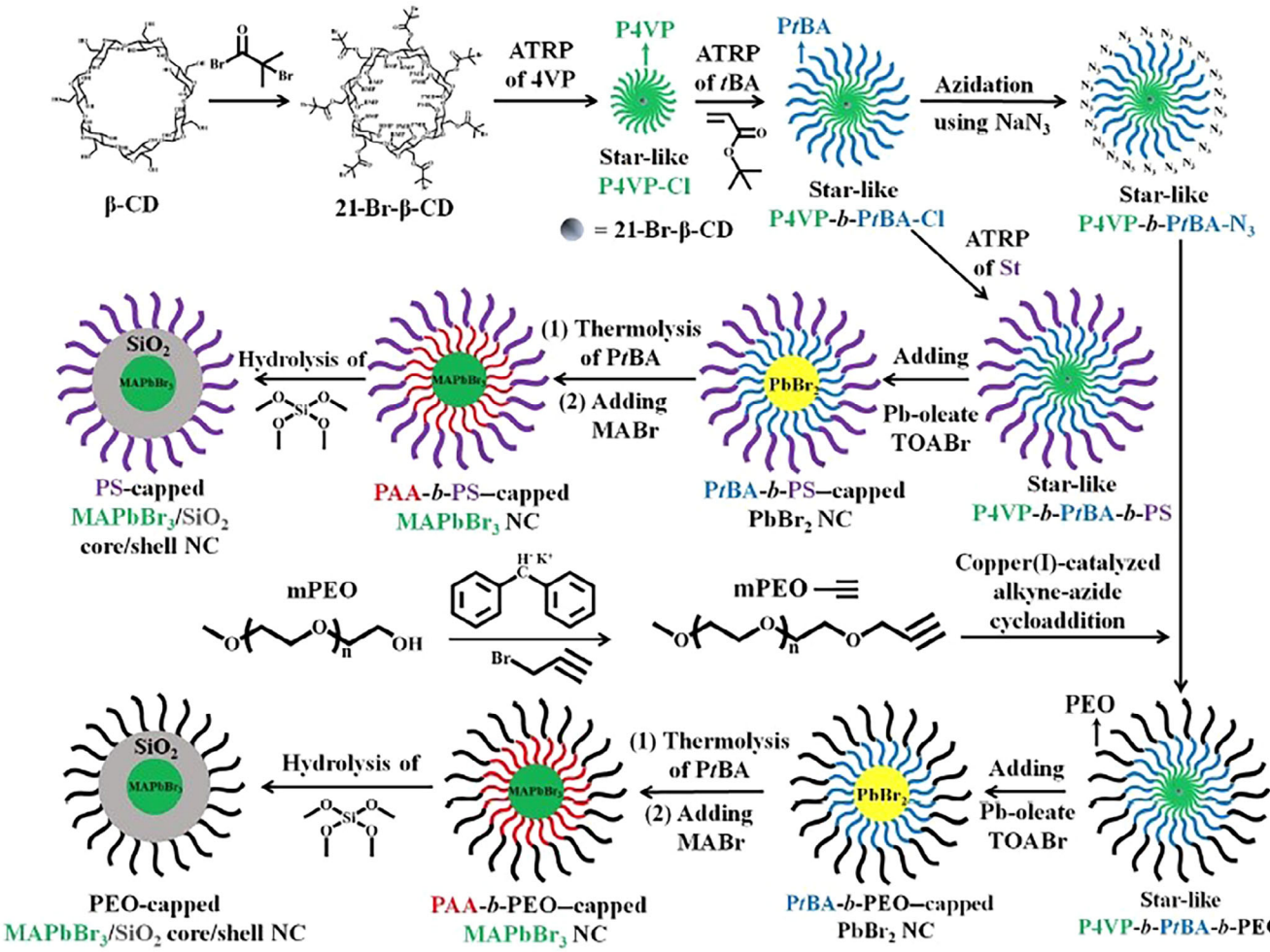

FIGURE 3 Schematic diagram showing the sequential synthesis of PS-capped and PEO-capped $MAPbBr_3/SiO_2$ NCs using P4VP-b-PtBA-b-PS and P4VP-b-PtBA-b-PEO, respectively. CD = cyclodextrin; BMP = 2-bromo-2-methylpropionate; and TOABr = tetraoctylammonium bromide. Reprinted with permission.[150] Copyright 2019, Science.

contains an amino group and another functional group that can react with the SiO_2 particles. The surface ligands of the perovskite QDs react with the amino group of the coupling agent to create a covalent link between the coupling agent and the QDs. The other functional group also reacts with the SiO_2 particles, forming another covalent bond between the coupling agent and the SiO_2 particles. The resulting composite material consists of perovskite QDs anchored onto the surfaces of monodispersed SiO_2 particles via covalent bonds. This method has a number of benefits, such as improved stability and the capacity to adjust the qualities of the final composite material. Yang et al. demonstrated a method for anchoring $FAPbX_3$ QDs onto the surface of amine-functionalized silica (A-SiO_2) spheres (Figure 4),[152] which involved a ligand-assisted reprecipitation (LARP) process at room temperature. The A-SiO_2 spheres acted as adsorption and nucleation sites for the QDs, enabling them to attach uniformly to the surfaces of the spheres. This method improved the photostability of the QDs as they were not in direct contact with each other. Yang et al. also found that the $FAPbBr_3$/A-SiO_2 composites produced low-threshold random lasing emission without the need for an additional cavity. This was caused by the effective optical gain of the QDs and the strong scattering phenomena of the A-SiO_2 spheres. These findings suggest that this new material could potentially be applied to integrated speckle-free imaging and HP lasers.

The advancement and widespread application of HPs@SiO_2 composites hold great promise in various technological fields, yet a number of challenges remain to be addressed. A fundamental concern pertains to the need for standardized protocols in evaluating the stability of HPs@SiO_2 composites. Presently, the variability in experimental conditions across research papers hinders meaningful comparisons. Establishing a uniform standard encompassing parameters such as power intensity and wavelength for photostability measurements is vital.

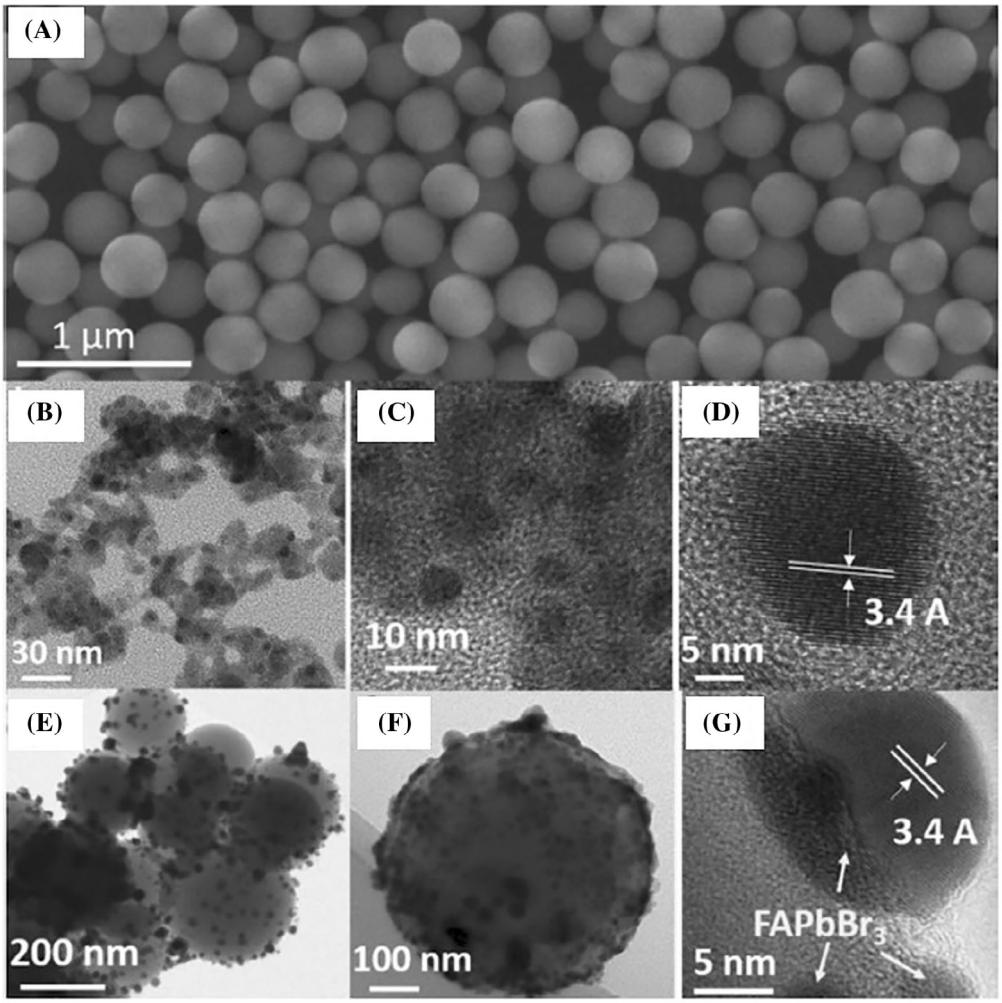

FIGURE 4 (A) SEM image of amine-functionalized silica (A-SiO_2) spheres, (B–D) TEM images of $FAPbBr_3$ QDs, and (E–G) TEM images of $FAPbBr_3$/A-SiO_2. Reprinted with permission.[152] Copyright 2020, Wiley-VCH.

Furthermore, maintaining standard environmental conditions, particularly relative humidity and temperature, under which storage stability is assessed, is essential for reliable and consistent results. The adoption of binary coating strategies represents a pathway toward enhancing the protective capabilities of these composites, safeguarding their functionality over time. There is also a need to transition the production processes of HP@SiO_2 composites from the laboratory scale to the industrial scale to improve their commercial potential.

While mesoporous silica is currently the dominant template material for the fabrication of HPs@SiO_2 composites, there exists a significant opportunity to diversify template options.[153–155] Templates such as mesoporous alumina and mesoporous TiO_2, with their distinct properties, can be used to tailor HPs@metal oxide (MO_x) composites for use in various applications. Encouraging research and exploration into these alternative templates can expand the versatility and adaptability of HPs@MO_x composites. Simultaneously, there has been a lack of research on atomic layer deposition (ALD) as a means to coat HPs@MO_x composites, with the majority of previous studies focusing on AlO_x coatings. Given the precision and versatility of ALD when depositing thin films, it is crucial to broaden the scope of ALD research to encompass other MO_x materials such as TiO_2 and ZnO. This would allow for the fine-tuning of the properties of HPs@MO_x composites to address specific application requirements and ensure long-term stability.

In addition to these immediate challenges, it is important that the scientific community pursues innovative strategies to propel the field forward. This involves exploring novel combinations of methods and techniques, with the aim to synergize the strengths of disparate approaches. Additionally, a strong emphasis on the development of solvent-free processes can mitigate the environmental impact and streamline production while enhancing the sustainability of HPs@MO_x composite manufacturing.

3.3 | Silanol

Silanol (Si-OH) groups have also been used to enhance the stability of halide perovskite materials, especially when integrated into composite structures such as HPs@SiO_x. By passivating the surface defects of HP materials, they mitigate non-radiative charge carrier recombination, bolster device efficiency, and reduce instability. Silanol groups also act as hydrophilic agents on the SiO_x surface, attracting and absorbing moisture, thus safeguarding HP materials against degradation caused by humidity. Moreover, their presence enhances the mechanical durability of HP films and devices, forming robust Si-O-Si networks that prevent cracking or delamination under mechanical stress. Additionally, the compatibility of SiO_x materials with solution-processing methods makes them well-suited for conformal coatings, preserving stability during device fabrication. Lastly, the tunability of silanol-rich SiO_x allows for the optimization of optical and electrical properties, facilitating tailored solutions for specific HP devices.

Silanols comprise a silicon atom bonded to a hydroxyl (—OH) group. Alkoxysilanes, aminosilanes, and halosilanes are typically hydrolyzed to produce silanols.[156]

$$R_3Si-Cl+H_2O \rightarrow R_3Si-OH+HCl$$

There are different types of silanols, which can be classified based on the nature of the Si atom, the number and position of the hydroxyl groups:

i. *Monosilanol*: This is the simplest silanol. Monosilanol comprises one hydroxyl group attached to a Si atom.
ii. *Disilanol*: Disilanol has two —OH groups bonded to a Si atom. It can be further classified into geminal disilanol and vicinal disilanol based on the structural arrangement of the —OH groups, where the two —OH groups are either attached to the same or the adjacent silicon atoms, respectively.
iii. *Trisilanol*: Trisilanol consists of three —OH groups attached to a Si atom.
iv. *Tetrasilanol*: Tetrasilanol consists of four —OH groups bonded to a Si atom.
v. *Cyclosilanol*: Here, the Si atom is part of a cyclic structure, such as in cyclosiloxanes. The number and position of the —OH groups can vary depending on the specific cyclosiloxane.

The properties of silanols are affected by their chemical composition, and they have various applications. In the material science field, silanols are frequently used as anchoring groups for chemical processes and in the functionalization of silica surfaces; in biochemistry, silanols play a vital role in the interactions between silica-based substances and biological systems, for example, in proteins and cells.

Silanols are highly sensitive to environmental factors, for example, pH and temperature, and the inclusion of other functional groups can modify their behavior. Alkoxysilanes such as TMOS and phenyltriethoxysilane (phTEOS) are commonly used as precursors in the production of silica-based materials. These alkoxysilanes undergo hydrolysis upon exposure to water, which results in the formation of Si—OH groups on the surface of the templated particles. These Si—OH groups can then undergo condensation reactions, where pairs of Si—OH groups react with each other to form Si—O—Si bonds, constructing a giant three-dimensional (3D) silica network. These condensation reactions can occur either directly between two Si-OH groups or via an alkoxy group (RO—) intermediate. The ratio of TMOS to phTEOS used can affect the formation of the silica network, creating materials with different properties. For example, increasing the phTEOS content may lead to the formation of a more cross-linked and rigid silica network.

Talianov et al. explored the synthesis of highly stable silica shell-coated $CsPbBr_3$ NCs in which silanol groups are condensed to form silica shells.[30] Liu et al. used a Lewis base silica tetraethoxysilane (TEOS), comprised of four —OH groups on a HP film, as a passivation additive (Figure 5).[157] The TEOS on the perovskite film was anchored onto lead and suppressed the defect states. There are many advantages associated with using TEOS as a passivation additive, as it self-crosslinks into a network after hydrolysis, which results in detachment from perovskite. TEOS contains an alkoxy functional group, that can be converted into silanol upon hydrolysis. Then, the hydrolyzed TEOS forms a cross-linked network. Hydrolyzed TEOS is polymerized in situ into a network as part of the perovskite phase formation method. Additionally, TEOS is connected to the perovskite layer as a result of the interaction between the oxygen on the TEOS network and the Pb^{2+} on perovskite. As a result of that, a composite of cross-linked TEOS and 2D HP film was developed. The TEOS network with oxygen consists of lone pair electrons coordinated with the uncoordinated Pb^{2+} ions in 2D perovskite, resulting in the passivation of surface defect states of the HP film. The resultant perovskite with TEOS was found to have a 40% higher PL intensity than the original, pristine perovskite.

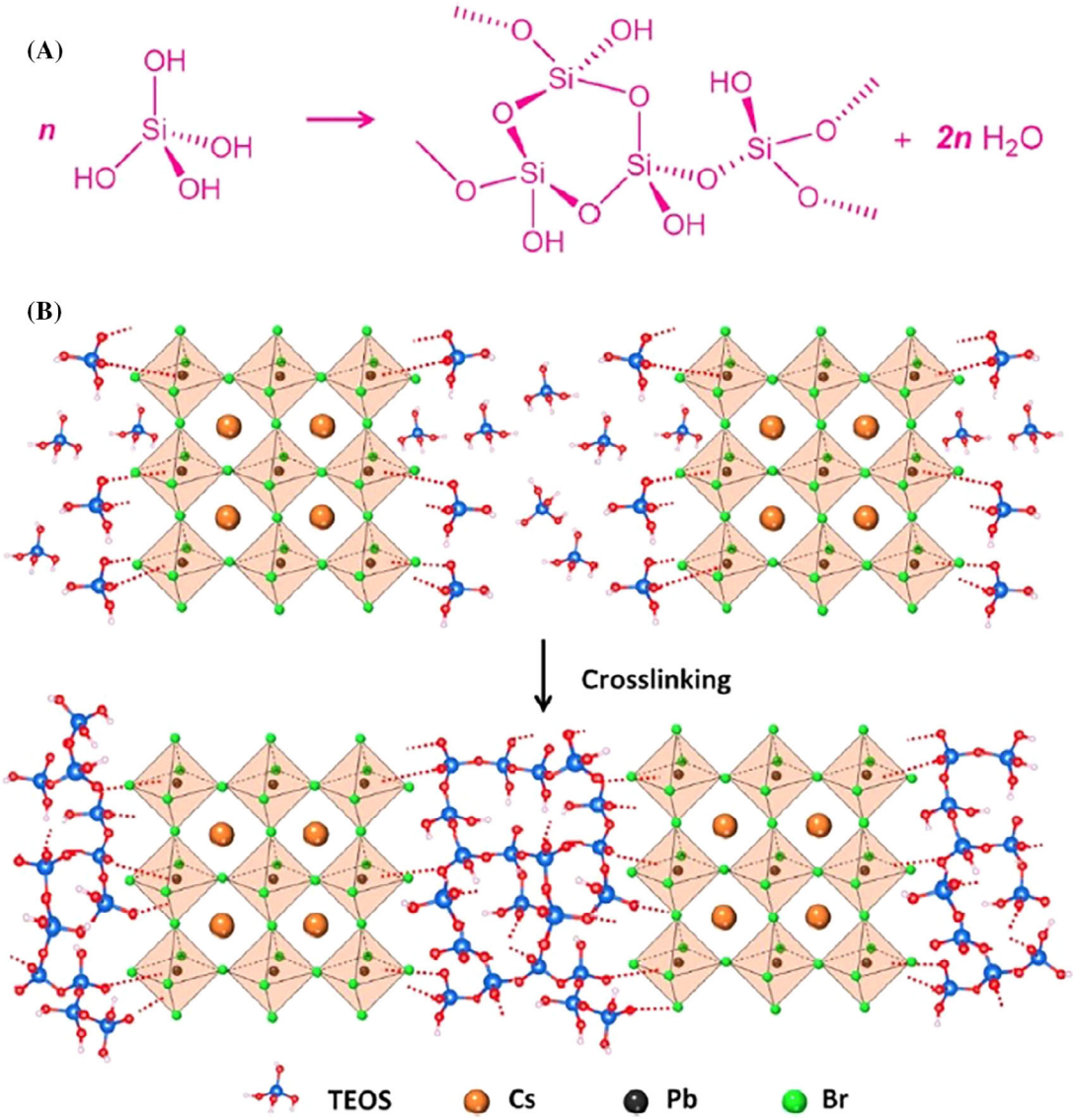

FIGURE 5 Schematic representation of the (A) cross-linked TEOS network and (B) cross-linked TEOS-2D HP composite film. Reprinted with permission.[157] Copyright 2020, Elsevier B.V.

3.4 | Silica gel

Silica gel is amorphous in nature and has a sporadic 3D structure, comprised of alternating Si and oxygen atoms as well as nanometer-sized holes and pores. Silica gel is amorphous in nature and has a sporadic 3D structure, comprising alternating Si and oxygen atoms as well as nanometer-sized holes and pores. Silica gel offers various benefits for the stabilization of HP materials, including shielding against moisture-induced degradation, the potential to passivate surface defects, ensuring thermal stability, compatibility with encapsulation materials, and greater long-term reliability. Generally, silica gel is synthesized via the sol–gel process:

a. *Hydrolysis*: First, silicic acid is produced by hydrolyzing a Si alkoxide (such as tetraethyl orthosilicate, TEOS) using an acid or basic catalyst.

$$Si(OC_2H_5)_4 + 2H_2O \rightarrow Si(OH)_4 + 4C_2H_5OH$$

b. *Condensation*: The silicic acid molecules then undergo condensation to form a network of connected silica particles. This step is typically performed in a basic environment, which aids in the condensation reaction.[158]

$$Si(OH)_4 \rightarrow SiO_2 + 2H_2O$$

c. *Drying*: The resulting silica particles are rinsed and dried to remove leftover solvent and to activate the drying agent.

Silica gel is a superior desiccant and moisture absorber due to the abundance of –OH groups on its surface that can interact with water molecules. It is also used as a catalyst in chemical reactions and as a chromatography medium in analytical chemistry. The silanol groups (—Si—OH) can be used to functionalize the HPs by covalently attaching other organic or inorganic functional groups to it. However, it is difficult to utilize all the available silanol groups due to steric hindrance and imperfect reaction conditions. Generally, a small capping agent with low steric hindrance is used for this, for example, trimethylsilylchloride. The second grafting procedure, known as endcapping, is then carried out to reduce silanol activity. There are two main advantages associated with endcapping. Bare silica gel for chromatography is polar and moderately acidic due to the free silanol groups (pKa 5). However, endcapping makes the silica non-polar and non-acidic. This polar interaction serves as the foundation for the separation in chromatography. Endcapping protects the surface from being attacked and hydrolyzed when functionalized silica is used under harsh conditions. The encapsulation of HP NCs with silica gel has been proposed as a potential method for preventing the degradation of these NCs against moisture, oxygen, and other environmental factors. The silica gel coating can be applied via various methods, including sol–gel synthesis, reverse microemulsion, and spray-drying. A silica precursor and a catalyst are combined with perovskite NCs as part of a sol–gel synthesis to promote the growth of a silica gel layer on the HP surface. The sol–gel coating improves the stability and the mechanical and optical properties of the NC; it also allows for the thickness of the layer to be controlled. In the reverse microemulsion process, perovskite NCs are dispersed in a water–oil emulsion, and a silica precursor is subsequently added to form a gel around the NCs. Reverse microemulsions are effective for the coating of perovskites with silica gel because these microemulsions can control particle size and distribution as well as reduce agglomeration and solvent usage. During the spray-drying step, silica precursor solution is sprayed into a hot gas stream with perovskite NCs to form a dry powder coated with silica gel.

HP NCs have demonstrated great potential for use in various electrochemical applications. However, the weak aqueous stability of the NCs restricts their use. The use of silica gel has been proposed to improve the stability of HP.[159] Silica gel is a porous and hydrophilic material that can absorb water and prevent HP from interacting with water, thus improving its stability. Encapsulating perovskite NCs with a waterproof shell (such as silica or other inert coatings) can improve the PL stability of HPs in the aqueous phase. However, silica gel coating can also hinder their electrochemical performance due to the poor electrical conductivity of the inert coatings. The inert coatings used to encapsulate perovskite NCs are typically insulators that can hinder the transport of charge carriers, which is crucial for many electrochemical applications. The poor electrical conductivity of the coatings can increase the resistance of the perovskite NCs, resulting in reduced electrochemical performance (reduced charge transport, inferior current density, and lower efficiency). Several methods to increase the electrical conductivity of the coatings have been put forth to address this issue. One approach suggests introducing conductive materials, such as carbon nanotubes, graphene, or metal nanoparticles, into the coatings to improve charge transport. Another approach suggests the use of conductive polymers as encapsulating materials, which can provide waterproofing and improve electrical conductivity. According to Li et al., encasing $CsPbBr_3$ NCs in a silica gel shell that is waterproof and conductive increases the NCs' aqueous stability and radiative-charge-transfer efficiency.[160] The resulting NCs exhibited strong electroluminescence (ECL) in aqueous media. ECL is a phenomenon where a luminescent signal is generated by an electrochemical reaction. The ECL of $CsPbBr_3$ NCs is believed to stem from the radiative recombination of injected electrons and holes in the NCs, which is induced by an electrochemical potential applied to the NCs. The ECL signal of $CsPbBr_3$ NCs is sensitive to various electrochemical parameters, which include the electrode potential, scan rate, and supporting electrolyte concentration. Lee et al. fabricated highly stretchable white-light electroluminescent devices using gel-type silica-coated $CsPbBr_3$ and $CsPbBr_xI_{3-x}$ NC inks.[161] Silica shell with 3-aminopropyltriethoxysilane (APTES) treatment has been shown to improve the stability of HP NCs. APTES is a type of silane coupling agent that can react with both the silica shell and the perovskite NC surface, forming a covalent bond and improving the stability of the NCs. Additionally, gel-type inks have been used to improve the dispersity of perovskite NCs in polymer matrices. The gel-type inks typically comprise a mixture of polymer and solvent and can form a 3D network structure when dried, which helps to trap the perovskite NCs in the polymer matrix and prevent aggregation.

3.5 | Silicate

Silicate compounds are a large class of compounds that contain the silicate ion (SiO_4^{4-}) as a building block, with additional elements such as aluminum, magnesium, iron, and calcium incorporated in varying amounts. Silicate

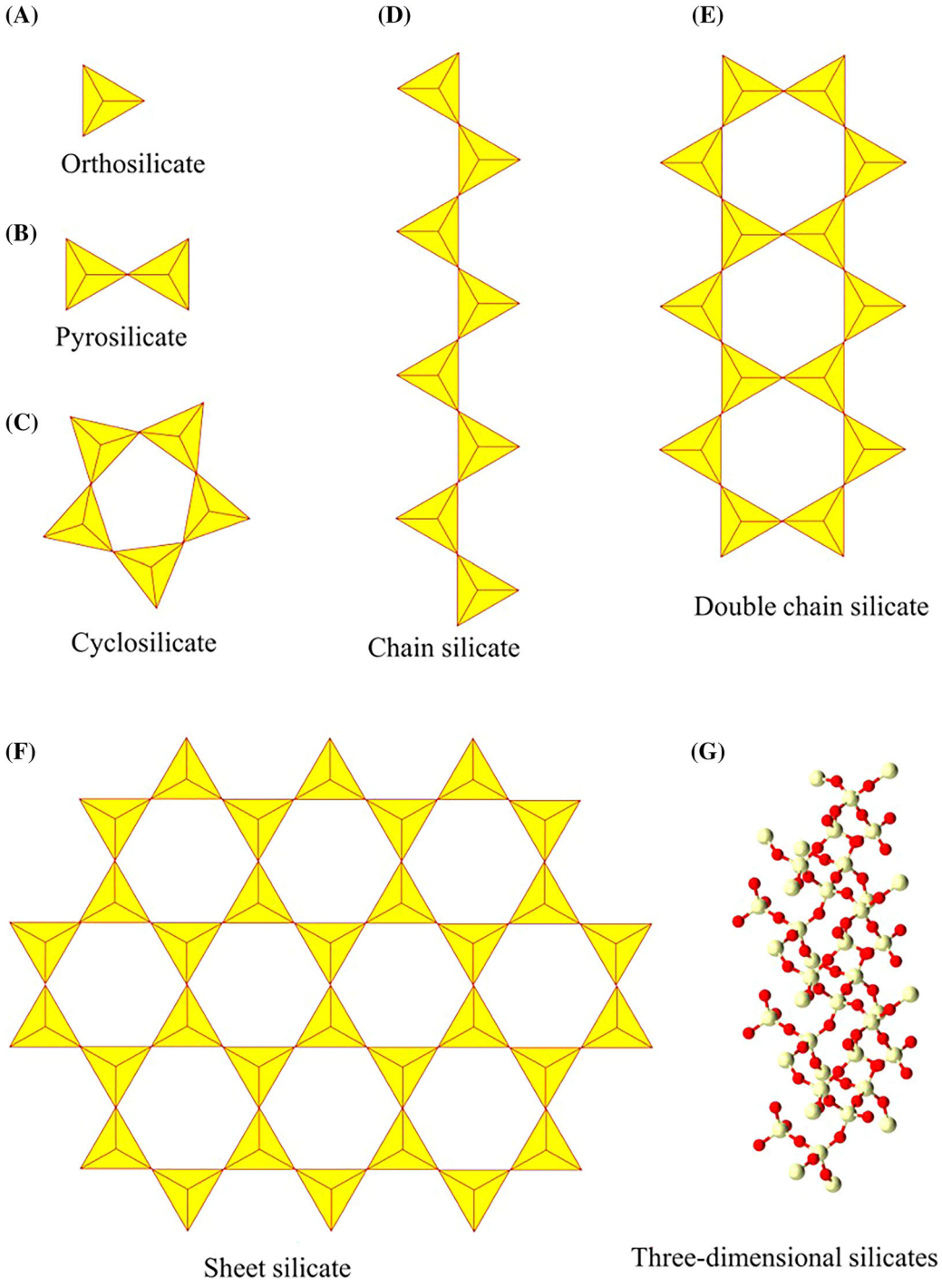

SCHEME 2 Various silicate structures. (A) Orthosilicates or nesosilicates; (B) Pyrosilicates or sorosilicates; (C) Cyclosilicates; (D) Chain silicates or inosilicates; (E) Double chain silicates; (F) Sheet silicates or phyllosilicates; and (G) Three-dimensional silicates or tectosilicates.

compounds are widely used in various industrial and commercial applications, such as glass production, construction materials, ceramics, detergent and soaps, fireproofing materials, agriculture, water treatment, and personal care products.

Silicates are instrumental in stabilizing halide perovskite materials. They serve multiple critical functions, including passivating surface defects to enhance device performance and stability, providing mechanical support to prevent physical damage, acting as a moisture barrier to guard against degradation, improving chemical stability for long-term functionality, ensuring compatibility with manufacturing processes, and offering tuneable properties for optimized device performance. Silicates are particularly viable for real-world renewable energy and optoelectronics applications.

Silicates can be classified into different groups based on their crystal structure (Scheme 2):

i. *Orthosilicates or Nesosilicates*: Nesosilicates are silicate minerals where the tetrahedral silica units are not linked together. Examples of this include willemite (Zn_2SiO_4), forsterite (Mg_2SiO_4), and phenacites (Be_2SiO_4).
ii. *Pyrosilicates or Sorosilicates*: Sorosilicates are silicate minerals where two tetrahedral silica units are linked together. Examples of this include zoisite ($Ca_2Al_3(SiO_4)(Si_2O_7)O(OH)$), epidote ($Ca_2(Al_2Fe(OH)(SiO_4)_3)$), thortveitite ($Sc_2[Si_2O_7]$), and hemimorphite ($Zn_4(OH)_2[Si_2O_7]\cdot H_2O$).
iii. *Cyclosilicates*: Cyclosilicates are silicate minerals where the tetrahedral silica units are arranged in rings. Examples of this include wollastonite-$Ca_3[Si_3O_9]$, beryl-$Be_3Al_2[Si_6O_{18}]$, tourmaline-Na $(Mg,Fe)_3Al_6BO_3Si_6O_{18}$.
iv. *Chain silicates or Inosilicates*: Inosilicates are silicate minerals where the tetrahedral silica units are linked together in chains. Examples of this include spodumene-$LiAl(SiO_3)_2$ and diopside-$CaMg(SiO_3)_2$.
v. *Double chain silicates*: Double chain silicates are formed by two simple chain silicates that are connected by oxygen. An example of this is tremolite ($Ca_2Mg_5[(Si_4O_{11})_2](OH)_2$).
vi. *Sheet silicates or Phyllosilicates*: Phyllosilicates are silicate minerals where the tetrahedral silica units are linked together in sheets. Examples of this include muscovite ($KAl_2(Si_3Al)O_{10}(OH)_2$), kaolinite ($Al_2Si_2O_5(OH)_4$), and pyrophyllite ($Al_2Si_4O_{10}(OH)_2$).
vii. *Three-dimensional silicates or Tectosilicates*: Tectosilicates are silicate minerals where the tetrahedral silica units are linked together in a 3D network. Examples of this include quartz (SiO_2), feldspar ($AlNaO_8Si_3$), and zeolites (Al_2O_5Si).

Various silicates, such as halloysite, kaolinite, montmorillonite, and pyrophyllite, are used to improve the stability of HP NCs.[44,45,162] Encapsulating HP NCs in silicate-based materials can aid in improving the stability and optical properties of the NCs as well as reducing toxicity of lead based HPs. Halloysite nanotubes (HNTs) are naturally occurring clay minerals that have a tubular morphology; HNTs are composed of stacked layers of aluminosilicate sheets, forming a hollow tubular structure with an inner diameter of approximately 15–100 nm and a length of 1–3 μm.[163] The structure of HNTs can be described as a rolled-up sheet of hexagonal rings made up of Si, oxygen, and aluminum atoms. The layers are stacked on top of one another. Each HNT comprises an inner lumen and an outer surface; the inner lumen consists of a single layer of alumina octahedral and silicate tetrahedral layers, while the outer surface consists of a double layer of the same units. The inner lumen is negatively charged due to the existence of —OH groups on its surface, which makes it a preferred site for positively charged ions or molecules. However, the outer layer can be modified to become positively charged in the presence of acid. which can be subsequently utilized for the self-assembly of HP QDs. Hao et al. were able to convert the surfaces and section edges of the surface hydroxyl (Sur-OH) groups within HNTs into Sur-OH_2^+ groups under acidic conditions (Figure 6).[45] Sur-OH_2^+ groups can further enhance the adsorption of negatively charged species such as Br^- ions, facilitating the growth of $CsPbX_3$ QDs. This is because the Sur-OH_2^+ groups can interact strongly with the negatively charged Br^- ions. When Br^- ions are adsorbed onto the HNT surface, a localized negative charge is formed. This negative charge can then attract positively charged Pb^{2+} and Cs^+ ions, which can bind to the surface via electrostatic interactions.[44,45] $CsPbBr_3$ crystals are formed when the adsorbed Pb^{2+} and Cs^+ ions reach a critical concentration and begin to nucleate on the HNT surface. Subsequently, the $CsPbBr_3$ crystals can grow by incorporating additional Pb^{2+} and Cs^+ ions from the surrounding solution. In HNTs, the $CsPbBr_3$ crystals can nucleate and grow preferentially at the surfaces and edges of the tubes because these areas have a higher concentration of adsorption sites for the Pb^{2+} and Cs^+ ions.

In particular, the edges of the HNTs contain many Al—OH groups, which serve as nucleation sites for the $CsPbBr_3$ crystals. As the $CsPbBr_3$ crystals continue to grow, regular nanowires are formed along the edges of the HNTs because the edges of the HNTs provide a template for the synthesis of the crystals, which can align in a regular pattern along the edges. The PL intensity of the $CsPbX_3$@HNTs as-synthesized by Hao et al. was found to remain at 80% of its original value when operated at 100°C. After being stored in an open environment for 28 days, there was almost no reduction in the PL intensity, indicating that the material is resistant to environmental degradation. The PL intensity was also maintained at 82% of its original value when exposed to UV light for 144 h, which suggests that the material is also resistant to photodegradation.

Pyrophyllite is a mineral that belongs to the phyllosilicate group; it has a layered structure of tetrahedral and octahedral sheets. In pyrophyllite, the octahedral sheet is sandwiched between two tetrahedral sheets, forming a 2:1 layer structure[164]; weak van der Waals forces keep these layers together. A third of the octahedral sites within the octahedral sheet are vacant, leading to isomorphous replacement and an abundance of unevenly distributed negatively charged ions on the pyrophyllite surface. This creates an uneven electrostatic attraction, which can influence the adsorption behavior

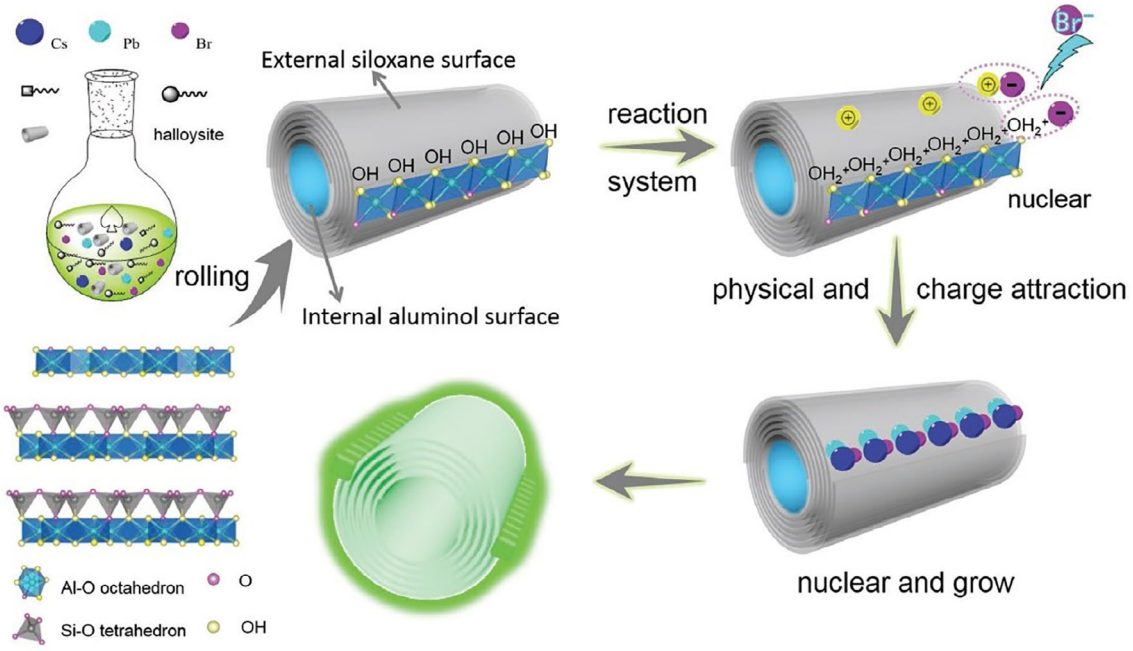

FIGURE 6 Schematic representation of the halloysite surface and its subsequent transformation into a positively charged surface, which facilitates the formation of $CsPbX_3$ QDs. Reprinted with permission.[45] Copyright 2019, Wiley-VCH.

of other charged species. The uneven distribution of these ions on the surface is a result of the isomorphous replacement of some of the octahedral sites with other elements, which can introduce charges into the structure of the mineral. The negatively charged layers in the octahedral sheet generate an uneven electrostatic attraction on the QDs. This electrostatic attraction coincides with the random distribution of NCs, which can form QDs on the pyrophyllite surface. Yuan et al. posited a technique for synthesizing $CsPbX_3$ NCs in pyrophyllite.[164] The initial fluorescence intensity of the synthesized $CsPbBr_3$@pyrophyllite was found to remain at 97% for more than 5 months in storage. Pyrophyllite reduces damage to the aquatic environment caused by lead diffusion by binding lead ions. The binding of lead ions by pyrophyllite is an important environmental remediation strategy that can help reduce the harmful effects of lead contamination in water bodies. The bound lead ions can be removed from the water by sedimentation or filtration, thereby reducing the exposure of aquatic organisms to toxic levels of lead. $CsPbX_3$@pyrophyllite composites were also used to fabricate white LEDs on an InGaN blue chip. The resulting LEDs exhibited a high color gamut of 117%.[164] Organic–inorganic lead bromide perovskite can also be attached to the surface of silicate clays, such as montmorillonite, kaolinite, and halloysite, to form perovskite-clay composites. Kaolinite (KLN) is a type of clay mineral that has a layered structure composed of octahedral gibbsite $Al(OH)_3$ sheets sandwiched between tetrahedral SiO_4 sheets; montmorillonite (MLN) has a layered structure composed of two tetrahedral sheets and one octahedral sheet with a negatively charged layer in both the tetrahedral and octahedral sites due to cation substitution. The —OH groups at the surface of these minerals play an important role in the formation of perovskite-clay composites. Jana et al. synthesized $MAPbBr_3$@clay composites (clay = KLN, MLN, and HNT) which exhibited improved thermal and luminescence properties.[162]

3.6 | Polysilsesquioxanes

Polysilsesquioxanes offer surface passivation through silanol groups, reducing trap states and enhancing charge-carrier dynamics. Their hydrophobic properties act as a moisture barrier, shielding the perovskite from degradation. Polysilsesquioxanes exhibit high thermal stability, ensuring consistent device performance, and are easily integrated into fabrication processes. Silsesquioxanes have the general formula of $[RSiO_{3/2}]_n$, in which R represents a H, alkyl, aryl, alkenyl or alkoxyl group. Silsesquioxanes are colorless solid compounds that contain tetrahedral Si vertices and polymeric structures made of Si—O—Si linkages. These are available in a molecular structure with 6, 7, and 8 Si vertices (Scheme 3). The cages are labeled T_6, T_7, and T_8. Three oxo groups connect each Si center to three neighboring Si centers, and the fourth group on Si is typically an alkyl,

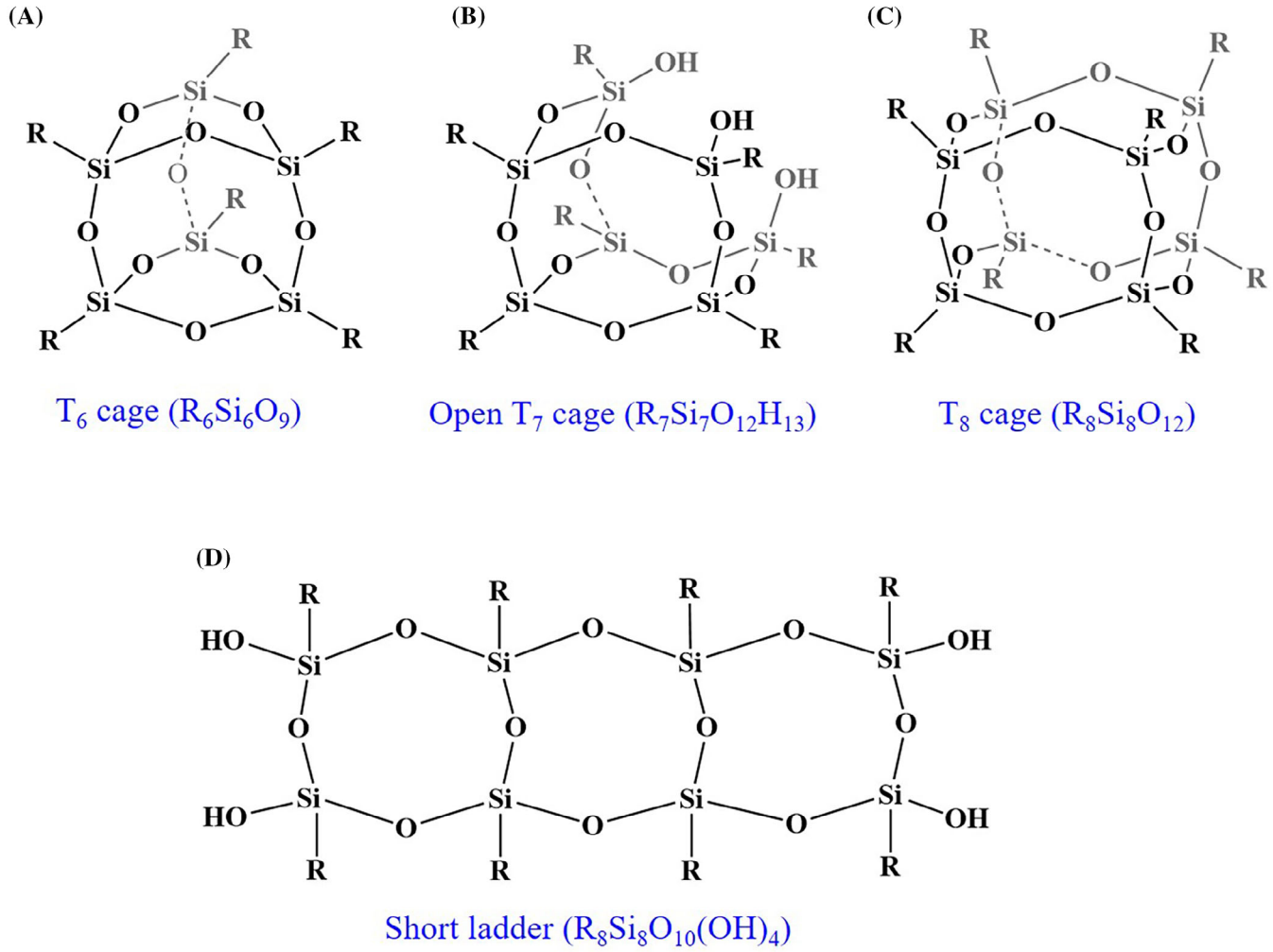

SCHEME 3 Schematic representation of various silsesquioxanes: (A) T_6 cage, (B) open T_7 cage, (C) T_8 cage, and (D) short ladder.

halide, hydride, and alkoxide. Typically, organotrichlorosilanes are hydrolyzed to produce silsesquioxanes as follows[165]:

$$8\,RSiCl_{3(l)} + 12\,H_2O_{(l)} = 8\,RSi(OH)_3 + 24\,HCl_{(aq)}$$

$$8\,RSi(OH)_3 = \left[RSiO_{3/2}\right]_8 + 12\,H_2O$$

Polysilsesquioxanes are used in various applications such as biomedical materials, coatings, and adhesives. Polysilsesquioxanes show great potential in drug delivery and tissue engineering due to their capacity to interact with biological systems under regulated circumstances. The type of capping ligand used affects the size, shape, stability, and optoelectronic properties of the resulting HP NCs. Polyhedral oligomeric silsesquioxane with an amino-group (NH_2-POSS) is an organosilicon compound with a branched structure that can provide steric hindrance and prevent HP NCs aggregation and degradation.[114]

Kataoka et al. reported on the synthesis of layered organic–inorganic HPs using metal halides and silsesquioxane as interlayers (Figure 7).[166] Propylammonium-functionalized silsesquioxane and various metal halide salts ($MnCl_2$, $CuCl_2$, $PdCl_2$, and $PbCl_2$) were used to self-assemble layered HP structures with high crystallinity. Micropores between the perovskite layers are created by the stiff silsesquioxane structure and may be filled with various molecules to modify the interlayer dielectric constants. This suggests that the resulting material could have tuneable electronic properties, which may be useful in electronic or optoelectronic applications.

3.7 | Silicone resin

Silicone resin is a critical component in stabilizing HP materials, especially in optoelectronic devices.[167] Its significance lies in its ability to create a protective

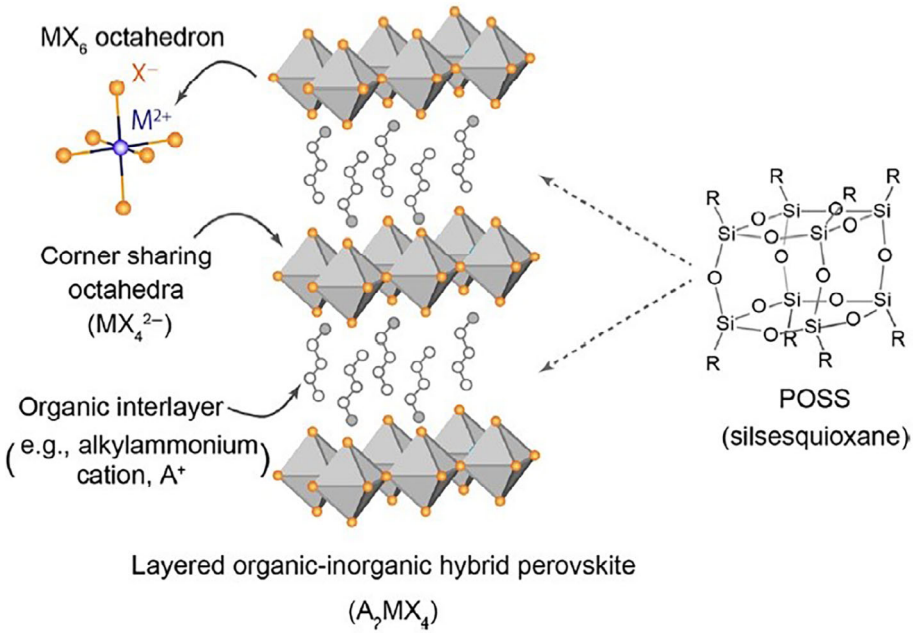

FIGURE 7 Structural representation of layered organic–inorganic HP and silsesquioxane (POSS). Reprinted with permission from.[166] Copyright 2015, American Chemical Society.

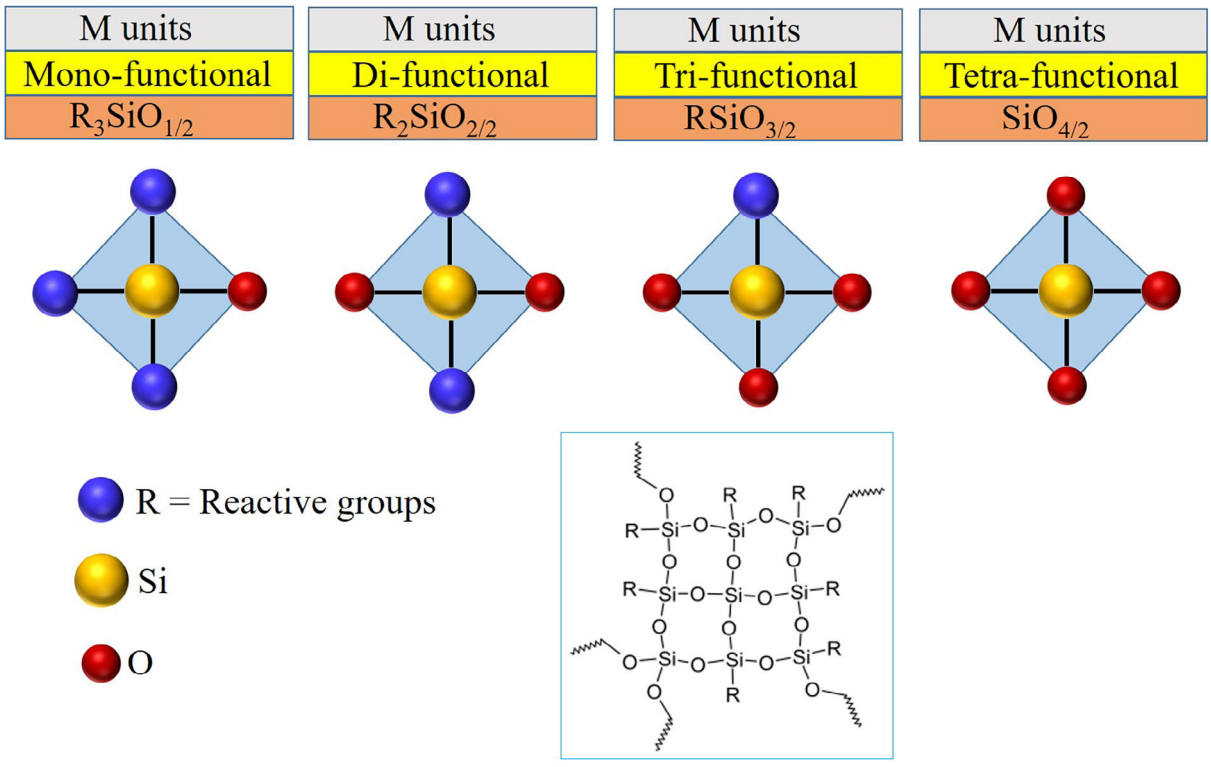

SCHEME 4 Schematic representation of various silicone resins. Inset: A typical silicone resin structure with R = CH_3, H or OH.

encapsulation barrier that shields the perovskite layer from environmental factors like moisture, oxygen, and contaminants, thus preventing degradation. Silicone resin also offers chemical, thermal stability, flexibility, and adhesion to various substrates, and optical transparency when needed. Its customizable properties allow tailoring to specific device requirements, optimizing performance and long-term stability. Silicone resins are

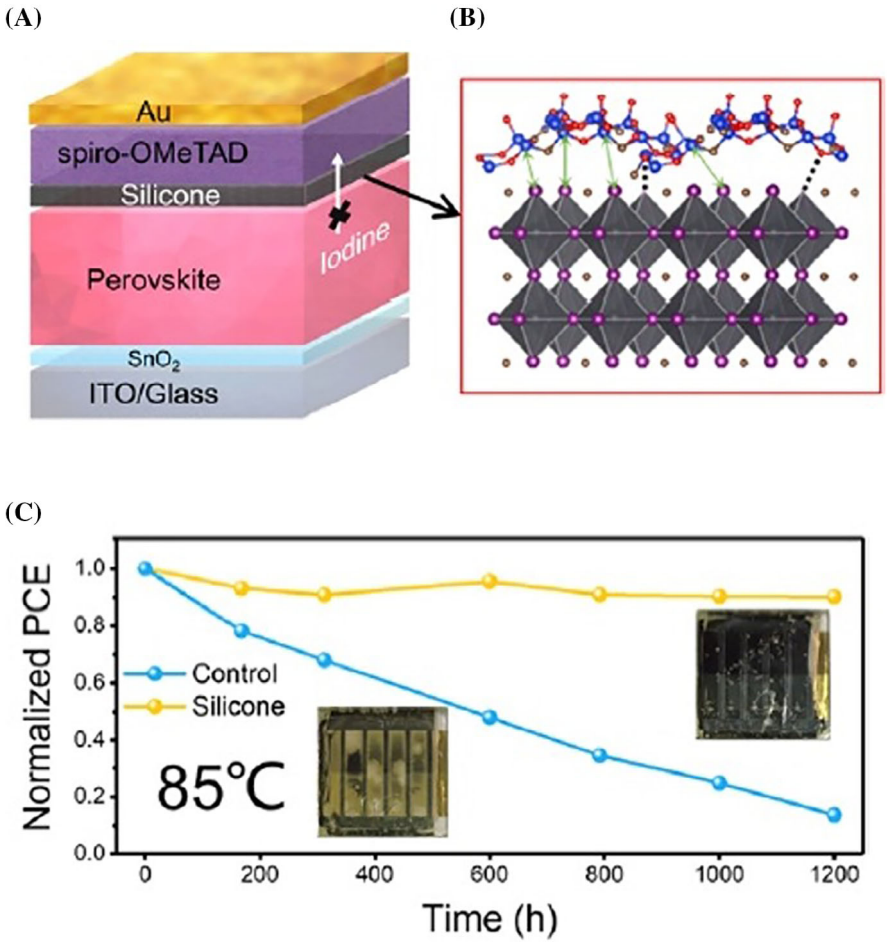

FIGURE 8 (A) PSC configuration using silicone resin, (B) Si–I and Pb–O bonds with HP, and (C) PCE trend with a silicone resin layer against time at 85°C. Reprinted with permission.[167] Copyright 2021, American Chemical Society.

utilized in various products, including electronics, coatings, adhesives, and sealants. Silicone resin is a type of synthetic polymer with the general formula $R_nSiX_mO_y$, where R represents a methyl or phenyl group, and X represents hydrogen (H), a hydroxyl group (OH), chlorine (Cl) or an alkoxy group (OR) (Scheme 4). Silicone resin comprises a silicone backbone and organic groups with alternating silicon and oxygen atoms known as siloxane bonds (Si—O—Si). Siloxane monomeric units are classified into four groups based on the number of substitutions of R on Si: "M," "D," "T," and "Q," which represent Me_3SiO, Me_2SiO_2, $MeSiO_3$, and SiO_4, respectively. The organic groups provide silicone resin with distinct properties, which include thermal stability, water resistance, and electrical insulation.

Silicone resin is an excellent material for the stabilization of HP NCs due to its hydrophobic properties. These NCs are highly ionic and the surfaces of these NCs are covered with dynamic ligands that are critical to the stability and optical properties of the NCs.

The hydrophobicity of the surrounding environment can significantly affect the surface ligands of the NCs, leading to changes in their stability, morphology, and luminescence properties. Silicone resins have tuneable hydrophobic properties that can be adjusted by varying the degree of cross-linking, the type and number of functional groups, and the curing conditions. This flexibility allows for the optimization of the hydrophobicity of the silicone resin to match the specific needs of the HP NCs. Wang et al. synthesized $MAPbBr_3$-silicone resin composites using two different silicone resins, that is, silicone sealant Dow corning (SSDC) and phenyl methyl silicone resin (PMSR).[168] The composite films exhibited an exceptional resistance to heat, water, and UV radiation, and have a maximum photoluminescence quantum yield (PLQY) of 62%. The long-term stability of hybrid PSCs has been a prevalent issue due to ion diffusion that can cause the degradation of the perovskite layer. To address this, Lin et al. developed a silicone resin layer that is both thermally stable and hydrophobic to act as an interface layer between the HP and the HTL (Figure 8).[167] Experimentally and theoretically, it has been demonstrated that the Si—O—Si unit generates Si—I

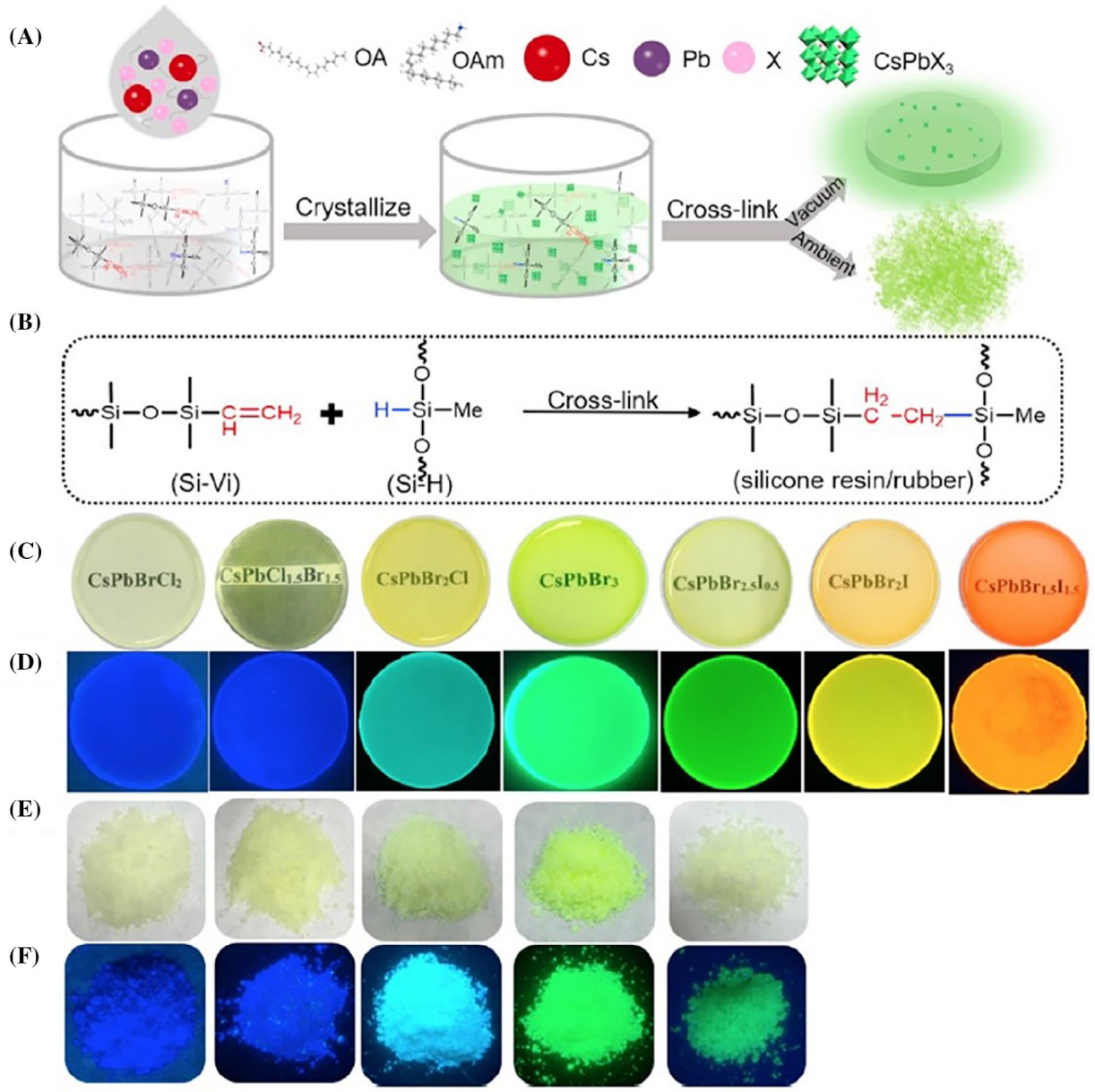

FIGURE 9 In situ synthesis of $CsPbX_3$ NCs via synergistic stabilization in polysiloxanes. (A) Diagrammatic representation of the in situ synthesis of silicone oils-mediated $CsPbX_3$ NCs and the subsequent formation of a cross-linked structure, (B) Reaction scheme for the synthesis of silicone resin from silicone oils, (C) Images of $CsPbX_3$-silicon resin monoliths made with various halide ratios under ambient light (D) and UV light, (E) Images of composite powders with various halide ratios under an ambient environment, under room lighting, (F) and UV light. Reprinted with permission.[169] Copyright 2020, Elsevier B.V.

and Pb—O bonds with HP, which chemically and physically stop iodine from diffusing and releasing on its own and increase the PSCs' long-term stability.

The formation of Si—I bonds plays a vital role in immobilizing I^- ions, while the uniform network structure of the silicone resin effectively suppresses iodine diffusion, thereby contributing to the enhancement of thermal and illumination stability in the perovskite material.[167] Despite these advancements, the migration of halides within the perovskite layer persists, indicating that surface treatment alone is insufficient to eliminate this issue. Consequently, it appears that enhanced stability results from the controlled release of organic cation, MA^+ rather than solely relying on surface treatments to address halide migration. This implies that while surface treatments may mitigate certain degradation mechanisms, controlling the release of organic compounds may play a more significant role in enhancing the long-term stability of perovskite materials.

Moreover, spiro-OMeTAD, which is frequently utilized as the HTL in PSCs, does not thermally crystallize in the presence of silicone resin layer. The efficiency and stability of the PSCs are further improved by interfacial energy-level engineering for hole extraction. The addition of a silicone resin coating increases the PCE of a perovskite solar cell to 21.11%. The devices were thermally aged at 85°C, and were found to retain more than 90.1% of its original PCE after 1200 h; the devices were also found to retain 99.6% of its original PCE after 2000 h at approximately 55 ± 5% of humidity. The silicone devices exhibited excellent photostability while retaining 83% of its initial PCE after 1037 h.

Wang et al. describe a novel approach for stabilizing $CsPbX_3$ NCs in a silicone resin matrix (Figure 9).[169] This approach involves the in situ preparation of HP NCs within the polysiloxane matrix. The silicone oils act as an antisolvent, which promotes the formation of $CsPbX_3$ NCs by initializing the precipitation of the perovskite precursor. This can be attributed to the lower solubility of the perovskite precursors compared to the polysiloxane matrix. On the other hand, the silicone oil precursors' cross-linking process is accelerated by the HP precursor solution, which acts as a catalyst. As a result, a stable network structure is formed within the matrix that encapsulates the NCs and improves stability. In an ambient environment, the $CsPbBr_3$-silicone resin composites prepared by Wang et al. remained stable when exposed to moisture, heat, and were able to emit PL after being exposed to air for a year and also submerged in water for 2 months. This study presents a novel method for addressing the formidable stability concerns associated with perovskite nanocrystals.

3.8 | Siloxane

Siloxane compounds have been commonly used as stabilizing agents for HP materials, particularly in PSCs and optoelectronic devices.[170–173] They serve as effective encapsulation materials, shielding perovskite layers from moisture, oxygen, and contaminants. Silicones are chemically stable, preventing reactions that could degrade perovskite materials, and exhibit high thermal stability to maintain consistent device performance. Their flexibility and adhesion properties reduce mechanical stress and support adherence to various substrates, ensuring long-lasting encapsulation. Some silicones offer optical transparency, preserving the device's optical properties, and their customizable attributes allow tailoring to specific device requirements. The fundamental building block of siloxanes is a straight or branched chain containing silicon and oxygen atoms alternately bonded to organic groups (such as methyl or phenyl groups). Examples of siloxanes include silicon (Si), oxygen (O), and, optionally, carbon (C) and hydrogen (H). Siloxane polymers have the general formula $(R_2SiO)_n$, where R corresponds to methyl or phenyl groups, and the polymer chain's repeating unit count is indicated by "n". A large variety of siloxanes with various properties and uses can be produced by changing the organic groups linked to the Si atoms. Siloxanes typically exhibit high stability, chemical resistance, and thermal resistance, and can be synthesized via the polymerization of siloxane monomers, the reaction of silanes with organic polymers, or the condensation of silanols. The properties of the resulting siloxanes can be modified by adjusting the number of organic groups, molecular weight, and cross-linking. Siloxanes are widely used as coatings, adhesives, and electrical insulators in a range of industrial applications. Additionally, siloxanes also serve as the primary building blocks in the production of silicone rubber and silicone polymers. Siloxane groups in organic compounds have recently been used to modify the surface of perovskite materials, which can ameliorate the stability of HP by passivating the surface trap-states and blocking the ingress of water and ions. Bai et al. passivated defects on both the top surface and grain boundaries (GBs) of $MAPbI_3$ perovskite solar cells using an oligomeric siloxane matrix Figure 10.[2] This was achieved by precisely regulating the hydrolysis and condensation properties of TEOS during HP crystallization. This led to an increase in open circuit voltage (V_{OC}) to 1.16 V, resulting in a champion PCE of 21.10% in p-i-n planar $MAPbI_3$ PSCs. This improved performance can be attributed to the coordination link formed between GBs and the oxygen atom of the —OCH_2CH_3 group of siloxane with the uncoordinated Pb^{2+} ions at the HP surface, which passivates the uncoordinated Pb defects. However, there are some issues associated with using siloxane derivatives to alter the top of the HP surface: (i) the hydrolysis and condensation capabilities of siloxane derivatives when exposed to water make it difficult to manage the concentration or thickness of the layer, (ii) the additional water vapor required for siloxane hydrolysis may be harmful to the perovskite films, and (iii) the alcohol by-product formed during the siloxane hydrolysis step is harmful to PSCs because of its high hydrophilicity and polarity. Organic molecules with siloxane groups can be employed to overcome the issues while employing pure siloxane derivatives for buried interface modification, which might prove to be a good alternative.

Notably, the formation of additional water vapor/toxic by-products can be avoided by inhibiting water-induced hydrolysis and suppressing the condensation properties of silicone derivatives, which helps to minimize the defects in the perovskite layer. In order to

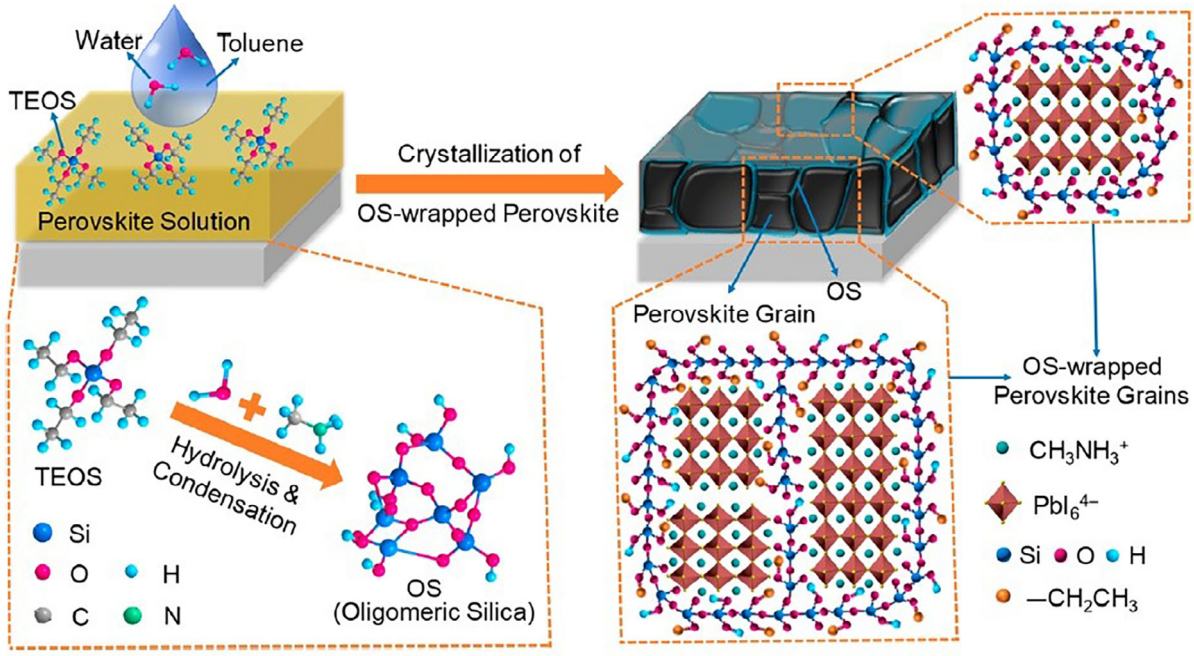

FIGURE 10 Schematic showing the in situ wrapping of perovskite by the oligomeric silica (OS) matrix and the hypothesized OS-wrapped perovskite nanostructures. Reprinted with permission.[2] Copyright 2019, American Chemical Society.

produce diethylphosphatoethylsilicic acid (PSiOH), which is a product of hydrolysis, Duan et al.[170] synthesized a novel siloxane derivative called diethylphosphatoethyltriethoxysilane (POSi). The Si—OH group in PSiOH interacts with adsorbed —OH on the TiO_2 surface to modify the energy band structure, improving the electrical characteristics of the TiO_2 layer, while the oxygen atoms in the P═O bonds in PSiOH help to eliminate unsaturated bonds in Pb^{2+} ions and any defects on the perovskite bottom surface. After PSiOH treatment, $FA_{0.83}Cs_{0.17}PbI_3$ PSCs were able to achieve a champion PCE of 24.20%. After 2200 h of storage in ambient air, the unencapsulated devices were found to have retained 83.73% of their initial efficiencies, while the encapsulated device was found to have retained 80.54% of its initial PCE after 500 h under continuous illumination.

Siloxane can also be used to improve the external quantum efficiency (EQE) of HP LEDs. The spin-coating process used in perovskite film fabrication can sometimes dissolve the underlying organic HTL, resulting in the transfer of excited perovskite emitters to indium tin oxide (ITO) because of the partial contact with the ITO anode layer. This can significantly affect the performance of LEDs; however, this issue can be solved by using siloxanes. Matsushima et al. added TEOS into poly(N-vinylcarbazole) (PVCz) and observed that TEOS was subsequently hydrolyzed, forming a giant siloxane network.[172] This prevented the PVCz films from dissolving in polar solvents and reduced excited-state quenching. Notably, the use of siloxane-blended PVCz HTLs resulted in perovskite LEDs that exhibited an EQE of 15.4 ± 0.3%, which is a 50% increase in EQE in comparison to devices without siloxane (10.4 ± 0.3%). HPs, such as $MAPbI_3$ and $FAPbI_3$, can interact with water molecules to form less stable hydrated species such as $PbI_2{\cdot}3H_2O$ or $PbI_2{\cdot}4H_2O$. Solar cells can be negatively affected or even fail completely in the presence of these hydrated species. A promising approach to improving the stability of PSCs is to passivate the GBs between perovskite grains.

These differences can create energy levels within the bandgap of the perovskite material, which can trap charge carriers and reduce the efficiency of the solar cell. When a photon is absorbed by the perovskite material, it creates an electron–hole pair that can move through the material and contribute to the current generated by the solar cell. However, if the electron and hole recombine at a GB, their energy is released as heat instead. This is called non-radiative recombination, which accelerates the degradation of the PSCs and significantly affects performance. However, passivating the GBs with materials such as polydimethylsiloxane (PDMS) can help to reduce the number of recombination centers and improve the efficiency of the PSCs. It has been demonstrated that PDMS can passivate both the perovskite and surrounding GBs when added during the spin-coating of PSCs. This passivation effect gives rise to multiple advantages associated with the stability and efficiency of the solar cell.

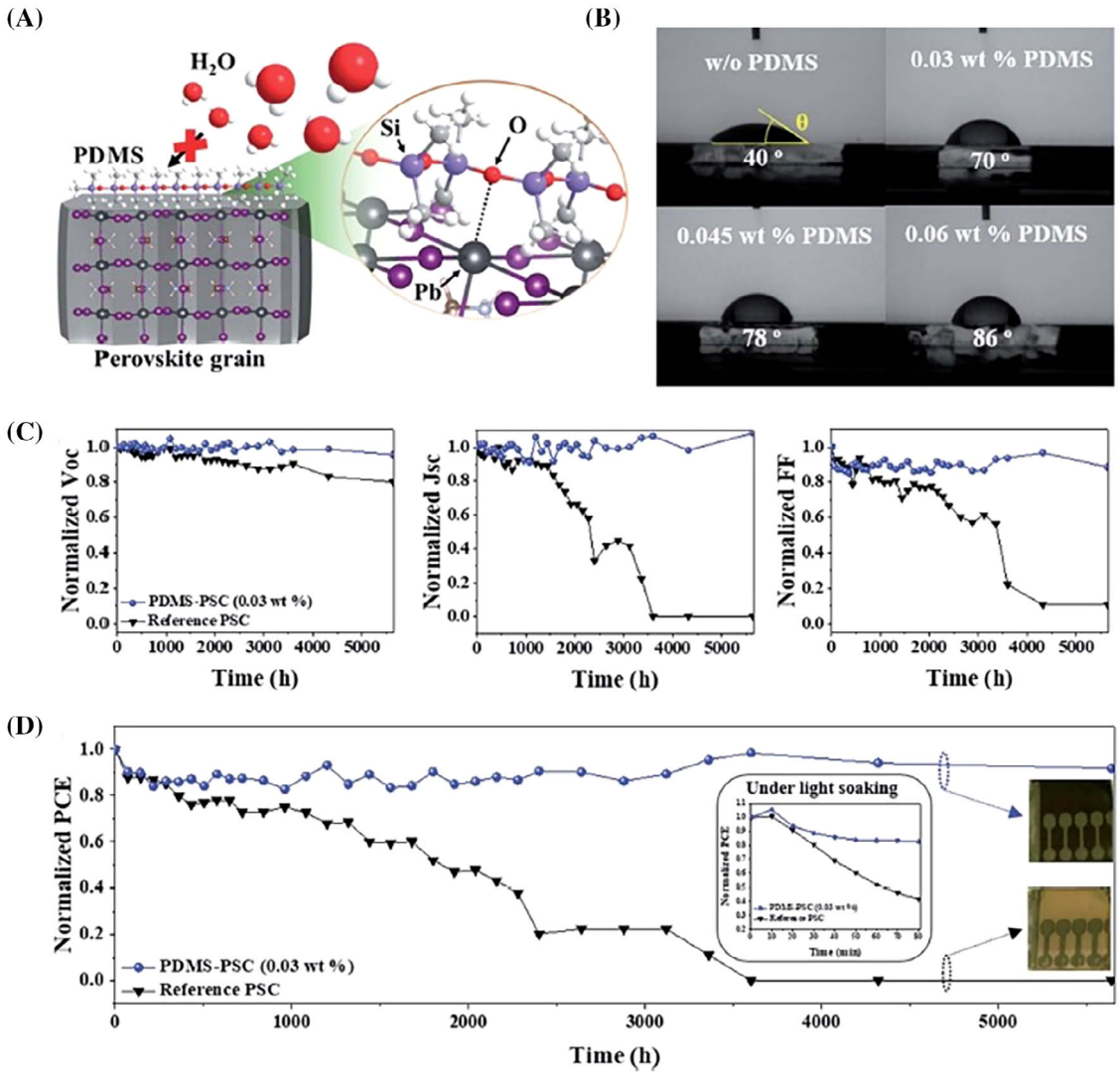

FIGURE 11 (A) Schematic of the PDMS-HP and inhibition of water, (B) contact angle measurements of water droplets on HP films with different wt% of PDMS, (C) V_{OC}, J_{SC}, and FF, and (D) PCE measurements. Inset: PCEs of the reference (without PDMS) and PDMS (0.03 wt%)-PSCs (1 Sun illumination). Reprinted with permission.[174] Copyright 2019, Royal Society of Chemistry.

First, PDMS can promote the formation of lead oxide (PbO) bonds between the perovskite material and the underlying substrate, which can prevent a water-perovskite reaction, which occurs when water molecules come into contact with the HP, leading to the decomposition of the perovskite and suboptimal device performance.[174] Second, PDMS can reduce the density of Pb defects in HP, resulting in reduced trap-assisted recombination reactions. Pb defects act as deep-level traps for charge carriers, leading to recombination and a reduction in PCE of the solar cells. By passivating these defects with PDMS, the number of recombination centers in the perovskite material can be reduced, subsequently improving the efficiency of the solar cell. The PSC with device configuration FTO/TiO_2/Perovskite ($FA_xMA_{1-x}PbI_3$)/Spiro/Au demonstrated remarkable power conversion efficiency (PCE) of over 25%, as reported by recent studies.[175] However, persistent challenges revolve around their long-term stability, especially in humid environments where water-induced decomposition poses a threat to their effectiveness. Jeong et al. highlighted this issue, noting a PSC with a PCE of 25.6% and operational stability limited to 450 h.[175] Achieving enhanced operational stability is crucial for the successful commercialization of PSCs. Notably, Kim et al. discovered that the PDMS-passivated PSCs retained over 90% of their initial PCE of 15% even after enduring 5000 h in a laboratory environment at 70% relative humidity (RH), as depicted in Figure 11.[174] PDMS passivation of perovskite grains and GBs facilitates the formation of PbO bonds, thereby preventing water-perovskite reactions and reducing defect density. This treatment significantly enhances

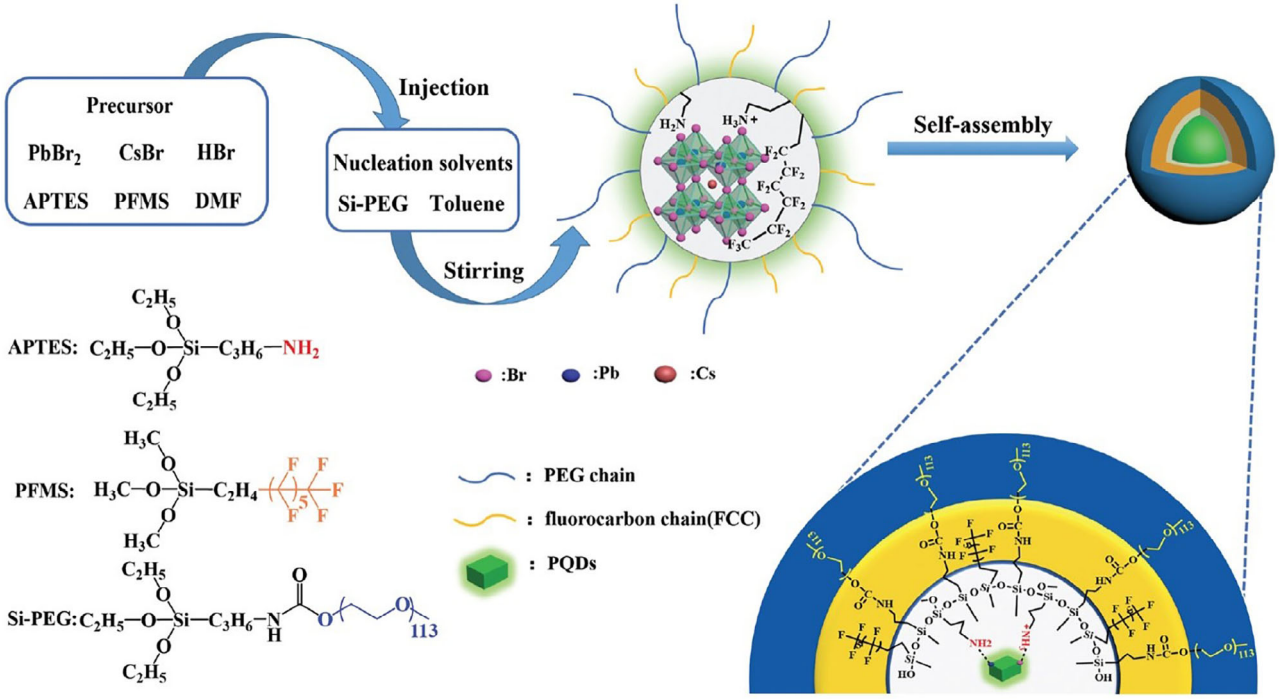

SCHEME 5 Schematic illustration of the LARP synthesis of water-dispersive silica-encapsulated perovskite QDs (PQDs@SiO_2-d) and their possible self-assembled structure in water. Reprinted with permission.[177] Copyright 2021, Royal Society of Chemistry.

photovoltaic performance compared with untreated PSCs, marking a substantial advancement toward the commercial viability of perovskite optoelectronic devices.

The moisture barrier properties of PDMS polymer films can be significantly improved using various methods, such as the addition of fillers or coatings. One approach suggests filling the free volume of PDMS with a barrier material, such as aluminum oxide (AlO_x). Choi et al. deposited AlO_x inside PDMS by thermal atomic layer deposition; the resulting film exhibited a water vapor transmission rate (WVTR) of 5.1×10^{-3} g m^{-2} d^{-1} at 65% RH and 45°C.[176] The PCE of the fabricated organic–inorganic PSC with PDMS/AlO_x was found to decrease by approximately 5% after 300 h (45°C and 65% RH).

Triple siloxane coupling agents can also be used in the encapsulation of perovskite QDs. Triple siloxane coupling agents are organic compounds that contain three different siloxane molecules with different chemical properties; this is typically made up of a hydrophobic silane, a hydrophilic silane, and a bridging silane. The three siloxane molecules are covalently bonded via condensation to produce a single molecule. The hydrophobic silane component typically comprises non-polar and hydrophobic long alkyl chains, which provide a protective layer around the encapsulated material that prevents degradation and preserves its optical properties. Generally, polar functional groups like amine, carboxylic acid, or hydroxyl groups are present in the hydrophilic silane component. These groups can potentially interact with water molecules, increasing the stability and dispersibility of the material in water-based systems. The hydrophobic and hydrophilic silanes are linked by the bridging silane in the triple siloxane coupling agent, maintaining stable contact between the encapsulated material and the surrounding water. The bridging silane is able to connect the hydrophilic silane to another component due to its shorter chain and lower polarity.

Shi et al. condensed superhydrophobic perfluorooctyltrimethoxysilane (PFMS), hydrophilic APTES, and hydrophilic polyethylene glycol (Si-PEG) as triple siloxane coupling agents for the encapsulation of perovskite QDs (Scheme 5).[177] The —NH_2 group of APTES was converted into protonated APTES ($APTES^+$) in the presence of acid and interacted with the surface of the perovskite QDs. The fluorocarbon chain in PFMS protects the perovskite QDs from the harsh experimental conditions. Balancing stability and dispersibility in polar solvents is particularly difficult. Herein, the ester group of Si-PEG was found to have improved the dispersibility of the perovskite QDs in polar solvents. The encapsulated perovskite QD@siloxane maintained a PLQY of 93% when stored under harsh conditions (acidic, alkaline, and ionic conditions).

3.9 | Polysilazanes

Polysilazanes are essential for stabilizing HP materials, offering key benefits for PSCs and optoelectronic devices. They provide surface passivation by chemically binding to surface defects, thus enhancing charge-carrier dynamics and overall device stability. Their hydrophobic properties shield against moisture, which is critical for long-term perovskite material stability. High thermal stability ensures consistent performance in varying temperatures. Polysilazanes can be seamlessly integrated into device fabrication processes and offer tuneable properties, allowing customization for specific device requirements. Polysilazanes are a ceramic precursor material that contain an inorganic–organic hybrid polymer chain backbone consisting of alternating silicon and nitrogen atoms, with organic functional groups bonded to the Si atoms (Scheme 6). The fundamental repeating unit in polysilazane is (—Si—NH—)$_n$, where n corresponds to the total number of repeating units. A 3D network structure can be created by establishing a coordinate link between the Si atom's unoccupied d-orbital in a neighboring unit and the lone pair of electrons on the nitrogen atom in the repeating unit. Polysilazanes can have a variety of properties and uses depending on the functional groups bonded to the Si atoms. The structure of polysilazane can be altered by varying the types and ratios of organic functional groups added as well as the reaction conditions during synthesis; which also enables the properties of the material to be tailored to certain applications. In the presence of a catalyst, polysilazanes can be synthesized via the polycondensation of organosilicon precursors like hexamethyldisilazane or tetramethyldisilazane. There are many different types of polysilazanes:

a. Poly(dimethylsilazane) (PDMSZ): This linear polysilazane comprises repeating units of dimethylsilazane (—Si—NH—Si(CH$_3$)$_2$—) monomers and is easily synthesized and soluble in organic solvents; it is also widely used as a starting material for the growth of silicon carbide ceramics.
b. Poly(methylsilsesquiazane) (PMSZ): PMSZ is a hybrid organic–inorganic polymer that contains both silicon and carbon atoms in its backbone. PMSZ has a highly cross-linked structure and is amorphous in nature. The basic repeating unit comprises a silsesquiazane (Si—N) cage, which contains three silicon atoms and three nitrogen atoms. This cage is capped with methyl groups (—CH$_3$) on each silicon atom, resulting in a polymeric chain with the general formula [Si(NR$_2$)$_3$]CH$_3$, where R typically represents a hydrogen atom or an alkyl group.
c. Poly(hydridomethylsilazane) (PHMS): PHMS is another hybrid organic–inorganic polymer that contains silicon, carbon, and nitrogen atoms in its backbone. It is a cross-linked polymer that is formed from a precursor molecule, hexamethyldisilazane, reacting with a reducing agent, such as lithium aluminum hydride. The basic repeating unit of PHMS comprises a silazane (Si—N—Si) cage with a hydridomethyl (—CH$_2$—SiH$_2$—) group attached to one of the silicon atoms. The general formula of the polymer is [HSi(NR$_2$)$_2$]CH$_2$, where R typically represents a hydrogen atom or an alkyl group.
d. Poly(silylcarbodiimide): The basic repeating unit of poly(silylcarbodiimide) consists of a silylcarbodiimide (Si—N═C—N—Si) cage with a carbon-containing side group attached to one of the nitrogen atoms. The general formula of the polymer is [Si(NR$_2$)$_2$]C═NR, where R typically represents an alkyl or aryl group.
e. Poly(silazane) (PSZ): The basic repeating unit of PSZ consists of a silazane (Si—N—Si) cage, which is similar to the silsesquiazane cage found in PMSZ without any additional carbon atoms. The general formula of the polymer is [Si(NR$_2$)$_2$]$_n$, where R typically represents a hydrogen atom or an alkyl group.

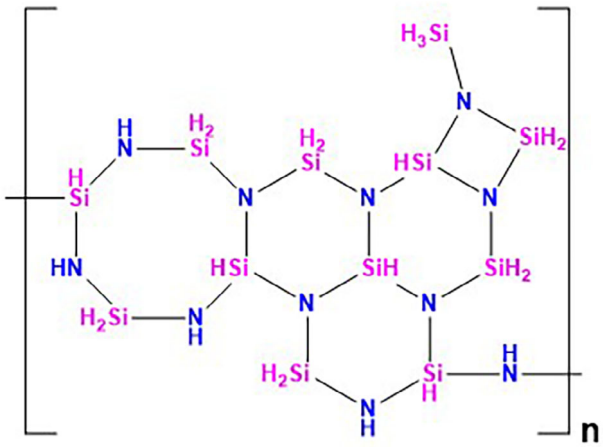

SCHEME 6 Structural representation of polysilazane.

HP NCs are prone to degradation when exposed to air and moisture, which limits their use. Yoon et al. synthesized the HP NCs by encapsulating the $CsPbBr_3$ NC solution with a Si—N/Si—O-based polysilazane (PSZ) matrix via the electrospray synthesis.[178] Furthermore, the surface passivation of Pb^{2+} defect sites, coupled with the addition of a SZ oligomer, not only enhances the photoluminescence quantum yield but also significantly improves the stability of the perovskite NCs, even after photodegradation. The $CsPbBr_3$-PSZ film exhibited a luminous efficacy (LE) of ~86 lm W^{-1} and a color-by-blue conversion efficiency of ~60%. This work demonstrates the simplicity and effectiveness of e-spray

deposition in creating stable and efficient perovskite NC films, offering a pathway toward the widespread adoption of perovskite-based optoelectronic devices.

4 | VARIOUS SYNTHETIC METHODS FOR PRODUCING PEROVSKITE@SILICON COMPOUNDS

4.1 | In situ synthesis

The in situ synthesis of perovskite@silicon compounds involves the simultaneous formation of perovskite and silicon components in a single step. This method typically involves the reaction of a silicon precursor, such as silicon alkoxide or silicon hydride, with a perovskite precursor, such as lead halides and organic halides, in the presence of a solvent, surfactant, or template molecule. This reaction can be carried out under a variety of conditions, including solvothermal, hydrothermal, or ambient conditions. The resulting perovskite@silicon compounds have special characteristics that make them appropriate for a variety of optoelectronic and energy conversion applications. For example, perovskite@silicon compounds can be used as photocatalysts in the conversion of solar energy into chemical fuels such as hydrogen gas. The introduction of silicon into the perovskite structure can also improve the stability and durability of HPs. The in situ synthesis of perovskite@silicon compounds is difficult due to the different reaction conditions required for the perovskite and silicon components. However, this method can potentially simplify the synthesis process and produce materials with enhanced properties compared to those synthesized using separate components.

Zou et al. suggested a post-treatment functional organotrichlorosilane (with the general formula R-$SiCl_3$, where R = —3,3,3-trifluoropropyl) for the fabrication of HP films for deep blue perovskite LEDs (PeLEDs).[179] It was shown that a part of the organotrichlorosilane molecules on the sky-blue HP film self-hydrolyzed into silanol molecules and produced hydrogen chloride as a by-product during the soaking process. Si-O-Si linkages are created during the condensation of —OH groups in the silanol and a cross-linked network. In addition, the hydrogen chloride diffused into the HP film and interacted with it via ion exchange, raising the chloride concentration in the perovskite lattice and changing the emission to the deep-blue region. The remaining cross-linked silane molecules interacted with the halide anions in the HP film to stop ion migration in the operating system and produce good commission internationale de l'Eclairage (CIE) stability.

Zhao et al. suggested hydrophobic molecule trichloro(octyl)silane (TC-silane) for the non-destructive surface modification of a perovskite film.[180] They were able to accommodate the synergistic effects of passivation and dipole polarization on the properties (i.e., performance and stability) of the HP film by choosing an appropriate TC-silane side chain length, which allowed them to manage the hydrolytic condensation and molecular arrangement. The fabricated TC-silane-passivated PSCs exhibited an efficiency of 20.03% and retained its 80% efficiency for more than 800 h. They showed TC-silane application for solar cells' bifunctional performance and stability improvement. Hu et al. demonstrated a facile method for synthesizing superhydrophobic (SH) SiO_2-coated $CsPbBr_3$ (SH-$CsPbBr_3$@SiO_2) nanoparticles (NPs) film.[181] The hydrolysis of TEOS realized the SiO_2 coating in ammonia to form $CsPbBr_3$@SiO_2 NPs. Hexamethyldisilazane was used to modify the surface of $CsPbBr_3$@SiO_2 NPs, enhancing the SH activity of the NP films. Additionally, Hu et al. synthesized $CsPbBr_3$@SiO_2 films via dip coating, and these films also showed SH activity and long-term stability.

4.1.1 | In situ synthesis of powder

Hu et al. synthesized perovskite NCs ($Cs_2AgBiBr_6$) inside three mesoporous silica templates (Figure 12)[182] and showed that the structure of the silica templates and the pore size influence the morphology and size of the perovskite NCs. They were able to control the formation of $Cs_2AgBiBr_6$ NPs using the mesoporous KIT-6, SBA-15, and MCM-41 silica templates. KIT-6 possesses a cubic 3D structure, while SBA-15 and MCM-41 have a two-dimensional (2D) hexagonal geometry. When $Cs_2AgBiBr_6$ is loaded onto these templates, it showed different configurations in different mesoporous silicon. One-dimensional (1D)-$Cs_2AgBiBr_6$ nanowires are positioned along in MCM-41 channels; in KIT-6, square (0D) NPs are neatly arranged within the channel; in SBA-15, 1D rod-shaped particles and 0D spherical particles extend across the channel. The differences in the morphology of $Cs_2AgBiBr_6$ NCs are attributed to the different pores present in mesoporous silicon templates. KIT-6 has a 3D tetragonal channel with a pore size of 6.12 nm. Although SBA-15 has a 1D channel, it contains smaller 0D NCs and longer 1D NCs due to the large pore size (5.81 nm). The pore structure of MCM-41 is similar to that of SBA-15, but the smaller pore size (3.07 nm) makes the formation of 1D NCs easier. The observation of different configurations of $Cs_2AgBiBr_6$ NCs within various mesoporous silicon templates highlights the importance

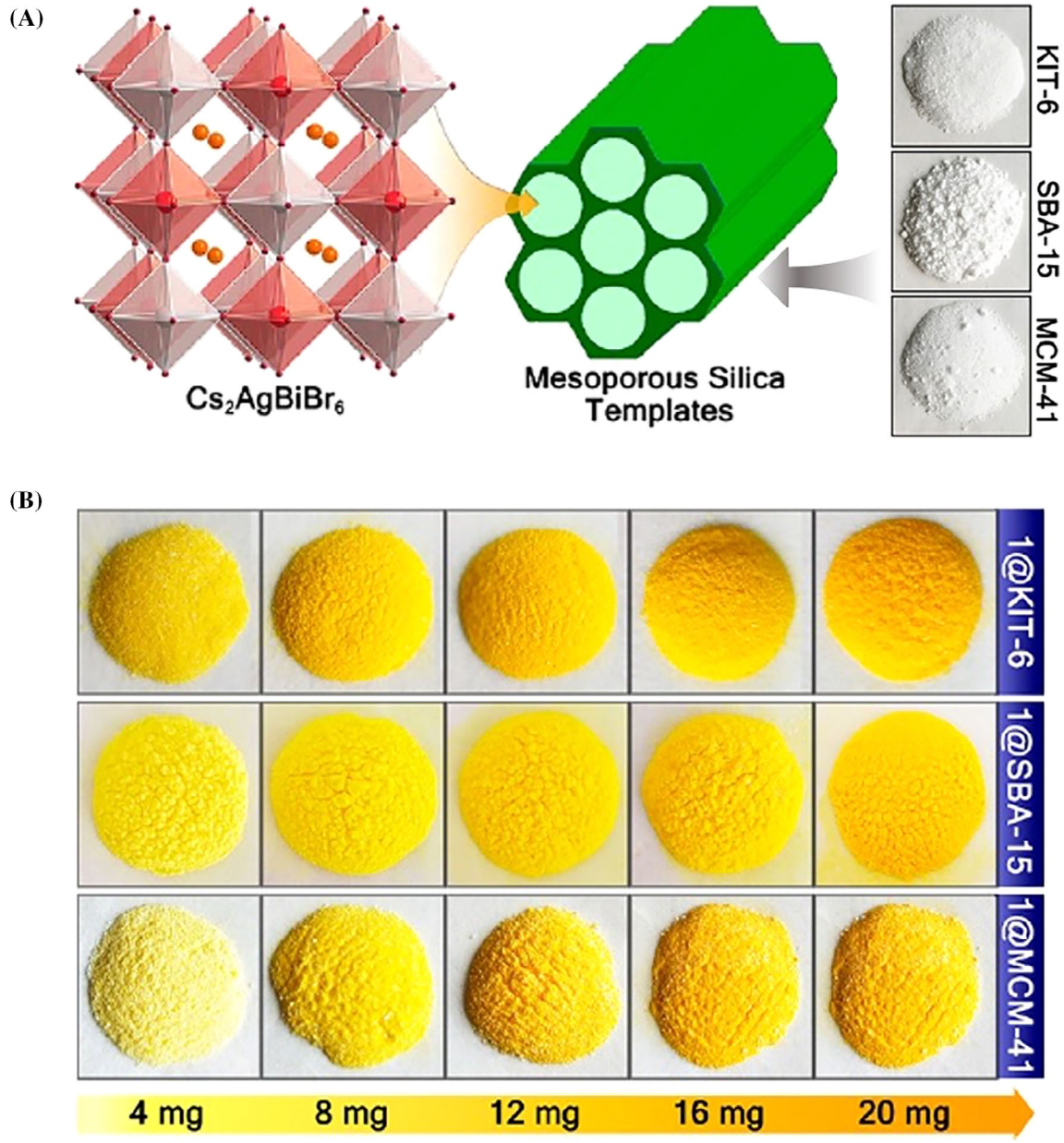

FIGURE 12 (A) Schematic diagram of a $Cs_2AgBiBr_6$ crystal structure, white powders of mesoporous silica (KIT-6, SBA-15, and MCM-41 templates), and $Cs_2AgBiBr_6$@mesoporous silica. (B) Images of $Cs_2AgBiBr_6$@KIT-6, $Cs_2AgBiBr_6$@SBA-15, and $Cs_2AgBiBr_6$@MCM-41. Reprinted with permission.[182] Copyright 2019, American Chemical Society.

of pore architecture in dictating the final morphology of the NCs. In addition, elucidating the relationship between pore size and the resulting NC morphology provides valuable insights for designing future nanomaterials with tailored properties.

4.1.2 | In situ crystallization synthesis

Yuan et al. reported on a strategy to introduce $CsPbBr_3$ QDs in the middle of TeO_2-based glass matrix containing suitable Cs/Pb/Br precursor sources in order to improve the stability of $CsPbBr_3$ QDs (Scheme 7).[183] The core technologies they develop are the design of correct glass configuration and the in situ nanocrystallization of $CsPbBr_3$ QDs from glass matrix. The $CsPbBr_3$ QD-embedded glass exhibited a high PLQY of approximately 70%, excellent photo/thermal stability, and excellent water resistance.

Rossi et al. demonstrated the silica overcoating of $CsPbBr_3$ NCs via the anhydride-induced transformation of Cs_4PbBr_6 NCs to obtain $CsPbBr_3$@SiO_2 core-shell NCs.[149] This core-shell structure offers several advantages, including enhanced stability, improved optical

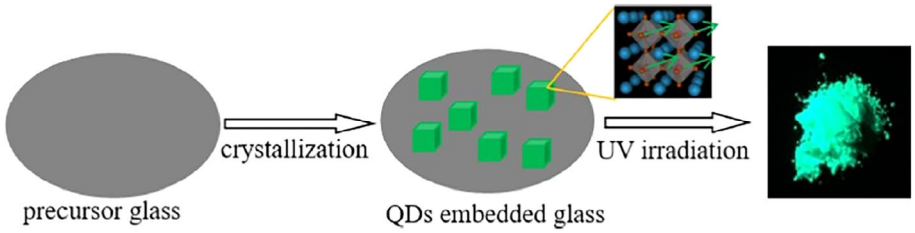

SCHEME 7 Schematic representation of the glass crystallization strategy for synthesizing $CsPbBr_3$ QDs-embedded glass. Reprinted with permission.[183] Copyright 2018, American Chemical Society.

properties, and compatibility with various applications. These Cs_4PbBr_6 NCs were converted into orthorhombic $CsPbBr_3$ by the anhydride-amine condensation process, highlighting a unique approach to synthesizing $CsPbBr_3$ NCs with desired crystal phases. This control over crystal phase is crucial for tuning the optical and electronic properties of the NCs. The reaction between maleic anhydride and Cs_4PbBr_6 NCs in toluene solution yielded maleamic acid and $CsPbBr_3$ NCs. After this, silica was coated all over the $CsPbBr_3$ NCs via alkoxysilanes hydrolysis to obtain $CsPbBr_3@SiO_2$ core-shell NCs.

4.2 | Ex situ synthesis

The ex situ synthesis of perovskite@silicon compounds involves the separate synthesis of perovskite and silicon components which are subsequently mixed to form a composite material. This typically involves the synthesis of perovskite and silicon components using established methods such as solution-based or vacuum-based techniques. The perovskite and silicon components are then combined using physical methods, for example, spin-coating, drop-casting, or spray-coating. The resulting perovskite@silicon compounds have unique optoelectronic properties that make them suitable for a range of optoelectronic and energy conversion applications. For example, perovskite@silicon compounds can be used to improve the efficiency and stability of PSCs. The incorporation of silicon into the perovskite structure can also improve the mechanical properties and durability of the material. The ex situ synthesis of perovskite@silicon compounds is relatively straightforward and compatible with existing fabrication techniques; however, this method can also result in a lower degree of integration between the perovskite and silicon components, leading to decreased device performance compared to in situ synthesis methods.

Zhenfu et al. reported on the synthesis of HP QDs encapsulated in magnesium silicate hollow spheres (MSHSs).[184] The resulting $MAPbX_3$ QDs-MSHSs nanocomposites exhibited high luminescence and stability. Zhenfu et al. posited a simple strategy that incorporates $MAPbX_3$ QDs into MSHSs via a modified LARP method under ambient conditions. The resulting nanocomposite exhibited high thermal stability and photostability, with tuneable emission peaks and high PLQY. Pan et al. developed an ex situ templated synthesis approach to attach the HP NCs on A-SiO_2 NPs (Figure 13).[185] In the two-step synthesis method, they first prepared functionalized silica NPs from a mixed APTES-TMODS precursor, which was subsequently used to induce the nucleation and growth of monodispersed $CsPbX_3$ NCs composites with SiO_2 NPs. The resulting $CsPbX_3$@octadecyl-/propylamine-capped silica (CA-SiO_2) nanocomposites exhibited significantly improved water stability, tuneable emission wavelength, and relatively high quantum yield compared to the free perovskite NCs. By manipulating the halide composition, the emission peak of the composite was tuned between 400 and 650 nm, whereas PLQY remained high at 76%.

Li et al. suggested the use of carbon dots (CDs) as a surface-passivating layer to modify the optoelectronic properties of HP.[186] To ensure superhydrophobic tunneling contact on top of the passivation layer of the CDs, cross-linked trichloro(3,3,3-trifluoropropyl) silane ($C_3H_4Cl_3F_3Si$) molecules were self-assembled; a maximum PCE of 21.12% with a high fill factor of 82.86% was subsequently observed in the perovskite devices. The trifluoromethyl groups (–CF_3) within $C_3H_4Cl_3F_3Si$ were found to increase the hydrophobicity of the CD self-assembled (CD-SAM) layers, protecting the bottom perovskite from water and oxygen damage. Wang et al. showed that hydrophobic trichloro (3,3,3-tri fluoro propyl) silane can act as a water-resistant layer and protect the HP film.[187] Fluoro-silane was also used as a tunneling layer to synthesize water-resistant perovskite solar cell devices. The fluoro groups were found to significantly increase the hydrophobicity of the fluoro-silane. Furthermore, it was also determined that fluoro-silane can be crosslinked when exposed to a trace amount of moisture. Wang et al. deposited fluoro-silane, which can initiate the hydroxylation of silanes into silanols, on top of the HP films, which contain a small amount of moisture.

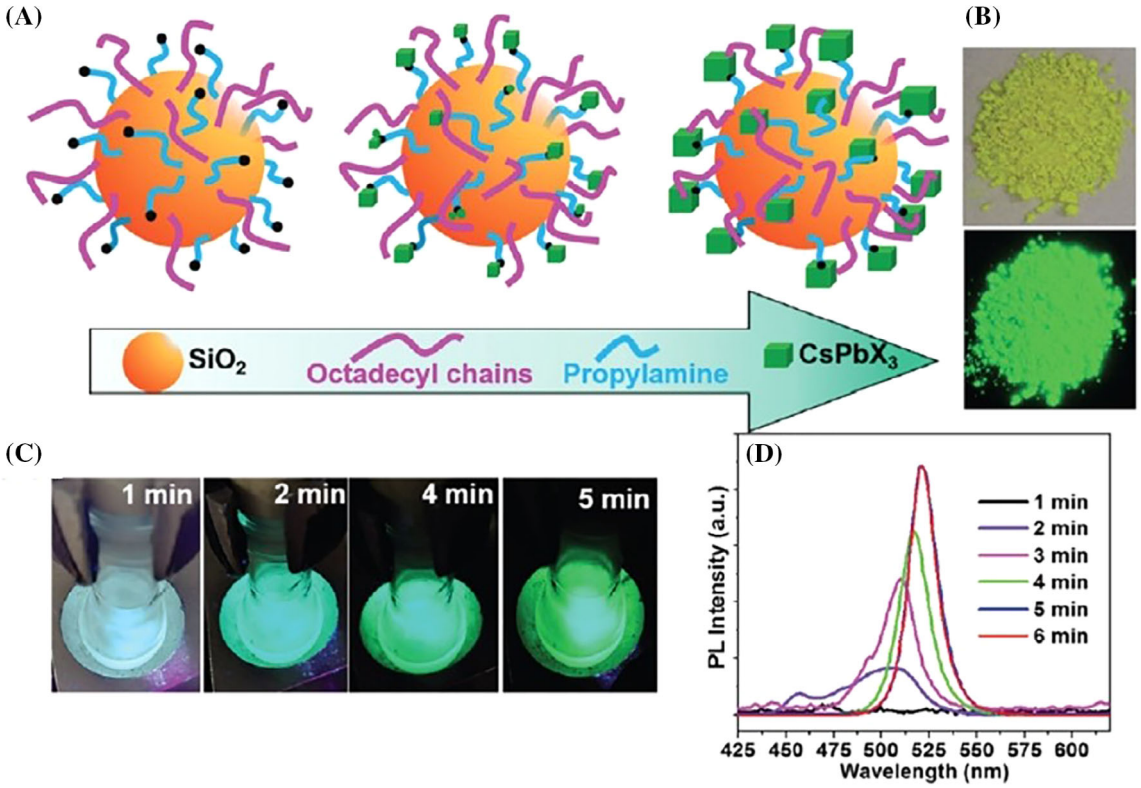

FIGURE 13 (A) Schematic of ex situ generation of $CsPbBr_3$@CA-SiO_2; (B) Photographs of the composites under daylight (top) and UV light (bottom); (C) Photographs showing the fluorescence color change with reaction time (0–5 min); and (D) PL spectra of the composites at different reaction times. Reprinted with permission.[185] Copyright 2019, Royal Society of Chemistry.

The silanols then crosslink automatically by forming Si—O—Si bonds, thus making the insulating layer durable enough to protect the perovskite films from water damage. The resulting hydrophobic fluoro-silane-protected solar cell devices exhibited an excellent efficiency of 18.9% with improved resistance to water destruction.

5 | APPLICATIONS OF PEROVSKITE@SILICON COMPOUNDS

Overall, the combination of perovskite and silicon in these hybrid materials offers a unique set of properties that make them attractive for a variety of biomedical and technological applications. In this section, we will discuss the potential use of silicon compounds in PSCs, LEDs, photocatalysis, and biomedical applications.

5.1 | Solar cells

Silanes can improve the PCE of solar cells by modifying the surfaces of the different layers in the device (Table 2). Silanes are able to improve the efficiency of PSCs via the following properties:

a. Enhanced interfacial contact: Silanes can increase interfacial contact between the different layers in a PSCs, including the perovskite layer, ETL, and HTL, which is crucial for ensuring efficient charge transport and collection in a solar cell.[196] However, the surfaces of these layers are not always perfectly compatible, which can result in poor interfacial contact and increased recombination losses. Silanes increase interfacial contact by modifying the surface chemistry of these layers; they contain functional groups, such as amino (—NH_2) or epoxy (—OCH_2CHCH_2O—) groups, that can react with the surface of the layers to form strong covalent bonds or hydrogen bonds. The improved adhesion between the layers can also give rise to enhanced interface charge transfer and reduced recombination losses. For example, in a perovskite solar cell, silanes such as APTES[190] or 3-glycidoxypropyltrimethoxysilane can modify the surface of the TiO_2 ETL and PEDOT:PSS HTL, respectively. Overall, using silanes to improve interfacial contact is an important strategy for increasing the efficiency of solar cells.

TABLE 2 Various silane compounds used in PSCs.

PSCs configuration	Structure of various silanes	PCE	References
ITO/P3HT: PCBM/3-Mercaptopropyltrimethoxysilane/ Au	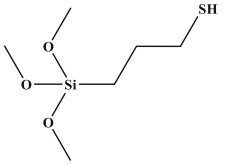 3-Mercaptopropyltrimethoxysilane	1.6%	188
ITO/PTAA/$CH_3NH_3PbI_3$/C60-SAM/Trichloro (3,3,3-trifluoropropyl)/BCP/Cu	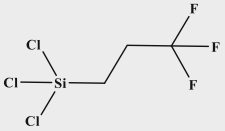 Trichloro(3,3,3-trifluoropropyl)	19.5% In forward scan	108
ITO/PEDOT:PSS/$CH_3NH_3PbI_{3-x}Cl_x$/PTS or OTS/PCBM/Ca/Al	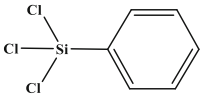 Phenyltrichlorosilane (PTS) 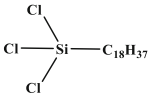 Octadecyltrichlorosilane (OTS)	12.63% (highest) 11.96% (average)	189
FTO/SnO_2/APTES/$CH_3NH_3PbI_3$/spiro-OMeTAD/Au	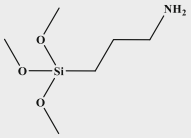 3-Aminopropyltriethoxysilane (APTES)	18.32% (17.74%) Reverse (forward) 17.54% Steady state efficiency	190
FTO/c-TiO_2/m-TiO_2/$CH_3NH_3PbI_3$/ Dodecyltrimethoxysilane/spiro-MeOTAD/Ag	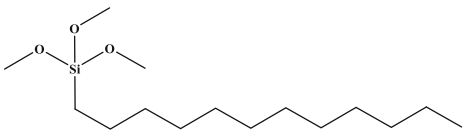 Dodecyltrimethoxysilane	13.74%	191
FTO/TiO_2/APTES/$CH_3NH_3PbI_3$@ZrO_2/C	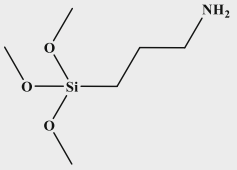 APTES	12.70% (maximum) 11.70% (average)	192
Glass (FTO)/TiO2/$(OC_2H_5)_3$–Si–$(CH_2)_3$–NH_3Br-$Cs_{0.05}(FA_{0.85}MA_{0.15})_{0.95}Pb(I_{0.85}Br_{0.15})_3$	$(OC_2H_5)_3$–Si–$(CH_2)_3$–NH_3Br (PASCA-Br)	21.66%	193
FTO/SnO_2/MPTMS/Cs $(FAPbI_3)_x(MAPbBr_3)_{1-x}$/Spiro-OMeTAD/Au	3-Mercaptopropyltrimethoxysilane (MPTMS)	20.03%	106
ITO/NiOx/$Cs_{0.05}(FA_{0.92}MA_{0.08})_{0.95}Pb$ $(I_{0.92}Br_{0.08})_3$/PCBM/PCBM with APTES/BCP/ Ag	APTES	18.62%	194
Glass/FTO/SnO_2/APTES, $Cs_{0.05}(FA_{0.85}MA_{0.15})_{0.95}Pb(I_{0.85}Br_{0.15})_3$/Spiro-OMeTAD/Ag	APTES	20.72%	195
FTO/SnO_2/Perovskite/TC-Silane/ lithiumbistrifluoromethanesulfonimidate (Li-TFSI)/Au	Trichloro(octyl)silane	20.03%	180

TABLE 2 (Continued)

PSCs configuration	Structure of various silanes	PCE	References
(ITO)/poly(bis(4-phenyl) (2,4,6-trimethylphenyl)amine) (PTAA)/ $CH_3NH_3PbI_3$/Carbon dots-self-assembled silane (CDs-SAM)/fullerene (C_{60})/ bathophenanthroline (BPhen)/Ag	Cross-linked trichloro (3,3,3-trichlorouoropropyl)silane ($C_3H_4Cl_3F_3Si$)	21.12%	186
Glass/ITO/SnO_2/$Cs_{0.05}(FA_{0.85}MA_{0.15})_{0.95}Pb(I_{0.85}Br_{0.15})_3$/3-iodopropyl trimethoxysilane	3-Iodopropyl trimethoxysilane	21.44%	105

b. Reduced charge carrier trapping: Silanes also help to reduce charge carrier trapping at the interface between the different layers in a solar cell.[188] When charge carriers (electrons or holes) move from one layer to another, they can get trapped at the interface between the layers, especially if there are defects or impurities present. This can result in recombination losses and reduced device efficiency. Silanes can overcome this by passivating the surface defects and reducing the density of surface trap-states. The functional groups in silanes can react with the surface of the layers to form a passivation layer, which helps to reduce the number of available trap states and prevent charge carrier trapping. For example, silanes such as 1H,1H,2H,2H-perfluorodecyltrichlorosilane or octadecyltrichlorosilane (OTS)[189] can be used to modify the surface of the perovskite layer in a PSC. Overall, using silanes to reduce charge carrier trapping is an important strategy for increasing the efficiency of solar cells and improving their stability.
c. Improved stability: Silanes can also improve the stability of solar cells by reducing the sensitivity of the different layers to moisture, oxygen, and other environmental factors. Silanes can modify the surface of the layers to form either a hydrophobic or hydrophilic surface depending on the silane used. As a result, the device will be protected from moisture and other environmental factors, reducing the likelihood of degradation and improving the stability of the device. For example, silanes such as trichloro (1H,1H,2H,2H-perfluorooctyl)silane (PFOTS) or perfluorooctyltriethoxysilane (PFOTES)[197] can be used to modify the surface of the layers in PSCs. Using silanes to enhance the stability of PSCs is an important strategy for increasing the longevity of the device and ensuring its performance over time.

SiO_2 has also been used to improve the PCE of PSCs; it is able to reduce surface recombination, improve stability, enhance light absorption, and facilitate charge transport, all of which contribute to the efficiency and stability of the device. SiO_2 can be used as a buffer between the perovskite and ETLs to increase interfacial contact and reduce recombination losses. The SiO_2 layer can passivate defects and reduce the density of trap states at the interface between the layers, improving charge transport and reducing recombination losses. The SiO_2 layer can also act as a barrier layer, preventing moisture and other impurities from entering the device and causing degradation. SiO_2 can also be used as an antireflective coating on the front surface of the PSC, which reduces the reflection of incident light and increases the amount of light absorbed by the HP layer, improving the efficiency of PSC. Notably, the thickness and properties of the SiO_2 layer can significantly affect the performance of PSC, which indicates that the optimization of these parameters is necessary to achieve the best results.

Four primary interfaces are responsible for the functionality of PSCs affecting the charge extraction, collection, and recombination processes: (1) the electron selective layer (ESL)/perovskite absorber layer interface, which is responsible for efficient electron extraction; (2) the perovskite absorber layer/hole selective layer (HSL) interface, which is crucial for hole extraction; (3) the front contact interface, which facilitates the entry of sunlight and electron transport; and (4) the back contact interface, which is responsible for collecting and completing the circuit for both electrons and holes.[198–202]

These interfaces play a pivotal role in the prevention of charge-carrier recombination and the efficient management of these charge carriers. This has become a central area of focus for engineers and researchers who are dedicated to improving the performance of PSCs in the conversion of solar energy. Recent research has illustrated the numerous benefits of utilizing self-assembled monolayers (SAMs) to modify these interfaces. SAMs have the ability to influence the energy levels at an interface by introducing a dipole moment, fine-tune the electronic states on the surface by passivating the inorganic surface states via chemical bonding, and influence the growth patterns of organic semiconductors, resulting in the fabrication of various structures. Due to these advantages, SAM treatment has emerged as a straightforward

yet highly efficient strategy for the optimization of the ESL/perovskite interface in PSCs, particularly for planar PSCs, where hysteresis is a concern. An example of this is the SAM 3-aminopropyltriethoxysilane (APTES), which has been effectively employed as an interfacial layer for ESL/perovskite interface modification in conjunction with SnO_2.[190,195] This treatment improves the interfacial contact and the perovskite film morphology and crystallinity, while also inducing dipoles at the interface. These dipoles affect the alignment of the energy bands, resulting in stronger built-in potential, thus facilitating the separation of photogenerated carriers and expediting charge extraction. The versatility of APTES increases their effectiveness; the alkyl chains can act as electrical insulators, reducing the transfer of electrons from the electrode to the perovskite layer and ultimately suppressing recombination. The terminal groups of APTES can also effectively passivate trap states on the perovskite surface through hydrogen-bonding interactions, thereby reducing the accumulation of charge and mitigating the recombination events associated with these traps.

5.2 | Light-emitting diodes

LEDs with HP NCs have garnered much attention due to properties such as fast crystallization kinetics, defect tolerance, low formation energy, and tuneable emission.[203–205] However, the poor structural stability of these LEDs (easily decomposes due to external factors) results in a low integrity crystal structure and low luminous efficiency (LE). Additionally, the thermal loss, agglomeration of QDs, and reabsorption loss associated with these LEDs significantly affects their suitability for practical applications.[206,207] However, most of these limitations can be addressed via encapsulation engineering. In particular, SiO_2-based encapsulation materials have proven to be crucial for enhancing the stability of PeLEDs (Table 3).

Various strategies involving surface engineering, encapsulation (shell), and compositional regulations are being developed to improve the stability of HP NCs.[11,216–223] In particular, oxide shells (TiO_2, SiO_2, ZrO_2, etc.) with silica is regarded as the optimal choice for encapsulation due to their excellent optical transparency, non-toxicity and chemical inertness.[15,136] Few studies have been reported on QDs embedded in PMMA polymer matrices to enable good processability, and they exhibited limited stability improvement compared to silica-based composite matrices. Additionally, the mixing of QDs is avoided due to the associated ion-exchange effects that can lead to the broadening of the emission spectra. Tang et al. reported the synthesis of ultrathin (approximately 2 nm) silica shell-coated Mn^{2+}-doped perovskite QDs using a versatile sol–gel method at room temperature (RT).[58] The resulting QDs exhibited a high PLQY, low toxicity, improved recombination, and improved water and thermal stability; the anion-exchange was found to have been blocked completely. No spectral shift was observed here, indicating a completely prevented anion-exchange. A maximum LE of 68.4 lm W^{-1} was observed at 10 mA with an excellent color rendering index (CRI) of 91. Su et al. proposed a method of assisting the dispersion of $CsPbBr_3/Cs_4PbBr_6$ NCs in a polymer using –OH-terminated mesoporous silica as a microcontainer.[224] It was observed that the composite silica microstructures containing NCs tend to disperse uniformly in the fabricated film. A small blue shift was observed in PL of the composite, which explains the formation of smaller particles within the silica microstructures. The blue-emitting chip was coated with red emissive CdSe/CdS/PMMA and green emissive composite HP NC/PMMA films.[224] The hydrogen bonding between —OH-terminated silica and PMMA polymer could potentially enhance interface compatibility and minimize external diffusion and external interactions. Thick silica shells can result in spectral shift/broadening and reduced PLQY; however, ultrathin silica shells can enhance the electroluminescence (EL) and chemical stability of HPs.[225] Philipse et al. reported the formation of a thin SiO_2 layer by exposing silica and QDs to a dilute aqueous sodium silicate solution for 2 h.[226] Liu et al. reported on the synthesis of dual-encapsulated HP NCs, that is, with lead-carboxylate and SiO_2, for the subsequent synthesis of ultra-stable $CsPbBr_3$ NCs.[227] The dual-encapsulated HP NCs exhibited excellent stability when exposed to air, water, and extreme temperatures, while the LED devices showed a positive decay of less than 15% after 1000 h under illumination. Choi et al. improved the processability of PMMA-grafted $CsPbBr_3@SiO_2$ NPs by controlling the PMMA brushes that act as a polymer matrix. Tuneable colors with a narrow spectrum could be observed by mixing red phosphors and green $CsPbBr_3@SiO_2$ NPs and subsequently using it to coat a blue LED chip.[228] Liu et al. synthesized $CsPbBr_3$/m-SiO_2 composites of varying sizes (100–300 nm) using a mixture of molten salts (KNO_3, $NaNO_3$, and KBr) as a reaction medium to facilitate the nucleation of HP NCs in m-SiO_2 particles.[229] m-SiO_2 is one of the best materials for HP NC encapsulation due to its excellent structural, chemical and thermal stability, low cost, low toxicity, and ease of fabrication. The surface of the m-SiO_2 can be modified to be either hydrophobic or hydrophilic depending on what is required. Liu et al. compared the optical properties and stability of the prepared HP NCs by changing the reaction

TABLE 3 The device configuration, performances, and stability of HP-based LEDs.

S. No.	Composite materials	LED device configuration	Luminous efficiency (lm W^{-1})	CIE (x, y)	Color gamut	Stability	References
1	$CsPbBr_3$/@SiO_2	LED chip/$CsPbBr_3$/mesoporous SiO_2/K_2SiF_6:Mn	–	(0.30, 0.31)	87% of Rec. 2020	–	[136]
2	$CsPbBr_3/SiO_2$	LED chip (blue)/$CsPbBr_3/SiO_2$/$CaAlSiN_3:Eu^{2+}$	94	(0.36, 0.35)	136% of NTSC	–	[208]
3	$CsPbBr_3$/MS	LED chip (blue)/$CsPbBr_3$/MS/$Sr_2Si_5N_8:Eu^{2+}$	47.6	(0.34, 0.34)	–	As the current increases from 20 mA to 120 mA, the CIE coordinates shift from (0.34, 0.34) to (0.32, 0.32).	[14]
4	$CsPbBr_3$/MS	LED chip (blue)/$CsPbBr_3$/MS/$CsPb(Br_{0.4}I_{0.6})_3$	30	(0.24, 0.28)	113% of NTSC; 85% of Rec. 2020	–	[209]
5	$CsPbBr_3$/MS@SiO_2	LED chip (blue)/$CsPbBr_3$/MS@SiO_2/KSF	85	(0.33, 0.32)	128% of NTSC; 96% of Rec. 1931 and Rec. 2020, respectively	–	[210]
6	$Cs(Pb_{0.66}/Mn_{0.34})Cl_3$@MSNs	LED chip (UV)/$CsPb(Br/Cl)_3$@MSNs/$Cs(Pb_{0.66}/Mn_{0.34})Cl_3$@MSNs	62.5	(0.34, 0.36)	–	35% of the initial intensity remains after 30 min at 10 mA	[211]
7	$CsPb(Br/Cl)_3/SiO_2$; $CsPbBr_3/SiO_2$; $CsPb(Br/I)_3/SiO_2$	LED chip(UV)/mixture of $CsPb(Br/Cl)_3/SiO_2$, $CsPbBr_3/SiO_2$, and $CsPb(Br/I)_3/SiO_2$	–	(0.33, 0.29)	–	No noticeable change in the PL spectrum after 8 h of operation at 20 mA	[142]
8	$MAPbBr_3$@SiO_2/PVDF	LED chip (blue)/$MAPbBr_3$ @SiO_2/PVDF/KSF adhesive	147.5	(0.29, 0.32)	120% of NTSC	–	[212]
9	DDAB-$CsPbBr_3/SiO_2$ QDs	LED chip (blue)/DDAB-$CsPbBr_3/SiO_2$ QDs/AgInZnS	63.4	(0.41, 0.38)	–	Small change in CRI when applied voltage increases from 2.5 to 3 V	[213]
10	$CsPbBr_3$-SiO_2	LED (blue)/$CsPbBr_3$-SiO_2/$CsPbBr_{1.2}I_{1.8}$	35.4	(0.33, 0.36)	127% of NTSC; 95% of Rec. 2020	–	[130]
11	Mn-doped $CsPbCl_3$-SiO_2/Al_2O_3	LED chip (blue)/Ce-PiG/Mn-doped $CsPbCl_3$-SiO_2/Al_2O_3	80.91	(0.38, 0.37)	–	–	[214]
12	DDAB-$CsPbBr_3$ @SiO_2	LED chip (blue)/DDAB-$CsPbBr_3$@SiO_2/	–	(0.35, 0.35)	–	Stable EL spectra after continuous	[56]

(Continues)

TABLE 3 (Continued)

S. No.	Composite materials	LED device configuration	Luminous efficiency (lm W^{-1})	CIE (x, y)	Color gamut	Stability	References
		DDAB-$CsPbBr_1I_2$@SiO_2				operation for 20 h at 30 mA	
13	$CsPbBr_3$@SiO_2	LED chip (blue)/ $CsPbBr_3$ @SiO_2/ KSF	63.5	(0.32, 0.30)	–	Shape and PL peak position remain the same after 13 h continuous operation at 6 mA	59
14	$CsPbBr_3$−$CsPb_2Br_5$@SiO_2	LED chip (blue)/ $CsPbBr_3$–$CsPb_2Br_5$@SiO_2/ $CaAlSiN_3:Eu^{2+}$	57.65	(0.34, 0.34)	–	87.4% of the initial LE remains after 120 min of excitation	126
15	$CsPbBr_3$Ds/$FSiO_2$	UV chip/ $BaMgAl_{10}O_{17}$:Eu/ $CsPbBr_3$QDs/ $FSiO_2$/(Sr,Ca) $AlSiN_3$:Eu	10.7	(0.33, 0.33)	–	–	125
16	$CsPbBr_3$@silicone	LED chip/ $CsPbBr_3$@silicone/ $CsPb(Br_{0.3}I_{0.7})_3$@silicone	–	(0.32, 0.30)	–	–	123
17	$CsPbBr_3$/SiO_2	LED chip (blue)/ $CsPbBr_3$/SiO_2/$CsPb(Br/I)_3$/SiO_2	35.32	(0.3, 0.31)	–	Stable after 40 h	13
18	$CsPbBr_3$@SiO_2	LED chip (blue)/ $CsPbBr_3$ @SiO_2/ CdSe	56 at 5 mA	(0.3, 0.32)	138% of NTSC	The CIE coordinate remains in the white region after 1 h	117
19	$CsPbMnCl_3$@SiO_2	GaN LED(UV)/ $CsPbBr_3$/ $CsPbMnCl_3$@SiO_2	68.4 at 10 mA	–	–	–	58
20	$CsPbBr_3$@ZrO_2	LED chip (blue)/ $CsPbBr_3$@ZrO_2/ CdSe	55 at 1 mA	(0.28, 0.33)	–	The PL intensity of the green emission drops only by 10% after 2 h	215
21	$CsPbBr_3$@SiO_2; $CsPb(Br/I)_3$@SiO_2	LED chip (blue)/ $CsPbBr_3$ @SiO_2/ $CsPb(Br/I)_3$@SiO_2	61.2	(0.33, 0.33)	120% of NTSC	Half lifetime = 227 h	15

temperature and precursor ratios. The NCs with 100 nm m-SiO_2 particles were found to exhibit the best performance; the 100 nm particles exhibited significantly enhanced properties even when compared to the reported 600 nm $CsPbBr_3$/m-SiO_2 composite.[229] They demonstrated excellent moisture, optical, and thermal stability of the $CsPbBr_3$/m-SiO_2 composite up to 1000 h while exhibiting a narrow green PL emission with a peak emission at 517 nm and a full width at half maximum (FWHM) of 18 nm. A high PLQY of 77% was observed in the 100 nm NCs. Additionally, a 7-in. liquid crystal display (LCD) was prepared with a polymer layer film containing 100 nm $CsPbBr_3$/SiO_2 particles as the green color conversion layer. The resulting device exhibited

favorable white light emissions with CIE color coordinates of (0.307, 0.327), which is a higher color gamut coverage than that of a commercial Dell XPS 157590 laptop LCD.

The most widely applied solution to address instability of HPs is to embed HP NCs in mesoporous polystyrene microspheres and subsequently encapsulate them with silica.[15,230,231] Although this protects the HP NCs from external factors, for example, oxygen and moisture, the preparation process is complex and the embedded HP NCs undergo uneven dispersion. An alternative method to improve stability is to embed HP QDs in the glass matrix; however, the resulting PLQY is low (<15%) due to the structural imperfections that arise during the fabrication process.[232] Zhao et al. embedded HP QDs into silica aerogels during aerogel synthesis.[233] Silica aerogel has a low density, high porosity, high optical transparency (which is crucial for embedding luminescent materials), and nanoscale mesoporous large surface area. The silica aerogel retains the HP QDs while the pore fluid evaporates during the pressure drying process.

Since the pore size of silica aerogel can be modified easily, the size of perovskite QDs is also easily adopted. The synthesized QDs also exhibited a tuneable PL (409–661 nm). The optimize QDs were found to exhibit a quantum efficiency of approximately 30% after 30 days of storage under illumination and high humidity. As the fluorescent decay lifetime of QDs decreased, a subsequent increase in the radiative rate was observed. To further evaluate the performance of the QDs in practical applications, a white LED (WLED) was fabricated using a blue-emitting GaN chip coated with commercial red phosphor and an optimize green-emitting composite. A driving current of 10 mA was applied to the device, and the resulting characteristics were observed. Three distinct peaks at 460 nm (blue), 520 nm (green QDs), and 618 nm (red) were observed in the EL spectra. The WLED demonstrated an LE of 29.3 lm W^{-1} with a CIE of (0.35, 0.35) and CRI of approximately 82. An excellent color gamut overlap of 117.8% of national television system committee (NTSC) standard was also observed. Recently, new strategies have been explored to enhance the stability of HP films using mesoporous SiO_2. However, there is little to no information on confining and improving the LE by reducing the reabsorption loss.[234] Fan et al. reported on an in situ growth strategy for the synthesis of efficient and stable perovskite QDs encapsulated in mesoporous silica (SBA-15),[234] which resulted in the deposition of HP QDs in the pores of SBA-15; the HP QDs were found to adopt an ordered mesoporous arrangement, which helped prevent agglomeration and reduced reabsorption loss. The ratio of silica composites to perovskite precursors were varied to find the optimal ratio (SBA-15). The reference perovskite QDs exhibited a PLQY of 24.8% with a FWHM of 20 nm, while the mesoporous SBA-15 encapsulated $CsPbBr_3$ QDs were found to have a PLQY 2.6 times higher than that of the reference QDs. This can be attributed to the matrix form of the SBA-15 composite, which prevents QD agglomeration. The PL lifetime of the $CsPbBr_3$/SBA-15 composite was also found to increase from 32.6 to 104.94 ns,[234] which can be attributed to the enhanced crystallinity and improved surface passivation effect. The non-radiative recombination of the $CsPbBr_3$/SBA-15 composite was also found to be lower than that of the $CsPbBr_3$ QDs. The relative refractive index (n_r) of mesoporous SBA-15 (defined as $n_{SBA\text{-}15}/n_{siliconeresin}$) was lower than 1; the pores act as a waveguide structure that inhibits light emission within SBA-15, which leads to reduced recombination losses. $CsPbBr_3$ and $CsPbBr_3$/SBA-15 composite layers were used to fabricate LED devices over an LED blue (460 nm) chip with an LE of 41.6 lm W^{-1}. The devices with the $CsPbBr_3$/SBA-15 composite film exhibited an increased LE of 183 lm W^{-1} due to the resulting waveguide effect and reduced self-absorption. A WLED was fabricated by adding a red composite to the monochromatic LED; notably, a lower LE of 116 lm W^{-1} was observed despite an excellent color gamut coordinate of (0.33, 0.31). This lower LE is due to the strong absorption of the red composite and its low contribution to the luminous function. The WLED devices were found to be stable by varying the driving currents. Wang et al. synthesized a mesoporous silica green HP QD nanocomposite that can be mixed with red-emitting HP QDs, achieving excellent thermal and photostability while preventing anion-exchange.[209] The mesoporous-coated $CsPbBr_3$ QDs demonstrated efficient thermal recycling with negligible loss, while the pristine $CsPbBr_3$ QDs experienced a 60% reduction in initial intensity after one heating cycle. A similar trend was also observed for photostability measurements. The green and red HP QDs (with and without mesoporous silica shells) were coated over a blue chip in silicone resin for the fabrication of an LED device. The LED devices without mesoporous QDs underwent a strong spectral shift from green to yellow due to the ion-exchange effect, while the mesoporous silica-coated QDs exhibited a CIE of (0.24, 0.28) and an LE of 30 lm W^{-1}. Similarly, Sun et al. reported on the synthesis of an HP QD/silica composite via the hydrolysis of APTES, which acts as a capping agent for QDs and a precursor for the silica matrix.[15] A bright WLED was also fabricated by coating green and red QD/SiO_2 over a commercial blue LED chip. The resulting WLED exhibited a maximum LE of 61.2 lm W^{-1} at 10 mA. When the current was increased from 10 to 120 mA, the intensities of the green and red PL spectral regions also increased similarly,

demonstrating that the phosphors do not exhibit saturation to blue light. The half-life of the WLED was determined to be 227 h. Xu et al. introduced a novel synthesis strategy for stable perovskite NCs via the hydrolytic polycondensation of APTES in the presence of ionic liquids (ILs).[16] The perovskite NCs that were synthesized with a molar n_{APTES}/n_{Pb} ratio of 2.0 exhibited the highest emission intensity, which can be attributed to the uniform and dense silica shell formation over the surfaces of the perovskite NCs. Additionally, the PLQY of the resulting perovskite NCs was determined to be approximately 85.7%, which is one of the highest reported PLQY values in silica-coated HP NCs. Additionally, from the time resolved PL (TRPL) study, the radiative lifetime of the resulting $CsPbBr_3@SiO_2$ NCs was found to increase to 98.51%. However, the radiative lifetime was found to decrease with an increase in the amount of APTES added due to the etching of the NC surface. The radiative lifetime decreases further when the ratio of n_{APTES}/n_{Pb} is increased, which could be due to the reduction in the particle size of $CsPbBr_3$ cores. A further increase in hydrolysis time leads to a partial phase transformation from $CsPbBr_3$ to Cs_4PbBr_6. The optimal hydrolysis time was determined to be 10 s with a shell size of 1–2 nm, after which, the $CsPbBr_3$ cores reduce in size due to the corrosion of the NCs by the alcohol and water produced from the hydrolysis of APTES. The conduction band minimum (CBM) and valence band minimum (VBM) positions were calculated from the ultraviolet photoemission spectroscopy (UPS) study, and a higher CBM and lower VBM was subsequently achieved. This could potentially help prevent the delocalization and quenching of excitons while promoting the radiative recombination of charge carriers due to the abundance of excitons. A $CsPbX_3@SiO_2$ color conversion layer was coated on a blue LED chip to evaluate the performance of the prepared NCs. To achieve a pure white emission, orange-red emitting CuInZnS (CIZS)/ZnS/PVP composites were mixed evenly with $CsPbBr_3@SiO_2$ NCs. The resulting device exhibited an outstanding CRI of 90.5, a CIE coordinate of (0.352, 0.343), and an LE of 41.57 lm W^{-1}. The resulting device also exhibited a stable CRI and CCT under varying current from 20 to 120 mA. This can be attributed to improved exciton confinement and radiative recombination probability. Zang et al. introduced a method to control the microstructure of the HP film to support the bending reliability of flexible perovskite LEDs (f-PeLEDs).[235] A reversible hydrolysis and condensation procedure was utilized to deposit a multifunctional silane molecule called (3,3,3-trifluoropropyl) trimethoxysilane (TFPTMS) onto HP films for obtaining an in situ crosslinked oxo-bridged silica network. Additionally, Lewis acid–base interactions may allow for the Si—O—Si groups to coordinate with uncoordinated lead ions. The hydrogen bonds between silanol groups and halides were found to greatly improve the flexibility of the HP film without affecting the optoelectronic properties of the film. The Si—O bond offers several advantages over the C—C bond, including a longer chain length (0.164 nm vs. 0.154 nm), higher bond energy (452 kJ/mol vs. 346 kJ/mol), and a larger valence angle (109° for the Si—O bond).[235] These characteristics highlight the potential of the Si—O bond to enhance the structural integrity and stability of materials. A longer chain length allows for greater spatial separation between atoms, whereas a higher bond energy indicates stronger interatomic interactions. In addition, a larger valence angle provides flexibility and resilience to the bond, making it less susceptible to deformation or breakage. Furthermore, the higher bond energy of the Pb—O bond (378 kJ/mol), particularly when oxygen is derived from the Si—O—Si linkage, compared with the Pb—Br bond (201 kJ/mol), indicates its significant role in the exceptional stability of the perovskite structure.

The fabricated TFPTMS-based f-PeLEDs exhibited a peak EQE of 19.2% in rigid devices; that of flexible devices was found to be 16.2%. Li et al. demonstrated the synthesis of $CsPbBr_3$ NCs within mesoporous SiO_2 nanospheres (MSNs) with the aim of improving their properties[236]; this involved the in situ crystallization of $CsPbBr_3$ NCs within the pores of MSNs. The use of MSNs allows for the regulation of the size distribution of the $CsPbBr_3$ NCs as well as the passivation of surface defects. Additionally, the MSNs serve as a protective barrier, shielding the NCs from water and oxygen. Even after being exposed to harsh conditions for 60 days, the composite powder was found to retain approximately 98% of its initial PL intensity. The film was also found to maintain a consistent RT PL intensity even after continuous heating–cooling cycles between 25 and 200°C. The LCD backlit based on the $CsPbBr_3$ NCs@MSNs composite was found to have a wide color gamut that covers 124% of the National Television Standards NTSC standard and 95.6% of the Rec. 2020 standard (Figure 14). This suggests that it is able to produce a wide range of colors that are more vibrant and accurate than those produced by displays with narrower color gamuts.

5.3 | Photocatalysis

HP NCs have unique electronic and surface properties, which can lead to high catalytic activity and selectivity in a variety of reactions. HP NCs can be used as heterogeneous catalysts, where the reaction takes place on the surface of the NC, or as photocatalysts, where light is

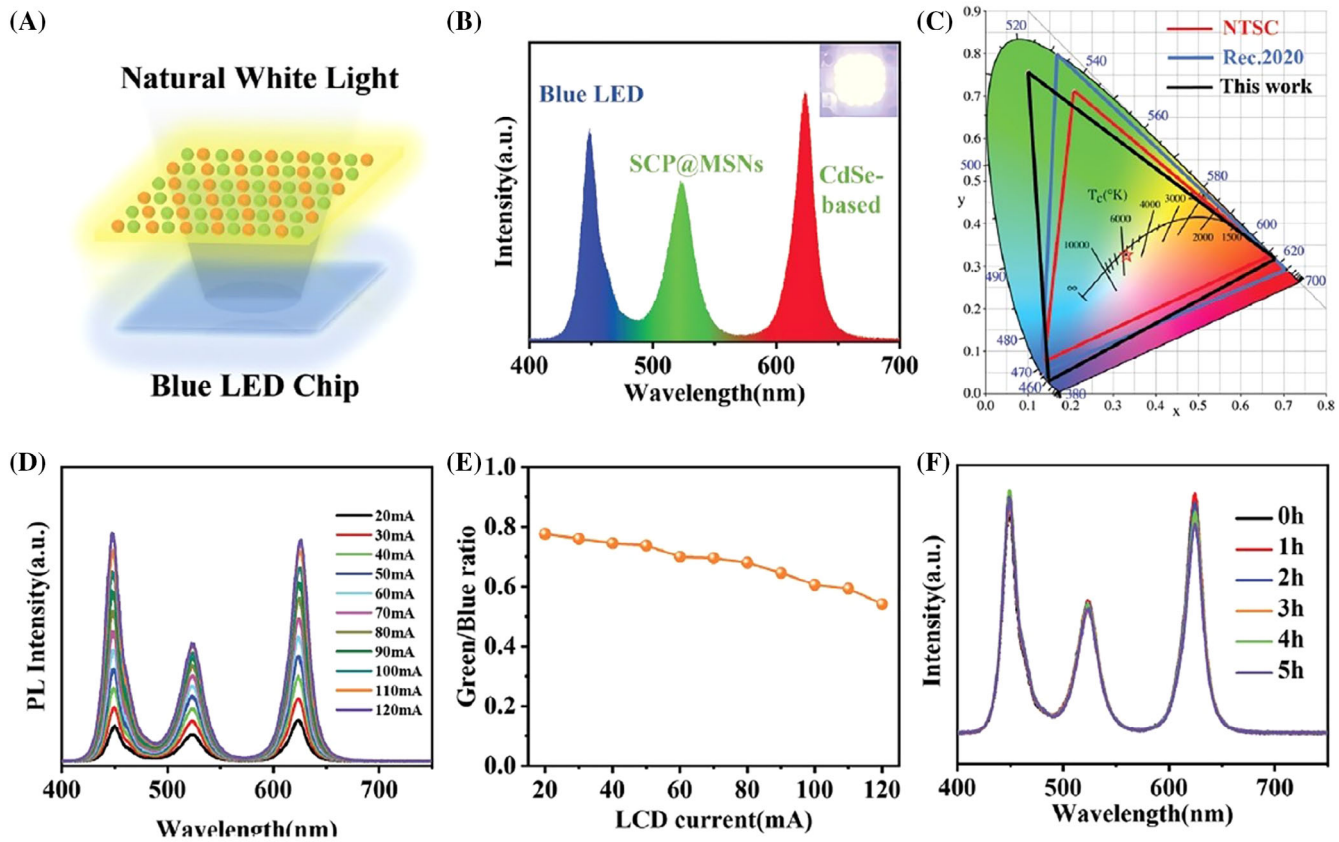

FIGURE 14 (A) Schematic diagram of the LCD backlight unit. (B) Entire spectrum of white LED (the inset image: white LCD backlit). (C) Color gamut of the LCD backlit-black line, NTSC TV standard-red line, and the Rec. 2020 standard-blue line. (D) PL spectra of the LCD at various applied currents (20–120 mA); (E) Ratio of green to blue intensity as a function of current; (F) PL spectra at various operating times. Reprinted with permission.[236] Copyright 2022, Wiley-VCH.

used to drive the reaction. HP NCs have been considered for various catalytic applications, including CO_2 reduction, water splitting, hydrogen evolution, and organic synthesis.[237–241] The tuneable composition and crystal structure of HP NCs allows for the optimization of their catalytic properties such as band gap and surface area, making them suitable candidates for future catalyst development. Gao et al. reported on the photocatalysis reaction of $CsPbBr_3$@SiO_2 composites for the degradation of tetracycline hydrochloride (TC-HCl) dye in water.[31] The photodegradation mechanism of TC-HCl is shown in Figure 15. $CsPbBr_3$ is a type of perovskite material that has a bandgap energy corresponding to the visible spectrum of light. When the $CsPbBr_3$@—SiO_2 composite absorbs photons with energies higher than the bandgap energy, electrons in the valence band (VB) of $CsPbBr_3$ can be excited into the conduction band (CB), leaving behind holes in the VB. These photo-excited electrons are called photogenerated electrons (e^-) and the corresponding holes are called photogenerated holes (h^+). The reduction potential of O^2/O^{2-} is approximately 0.33 V vs. the normal hydrogen electrode (NHE), which means that O^2/O^{2-} has a tendency to accept electrons and undergo reduction. On the other hand, the CB of $CsPbBr_3$ exhibited a more negative potential of approximately 0.39 V, which indicates that the e^- at the CB of $CsPbBr_3$ have a higher potential energy than the O^2/O^{2-} reduction potential; this allows the e^- to accepted by the O_2 molecules adsorbed on the surface of the $CsPbBr_3$@—SiO_2 composite, undergoing reduction to form O^{2-}. The generation of O^{2-} via the photoexcitation of the $CsPbBr_3$@—SiO_2 composite can potentially be applied in photocatalysis, where O^{2-} can oxidize organic molecules. This can also be applied to the production of renewable energy by converting sunlight into chemical energy and storing it in the form of O^{2-}. The VB of $CsPbBr_3$ has a lower potential energy than the $OH^{\bullet}/OH^-$ oxidation potential, which means that the h^+ in the VB of $CsPbBr_3$ do not have sufficient energy to oxidize OH^- into $OH^{\bullet}$. Instead, the h^+ can react with the adsorbed H_2O on the surface of the $CsPbBr_3$@—SiO_2 composite, forming hydroxyl radicals ($^{\bullet}OH$) which are strong oxidizing agents. These hydroxyl radicals can then react with and decompose organic pollutants. This process can

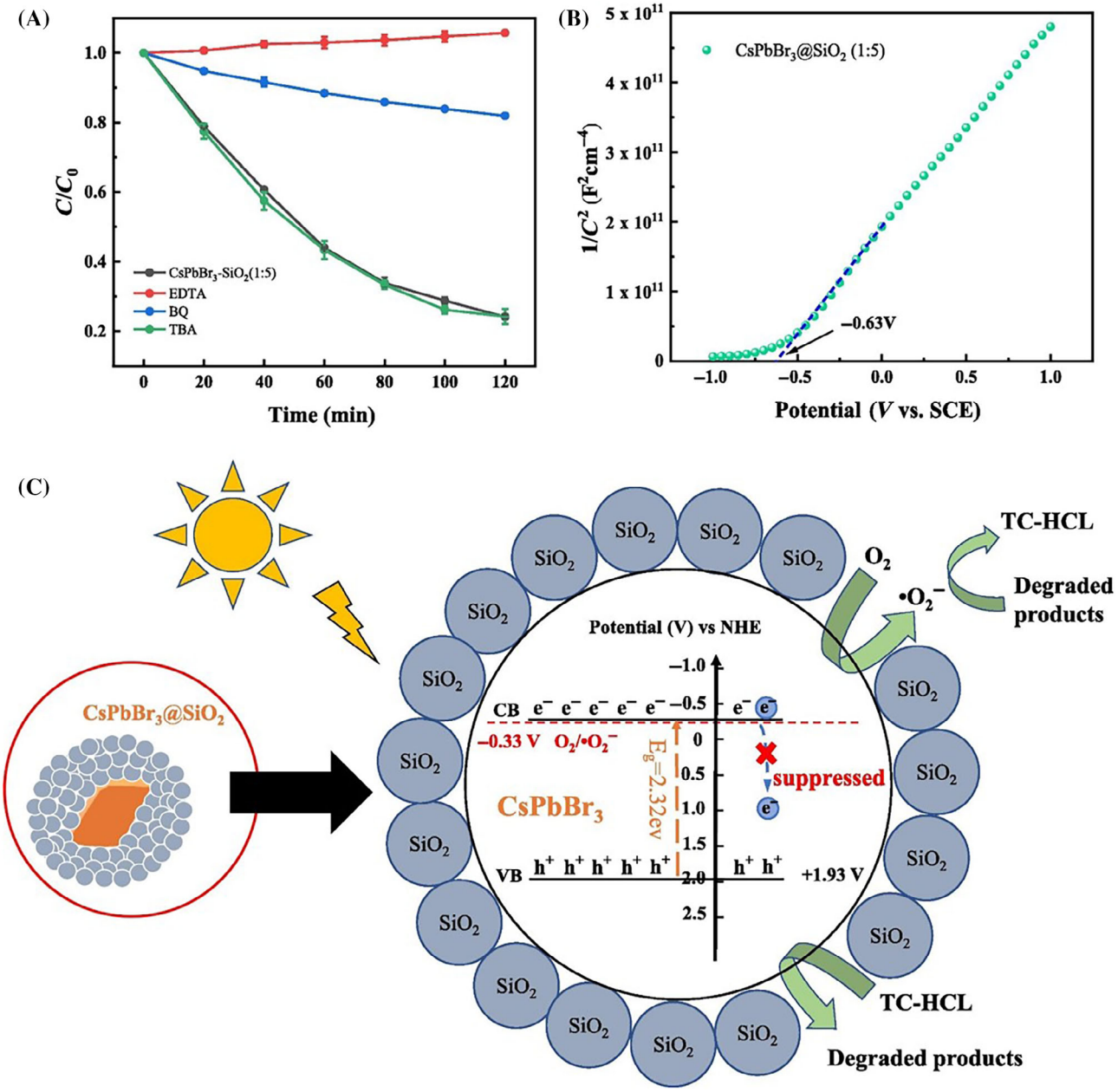

FIGURE 15 (A) Photocatalysis of TC-HCl; the photodegradation of TC-HCl (studied at the absorption peak of 356 nm); (B) Mott–Schottky graph of the $CsPbBr_3@SiO_2$ (1:5) composite; (C) Illustration of the photodegradation mechanism of the $CsPbBr_3@SiO_2$ composite. Reprinted with permission.[31] Copyright 2022, Elsevier B.V.

potentially be applied in the photocatalytic degradation of organic pollutants in water, such that the hydroxyl radicals generated by the photoexcitation of the $CsPbBr_3$@—SiO_2 composite can react with and decompose organic pollutants.

Huo et al. reported a one-pot strategy for the synthesis of a composite photocatalyst by anchoring $FAPbBr_3$ QDs on amine-functionalized silica (A-SiO_2) via N—H bonding (Figure 16).[242] The surface of A-SiO_2 contains an abundance of NH_x groups, which act as nucleation and growth sites for the HP QD that prevent the agglomeration of $FAPbBr_3$ and increase the number of active sites. The N—H bonds between the NH_x groups and the FA cation greatly improve the photodegradation activity of $FAPbBr_3$/A-SiO_2 composite. The $FAPbBr_3$/A-SiO_2 composites exhibited superior photocatalytic activity for the removal of NO compared to the pristine $FAPbBr_3$; This is due to the composite system's increased charge transfer efficiency and decreased photogenerated electron–hole pair recombination rate. This composite material is a suitable candidate for photocatalysis applications, particularly for the removal of NO from air pollutants.

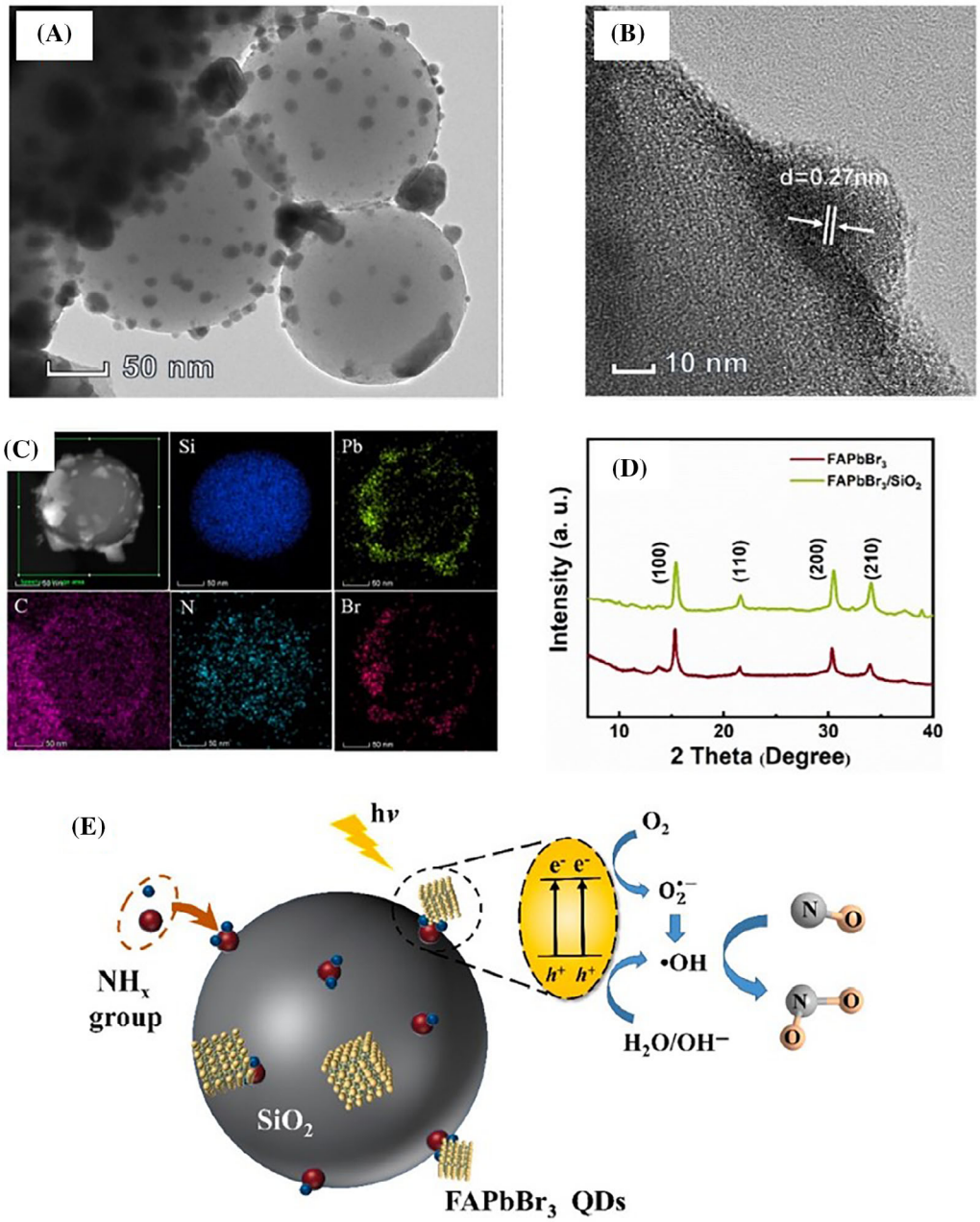

FIGURE 16 (A) TEM and (B) HRTEM images of a $FAPbBr_3$/A-SiO_2 composite, (C) Presence of Si, Pb, C, N, and Br in the composite confirmed by elemental mapping, (D) XRD spectra of composite and $FAPbBr_3$ NCs, and (E) Illustration of the photocatalytic process using $FAPbBr_3$/A-SiO_2 composite. Reprinted with permission.[242] Copyright 2021, Elsevier B.V.

5.4 | Biomedical applications

HP NCs have high PLQY, narrow emission spectrum, and tuneable emission wavelength, which make them ideal for use in the fluorescence imaging of cells where they can be used to label specific structures or biomolecules and visualize dynamic biological processes in real-time.[21,29,243,244] The bright and stable emissions exhibited by HP NCs allows for long-term imaging, while the tuneable emission spectrum allows for multiplexed imaging, where multiple structures or processes can be imaged simultaneously using different color-emitting HP NCs. Additionally, HP NCs can be easily functionalized with targeting moieties, such as antibodies or peptides, for the specific imaging of cells or tissues. However, the limited stability under ambient conditions and potential toxicity associated with HP NCs have hindered the widespread application of these NCs in biological imaging. A potential approach to overcoming these limitations is to embed HP NCs into a silica matrix.[22–24,245,246] Silica is

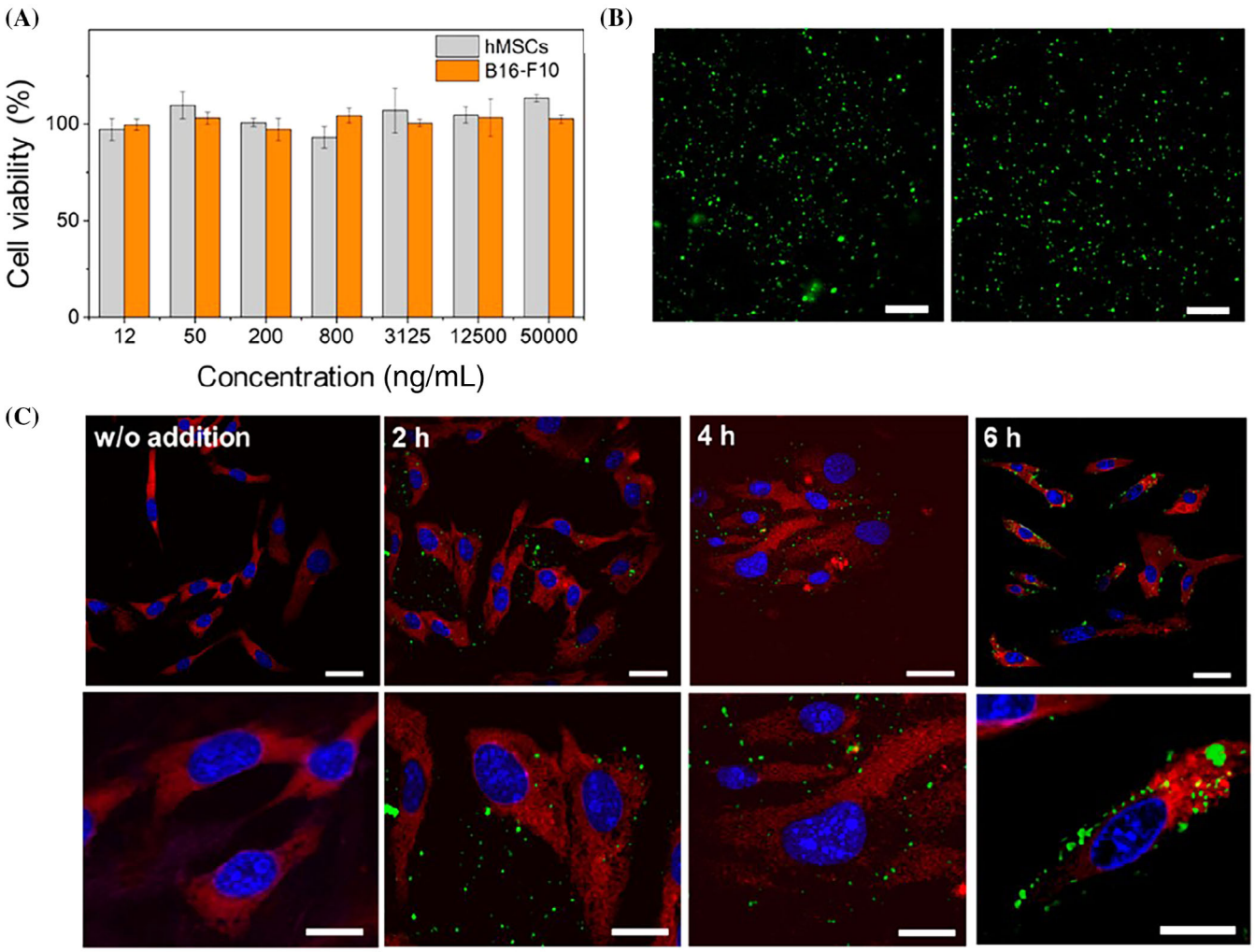

FIGURE 17 Silica-based shell@$CsPbBr_3$ NCs in biological fluids. (A) Human mesenchymal stem cells (hMSCs) and Murine melanoma (B16–F10) cells were used to test the cytotoxicity of phTEOS-TMOS@$CsPbBr_3$ NCs dispersed and incubated in PBS for 1 h, (B) Confocal scanning microscopy (CLSM) image of phTEOS-TMOS@$CsPbBr_3$ NCs; scale bar represents 30 μm, (C) CLSM image showing phTEOS-TMOS@$CsPbBr_3$ NCs (green) interacting with labeled B16–F10 cells (membrane in red, nuclei in blue). B16–F10 cells were incubated with phTEOS-TMOS@$CsPbBr_3$ NCs for 0, 2, 4, and 6 h (from left to right). Scale bar: 40 μm (upper row) and 10 μm (bottom row). Reprinted with permission.[30] Copyright 2021, American Chemical Society.

biocompatible, stable, and can protect the HP NCs from environmental factors such as moisture, oxygen, and light. Furthermore, the silica matrix can be functionalized with biomolecules such as antibodies or peptides to specifically target certain cellular structures or biomolecules. $CsPbBr_3$ NCs coated with a silica shell exhibit improved upconversion and fluorescence properties, making them ideal for use in imaging living cells. The silica shell can also prevent the toxic release of lead ions from the NCs. Talianov et al. encapsulated $CsPbBr_3$ NCs with silica using TMOS and phTEOS and observed the subsequent interactions in murine melanoma cell lines (B16–F10 cells) and human mesenchymal stromal cells (hMSCs) (Figure 17).[30] A staining method that involved rhodamine 800 and propidium iodide was used to visualize the interaction of phTEOS-TMOS@$CsPbBr_3$ NCs with the cells. Rhodamine 800 is a fluorescent dye that stains the cell membrane, and propidium iodide is a fluorescent dye that binds to deoxyribonucleic acid (DNA), staining the nuclei of cells. After incubating the phTEOS-TMOS@$CsPbBr_3$ NCs with hMSCs and murine melanoma (B16–F10) cells, Talianov et al. observed that the NCs exhibited intense fluorescence under the excitation of a 488 nm continuous-wave argon laser. This indicates that the phTEOS-TMOS@$CsPbBr_3$ NCs were not only stable in water but also in a bio-organic environment, as the fluorescence intensity of the NCs were maintained without risk of degradation and aggregation in the presence of cells. The stability of NPs in biological environments must be considered during the

development of these NPs for biomedical applications, as the NPs must be able to retain all properties in the complex and dynamic environment within living organisms. The use of fluorescent dyes to visualize the interaction of NPs with the cells is commonly used in nanobiotechnology and can provide valuable insights into the behavior of NPs in biological systems. An important factor to be considered is the biotoxicity of lead-based HP NCs (particularly the toxicity of lead, which is a component present in most HP NCs). While the toxicity of HP NCs is still being studied, it is clear that their biocompatibility needs to be improved for use in biomedical applications. Researchers are exploring various strategies to reduce the toxicity of HP NCs, including the use of lead-free alternatives and the encapsulation of NCs with biocompatible materials. The use of an amphipathic phospholipid as the encapsulating agent is promising as it can self-assemble into a bilayer structure with a hydrophobic and a hydrophilic end. This allows the phospholipid to form a stable coating around the NCs, with the hydrophobic end facing the particle surface and the hydrophilic end facing outward toward the water.[28] The resulting encapsulated material is stable and can be readily dispersed in water, making it ideal for bioimaging applications.

Song et al. reported a dual-passivation method involving all-inorganic HP NCs, for example, $CsPbBr_3$, $CsPbBr_2I_1$, $CsPbBr_{1.5}I_{1.5}$, and $CsPbBr_1I_2$ QDs for bioimaging (Figure 18).[247] The $CsPbI_3/3I@SiO_2$ QDs were passivated by halide and silica, which was produced from the hydrolysis of (3-iodopropyl)trimethoxysilane (3IS). A passivation strategy involving the 3IS molecule and silane can be applied to ionic $CsPbI_3$ QDs, such that the 3IS molecule acts as a passivation additive to minimize surface defects and can also passivate uncoordinated lead atoms on the surface of the QDs. This reduces the density of surface states, which leads to reduced non-radiative recombination and improved PL efficiency. Silane acts as a precursor of SiO_2, which isolates moisture and can inhibit halide migration. Moisture can lead to the degradation of the $CsPbI_3$ QDs, so by isolating it, the long-term stability of the QDs can be improved.

Additionally, the confinement of halide migration helps to prevent halide segregation and subsequently, the degradation of performance of the QDs. $CsPbI_3/3I@SiO_2$ NCs were also encapsulated by amphipathic phospholipid in order to improve water dispersity, which also helps to enhance the stability of HPs. Moreover, this change in surface could help to reduce lead leakage and enhance biocompatibility, which is advantageous for cellular labeling.

5.5 | Photodetectors

Perovskite-based photodetectors have been extensively developed for their exceptional sensitivity.[248–255] However, they face intrinsic limitations due to the narrow optical band gap of perovskite materials, which restricts their ability to detect a wide spectrum of light, particularly in the near-infrared range. Moreover, single-crystal (SC) perovskite devices often exhibit sluggish response times, exceeding 10 μs. To unlock the full potential of perovskite technology for photodetection, a more impactful avenue of research involves the integration of perovskite with silicon. This synergistic approach not only addresses the spectral limitations of perovskite but also harnesses the well-established infrastructure and rapid response capabilities of silicon, offering the promise of achieving both broad-spectrum and high-speed photodetection in a single, transformative platform. The integration of SC perovskite onto silicon substrates using functional groups at the interface has been a notable development in the field,[256] although it is accompanied by the potential drawback of introducing trapping states at the Si–SC perovskite interface, which could lead to an undesirable increase in the response time for the photodetector.

Due to this limitation, more direct and simplified methods for growing SC perovskite directly onto Si wafers while concurrently enhancing the interface quality are required. This would reduce the response time of the resulting photodetector and would represent an important milestone in the overall performance and versatility of hybrid perovskite-Si devices. Geng et al. directly integrated $MAPbBr_3$ SC onto silicon wafers using an antisolvent vapor-assisted crystallization method, leading to a significantly improved interface between these materials.[257] A fabricated $Si/MAPbBr_3/Au$ heterojunction photodetector exhibited a wide spectral sensitivity spanning from 405 to 1064 nm, an exceptional detectivity of up to 5.9×10^{10} Jones at a bias voltage of −1 V, and an exceptionally rapid response time of just 520 ns. The key driver for these results was the enhanced interface quality between the Si substrate and SC perovskite material. This study underscores the pivotal role of interface engineering in advancing photodetection technology, promising high-performance photodetectors with broad spectral coverage, sensitivity, and rapid response times.

Silica coatings offer numerous benefits for perovskite-based photodetectors,[258] including acting as a passivation layer, thus mitigating surface defects that can trap charge carriers and reduce the efficiency of the device. It can also serve as a protective barrier against moisture and oxygen, enhancing the stability and longevity of the

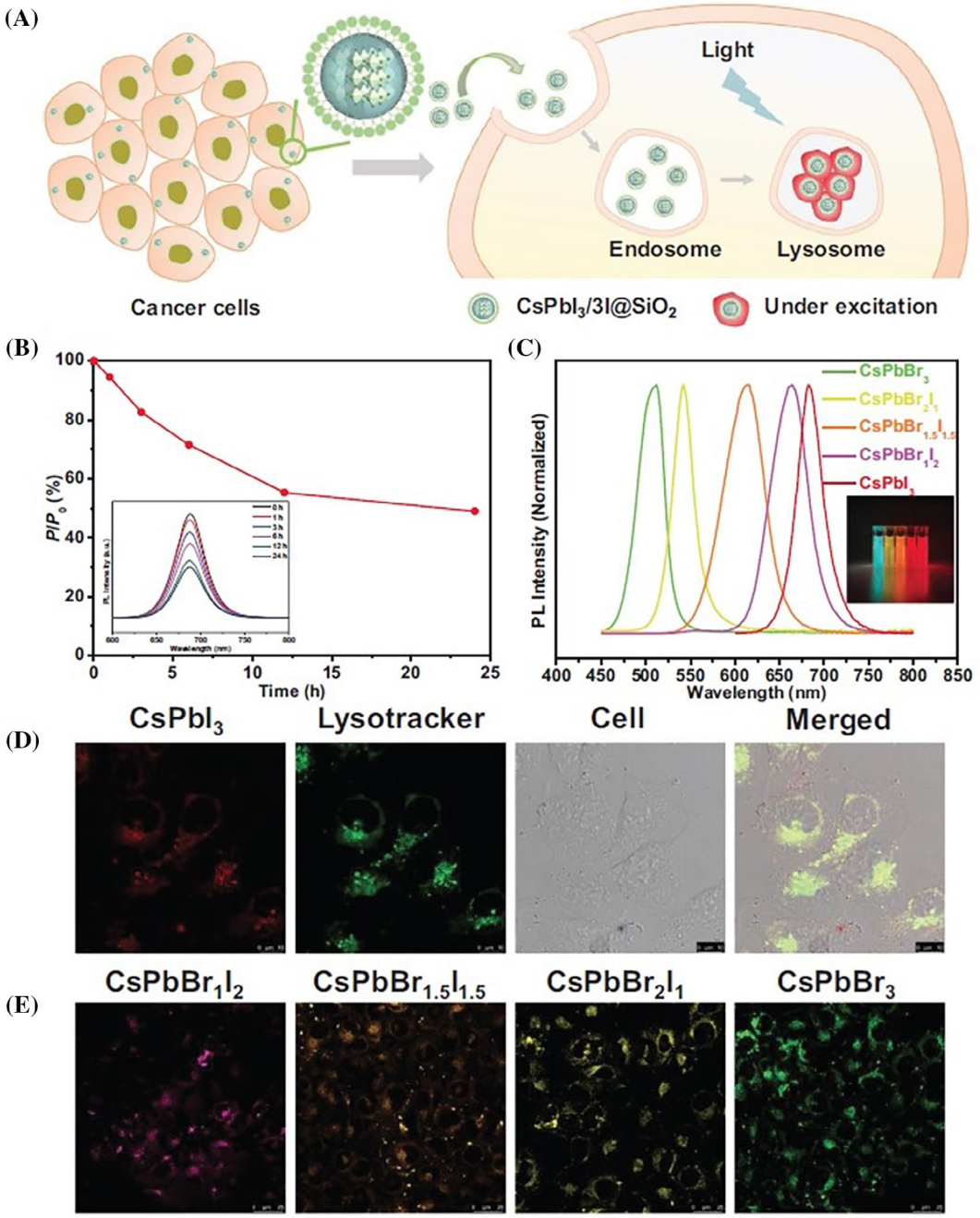

FIGURE 18 Bio-imaging of all-inorganic HP NCs. (A) Schematic representation of $CsPbI_3/3I@SiO_2$ phospholipid micelles; (B) Stability test: emission intensity and PL spectra of $CsPbI_3/3I@SiO_2$ phospholipid micelles kept in water for 24 h; (C) Emission spectra of $CsPbBr_3$ (emission: 510 nm), $CsPbBr_2I_1$ (emission: 542 nm), $CsPbBr_{1.5}I_{1.5}$ (emission: 616 nm), $CsPbBr_1I_2$ (emission: 664 nm), and $CsPbI_3$ (emission: 680 nm) QDs; the inset shows the photo image of the perovskite samples; (D) CLSM images of MDA-MB-231 cells upon incubation with $CsPbI_3/3I@SiO_2$ phospholipid micelles; scale bars represent 10 μm; (E) CLSM images of MDA-MB-231 cells upon incubation with $CsPbBr_3$, $CsPbBr_2I_1$, $CsPbBr_{1.5}I_{1.5}$, and $CsPbBr_1I_2$ QDs; scale bars represent 25 μm. Reprinted with permission.[247] Copyright 2022, Wiley-VCH.

perovskite material. Additionally, the engineered refractive index of silica coatings minimizes optical reflection, thus maximizing light absorption within the perovskite layer. Silica coatings also create a smoother surface, reducing scattering-induced losses and improving overall photodetector performance. They also offer greater mechanical strength, making them valuable for flexible photodetector applications. Finally, in tandem photodetectors, silica can act as an optical spacer, optimizing the optical path length and enhancing device efficiency.[259,260]

5.6 | Optoelectronic synaptic device

The emergence of optogenetics, a revolutionary technique in neuroscience, has sparked increased enthusiasm for the advancement of optoelectronic synaptic devices.[261,262] This surge in research is driven by the crucial role of the visual cortex system in processing information. These devices are intricately designed to replicate the nuanced functionalities of biological synapses under optical stimulation. The significance of these optoelectronic synaptic devices lies in their pivotal contribution to realizing artificial neural networks through the integration of optoelectronic components. The primary goal of this study is to meet the growing demands for high-performance neuromorphic computing, which seeks to replicate the intricate processes of the human brain.[263–266] To facilitate the widespread adoption of such computing systems, the strategic advantage of incorporating advanced silicon (Si) technologies, particularly Si photonics, is acknowledged. Consequently, the focus has shifted toward advancing the development of optoelectronic synaptic devices by leveraging Si materials. Within this realm, the Si nanomembrane (NM) stands out as a prominent candidate, given its potential for ultralow energy consumption, which is an essential attribute for efficient synaptic devices. However, the limited light absorption of Si NMs significantly hinders the achievement of high sensitivity to optical stimulation. Addressing this challenge requires exploring hybrid structures that seamlessly integrate Si NM with an optoelectronic material with superior optical absorption. This direction stands as a compelling focus for further research and development, holding the potential to overcome current limitations and unlock new possibilities in the field of optoelectronic synaptic devices.

Yin et al. successfully demonstrated the implementation of synaptic transistors using a hybrid structure that incorporates Si NM and perovskite materials.[267] This innovative hybrid design leverages the synergistic combination of the carrier transport capabilities of Si NMs and the superior optical absorption of perovskite. The functionality of these devices heavily relies on photogating, a process facilitated by the Si-NM/perovskite heterojunction, which plays a central role in the operation of synaptic transistors. Notably, the tuneability of the excitatory post-synaptic current is achieved through back gate-enabled adjustments, mimicking visual learning and memory processes. The dynamic adaptability of these synaptic devices is particularly evident in various mood states modeled by long-term memory. Impressively, these devices exhibit responsiveness to low optical power densities, specifically at 1 $\mu W/cm^2$, highlighting their efficiency in optical stimulation. Furthermore, the energy consumption of these devices is remarkably low, approximately 1 pJ, especially at a drain voltage of 0.01 V. The current state-of-the-art performance achieved through the hybrid structure of Si NM and perovskite has significant implications for advancing neuromorphic computing. By leveraging the benefits of Si-based optoelectronic integration, these devices can be used to develop high-performance and energy-efficient neuromorphic computing systems.[268]

6 | CHALLENGES, FUTURE IMPLICATIONS, AND OPPORTUNITIES FOR RESEARCH

6.1 | Surface functionalization of silica

The surface functionalization of silica refers to the process of modifying the surface of silica particles with different functional groups or molecules. This can be achieved by attaching organic or inorganic molecules onto the silica surface via covalent or non-covalent interactions. The functionalization of silica particles can give rise to new properties, such as hydrophilicity, hydrophobicity, and specific chemical or biological reactivity. Some common methods for the surface functionalization of silica particles include silanization (reaction of silane molecules with the hydroxyl groups within silica) and surface coating (involves depositing a layer of material onto the surface of silica via physical or chemical methods). Surface-functionalized silica particles have been used in a variety of applications, including drug delivery, catalysis, sensing, and separation science. There are many challenges associated with this method:

i. Surface reactivity: HP NCs have a high surface area-to-volume ratio, implying that most atoms within the NCs are located at the surface. The high surface reactivity can lead to the formation of surface defects and trap states that can reduce the stability and performance of the NCs. Additionally, the high reactivity of the surface can make it difficult to form a stable and uniform silica coating, as the silica precursors may react with the surface of the NCs before a complete coating is formed. To address this, researchers often use surface passivation techniques to stabilize the surface of the HP NCs before functionalizing with silica. These passivation techniques include the use of organic ligands or inorganic coatings to protect the surface of the NCs and reduce the formation of surface defects during the functionalization process.

ii. Colloidal stability: HP NCs are typically synthesized via a solution-based process and are often suspended in a solvent or capped with organic ligands to maintain colloidal stability. However, this can make it difficult to control the aggregation and sedimentation of the colloidal particles during the functionalization process. Aggregation can lead to the formation of larger particles and the loss of desirable properties, while sedimentation can result in non-uniform functionalization and deposition. To combat this, researchers use various techniques to control the colloidal stability of the HP NCs during functionalization; this can include the optimization of the surface passivation and functionalization conditions to minimize aggregation and sedimentation, as well as techniques such as centrifugation or size exclusion chromatography to purify the NCs and subsequently separate them from any aggregated or sedimented particles. Additionally, alternative synthesis methods that produce HP NCs with improved colloidal stability can also be explored, such as using inverse micelle methods or encapsulating the NCs in mesoporous silica matrices.

iii. Silica coating thickness: The thickness of the silica coating in perovskite materials is crucial because of its multifaceted impact on device performance and stability. First, it serves as a protective barrier, shielding the perovskite layer from environmental factors such as moisture, oxygen, and UV radiation, which could degrade the material over time. Second, optimal silica thickness contributes to structural stability by preventing degradation mechanisms such as ion migration and phase transitions induced by external stimuli. Moreover, controlling silica thickness contributes to surface passivation, thereby reducing surface defects and trap states that can impede device efficiency by minimizing non-radiative recombination. In addition, the thickness of the silica coating plays a pivotal role in tuning the optical properties of perovskite materials, thereby influencing the characteristics related to light absorption and emission. Furthermore, ensuring the appropriate thickness ensures compatibility with other device components, thereby facilitating efficient charge extraction and transport. In essence, precise control over silica coating thickness is fundamental for maximizing the performance, stability, and longevity of perovskite-based optoelectronic devices.

iv. Surface passivation: Surface passivation is a critical step in the functionalization of HP NCs. Surface defects and trap states can form on the surface of the NCs, and these defects can act as charge recombination centers and reduce the PL efficiency of the NCs. Therefore, surface passivation is used to protect the surface of the NCs and reduce the formation of these defects. Passivation can be achieved using a variety of organic or inorganic ligands, such as alkylamines, phosphonic acids, or metal halides. These ligands bind to the surface of the NCs and form a barrier that prevents the formation of surface defects. Additionally, passivation also improves the stability of the NCs by protecting them from oxidation and other reactions. Therefore, surface passivation is an essential step in the functionalization of halide perovskite nanocrystals to ensure their optimal performance and stability.

v. Reproducibility: Reproducibility and scalability are critical factors to be considered in the synthesis and functionalization of HP NCs. It is essential to develop reliable and reproducible synthetic methods that can produce high-quality NCs with consistent properties. This requires a deep understanding of the underlying mechanism of the NCs and the functionalization process. Additionally, the functionalization process needs to be scalable to enable the synthesis of large amounts of NCs for commercial applications. A notable approach to achieving sufficient reproducibility and scalability involves developing standardized protocols and quality control procedures that can ensure the consistency of the synthesis and functionalization processes across different batches and laboratories. This can involve the rigorous characterization of the NCs and the functionalized materials using techniques such as X-ray diffraction, transmission electron microscopy, and PL spectroscopy. Additionally, automated synthesis and functionalization platforms can also be developed to reduce the variability in the process and increase the throughput.

Overcoming these challenges requires a combination of advanced synthetic and analytical techniques, as well as a deep understanding of the surface chemistry and physics of HP NCs. Su et al. developed an approach for the in situ synthesis of $CsPbX_3$ NCs on porous colloidal silica spheres, effectively preventing anion exchange and enhancing photostability. The synthesized $SiO_2/CsPbBr_3$ composite material was then used to make single-layer WLEDs.[142] The silica spheres were first coated with polyvinylpyrrolidone (PVP) to prevent the total dissolution by NaOH during the consequent etching steps. The resulting PVP silica spheres were then etched with NaOH. The porous SiO_2 spheres were then transferred to tri-n-octylphosphine (TOP) to obtain an excellent dispersion in toluene. The silanol groups that contain oxygen

can bond to the TOP molecules and change the hydrophobic property of the silica particles to confirm that the porous silica was uniformly well-dispersed in the nonpolar toluene solvent. Finally, the obtained dispersion was quickly added to the container containing the $PbBr_2$ precursor to yield the $SiO_2/CsPbBr_3$ composite. The resulting composite exhibited exceptional stability and a narrow emission line width.

The functionalization of MSNs involves the introduction of specific chemical groups onto the surface of the NPs with the aim of modifying surface properties such as charge, hydrophobicity, and reactivity. This can be achieved via several methods, including covalent attachment, electrostatic adsorption, or the physical encapsulation of functional molecules onto the surface of the MSN. Notably, Kumari et al. systematically functionalized MSNs as peroxidase mimics for protein detection.[269] The azide group was found to reside primarily inside the pores of the spherical MSN. Kumari et al. also controlled the azide functionalization from 1% to 10% (N_3-MSN). Additionally, they also grafted 3-aminopropyl triethoxysilane onto the surface of synthesized N_3-MSN (NH_2-N_3-MSN); a biuret-modified Fe-tetraamido macrocyclic ligand (Fe-TAML) was then "clicked" onto NH_2-N_3-MSN via copper-catalyzed azide-alkyne cycloaddition (*CuAAc*) reactions. The hybrid material exhibited a significantly higher catalytic activity (1000-fold) than natural horseradish peroxidase. These materials can be used to stabilize the HP NCs and applied for catalytic applications. With the ongoing research and development in this field, it is expected that novel coating methods will emerge, leading to the improved stability and durability of perovskite QDs for various applications.

6.2 | Phase purity of perovskite nanocrystals

The phase purity of perovskite NCs refers to the degree to which the NCs are composed of a single crystalline phase. In other words, it indicates the purity of the perovskite material. High phase purity is crucial for the performance of perovskite NCs, as it affects the optical and electronic properties of the resulting NCs. For example, a high phase purity can lead to improved light absorption, enhanced charge carrier mobility, and improved NC stability. Silica is important for the synthesis of phase-pure HP NCs in that it provides a controlled environment for crystal growth. The silica added to the synthesis solution acts as a template for the nucleation and growth of the perovskite crystals, promoting the formation of phase-pure NCs with well-defined sizes and shapes. Silica also acts as a capping agent for the perovskite NCs, helping to stabilize the crystal structure and preventing the formation of undesired phases or defects. This is achieved by functionalizing the surface of the NCs with silica, which in turn protects the crystal surface and prevent unwanted reactions with the surrounding environment. Furthermore, the presence of silica in the synthesis solution promotes the diffusion and transport of the precursor species for crystal growth, which can help to control crystal growth kinetics and improve the crystal size and morphology. This is particularly useful for controlling the crystal size and shape of perovskite NCs, which has a significant impact on their resulting optical and electronic properties.

6.3 | Homogeneous distribution of perovskite nanocrystals inside silicon matrices

The homogeneous distribution of perovskite NCs is important for optoelectronic devices because it ensures that the properties of the material are consistent throughout the device, which subsequently leads to improved device performance and stability. Non-uniformly distributed perovskite NCs can result in defects, uneven charge transport, and reduced efficiency, which can shorten the lifespan of the device. Additionally, homogeneous distribution also improves the reproducibility of the device.

6.4 | Thin-film fabrication

There are several challenges associated with the thin-film fabrication of HP–SiO_2 composites:

i. Interfacial engineering issues: HP and SiO_2 have different crystal structures, thermal expansion coefficients, and chemical properties, which makes it difficult to achieve a stable and compatible interface between the two materials. The crystal structure of HP is typically cubic or tetragonal, while SiO_2 has a hexagonal or rhombohedral crystal structure. The difference in crystal structures can result in lattice mismatch and strain at the interface, which can lead to defects and reduced device performance.
ii. Quality: The quality of a thin-film is crucial to the performance of the device. However, the deposition process for HP–SiO_2 composites is complex and requires the precise control of deposition parameters such as temperature, pressure, and deposition rate. Any deviation from the optimal conditions can lead to poor film quality, which can have a negative

impact on the efficiency and performance of the resulting devices.

For example, a non-uniform thickness or composition of a thin-film can result in variations in the optical and electronic properties, which affects light absorption and carrier transport in the device. Cracks or pinholes in the thin-film can lead to current leakage and reduced device stability. Defects such as trap states or GBs can also reduce the carrier mobility and increase the recombination rate, which can lower the efficiency of the device.

iii. Morphology: The morphology of a thin-film (grain size, orientation, and crystallinity) also affects the performance of the resulting device. However, it is difficult to control the morphology of HP–SiO_2 composites due to the complexity involved in the deposition process and the determination of composition and post-treatment conditions. For example, the grain size and orientation of HP can affect the charge transport and recombination rate in the resulting device. However, it is difficult to control the grain size and orientation of HP due to the nucleation and growth of HP during the deposition process.
iv. Reproducibility and scalability: The reproducibility and scalability of HP–SiO_2 thin-film composites still presents as a prevalent issue, as device performance must be consistent across batches, and the fabrication process must be reliable and reproducible. The scalability of these processes for commercial applications is also difficult.

In summary, we expect that these challenges will be addressed in the coming years and that silicon compounds will play a critical role in enhancing the stability and performance of HP based-optoelectronic devices.

6.5 | Cost control for the use of silicon compounds in perovskite nanocrystal stabilization and device fabrication

Controlling the cost of material synthesis and device fabrication when using silicon compounds for perovskite NCs is a critical consideration for researchers and industrial applications. While these compounds are essential for stabilizing and encapsulating perovskite NCs, efficient use, recycling, and collaboration can help reduce the overall cost of production. In terms of material selection, researchers should carefully select cost-effective silicon compounds, striking a balance between performance and price. Additionally, they should assess the availability of these compounds from various suppliers to ensure a stable supply chain, avoiding potential disruptions. Recycling and reuse strategies are also critical for cost reduction. By implementing protocols for recycling silicon compounds, researchers can significantly cut costs. In particular, after encapsulating or stabilizing perovskite NCs, these compounds can be recovered and repurposed in subsequent processes, effectively extending their utility and reducing the need for fresh materials.

Process optimization is another key factor in cost control. Researchers can fine-tune the synthesis and fabrication processes to minimize the quantity of silicon compounds required. This may involve exploring alternative methods or techniques that require a lower quantity of silicon compounds while maintaining the desired product quality. Collaboration and information sharing within the research community are also valuable strategies. Collaborative efforts among research institutions, universities, and industry players can facilitate the exchange of cost-saving strategies and best practices. Sharing information regarding efficient silicon compound usage can benefit the research ecosystem as a whole, collectively reducing costs and promoting more cost-effective approaches. Furthermore, scale-up efforts can lead to economies of scale, effectively reducing the per-unit cost of silicon compounds as the demand for perovskite-based devices grows.

However, it is crucial to balance this with the fabrication of materials and devices with consistent quality. Rushed scaling efforts that compromise quality can ultimately prove counterproductive. Nevertheless, cost control efforts come with their own set of challenges and considerations. As perovskite-based technologies continue to advance, achieving a balance between cost-effectiveness and product quality is key to their successful commercialization.

6.6 | Various properties and advantages of silicon-based compounds for improving the stability of perovskites

The selection of suitable silicon-based compounds for stabilizing specific halide perovskite materials involves a nuanced consideration of several key requirements. With the diverse family of HP characterized by varying structures, forms, and dimensions, the compatibility of silicon-based compounds becomes crucial. First, chemical compatibility is paramount, ensuring that the chosen silicon material harmonizes with the chemical composition of the targeted halide perovskite to prevent adverse interactions. The ability to fine-tune surface passivation is essential, given that different halide perovskite compositions exhibit unique surface properties, requiring silicon

compounds capable of effectively mitigating surface defects. Band alignment is a critical consideration, requiring the energy bands of the silicon layer to align appropriately with those of the halide perovskite to facilitate efficient charge transport and extraction. The silicon-based compound should also possess barrier properties tailored to the environmental sensitivities of the specific halide perovskite, safeguarding against degradation from factors such as moisture and oxygen. Optical properties, including refractive index and transparency, must be considered to optimize light management within the solar cell according to the optical characteristics of the targeted perovskite. Finally, fabrication compatibility is essential to ensure that the silicon-based material seamlessly integrates into the manufacturing processes employed for the specific halide perovskite solar cell, allowing for efficient and scalable production. This holistic approach considers the intricacies of both silicon compounds and the diverse range of halide perovskite structures, enabling the tailored design of stable and efficient solar cell systems. Ongoing research will endeavor to refine the understanding of these requirements, aiming to unlock the full potential of silicon-based compounds in enhancing the stability of diverse halide perovskite materials.

The choice of silicon-based compounds to stabilize halide perovskite active layers depends on the specific requirements of various device applications. In solar cells, prioritizing light absorption, which is crucial for optimization, requires silicon compounds to exhibit chemical compatibility with halide perovskite, effectively passivate surface defects, enhance optical properties for improved absorption, and promote efficient charge transport. For LEDs, silicon materials must facilitate effective carrier injection and transport within the perovskite layer. This entails optical compatibility to minimize the absorption losses of the emitted light. In photodetectors, the focus is on responsivity and charge collection, necessitating silicon-based compounds that enhance light absorption and facilitate efficient charge extraction. In transistors, high charge mobility is vital, requiring silicon layers that promote effective charge transport and ensure a high-quality interface with the perovskite active layer. Memory devices based on HP need silicon compounds that aid charge retention within the perovskite layer and influence switching characteristics for reliable write and erase operations. Designing silicon-based materials to fit these specific needs ensures their effectiveness in stabilizing halide perovskite active layers across various device applications. This, in turn, paves the way for the wider use and integration of perovskite technologies across diverse technologies.

Silicon-based compounds have emerged as pivotal elements for enhancing the stability of perovskite solar cells, thereby addressing a key barrier to their widespread adoption. Their unique properties play a significant role in mitigating degradation issues associated with perovskite solar cells. These compounds excel in passivating defects on the surface of the perovskite film, effectively minimizing non-radiative recombination and thereby preserving the cell's performance and stability. Moreover, these compounds excel as barrier layers, shielding the perovskite film from detrimental factors such as moisture and oxygen, which can induce degradation. They can also serve as electron or hole transport layers, thereby boosting charge extraction and overall device efficiency. Importantly, their compatibility with common fabrication processes simplifies integration into existing manufacturing techniques. Furthermore, the tuneable optical properties of silicon-based materials enable researchers to optimize light management within the solar cell, thereby enhancing light absorption. Benefitting from commendable thermal stability and cost-effectiveness attributed to the abundance of silicon, these compounds present themselves as promising candidates for enhancing the durability and commercial viability of perovskite solar cells on a large scale. Ongoing research endeavors persist in exploring and refining the potential of silicon-based materials in effectively addressing the stability challenges associated with perovskite solar technology.

ACKNOWLEDGMENTS

This work was supported by the National Research Foundation of Korea (grant nos. 2021R1F1A1062528, 2021R1A4A5031805, 2021R1A2C1006113, and BrainLink RS-2023-00236798).

CONFLICT OF INTEREST STATEMENT

The authors declare no conflict of interest.

ORCID

Atanu Jana https://orcid.org/0000-0001-6566-0438
Hyunsik Im https://orcid.org/0000-0002-4461-8078

REFERENCES

1. Cui X, Chen Y, Zhang M, et al. Tailoring carrier dynamics in perovskite solar cells via precise dimension and architecture control and interfacial positioning of plasmonic nanoparticles. *Energy Environ Sci*. 2020;13(6):1743-1752.
2. Bai Y, Lin Y, Ren L, et al. Oligomeric silica-wrapped perovskites enable synchronous defect passivation and grain stabilization for efficient and stable perovskite photovoltaics. *ACS Energy Lett*. 2019;4(6):1231-1240.
3. Hwang SH, Roh J, Lee J, Ryu J, Yun J, Jang J. Size-controlled SiO_2 nanoparticles as scaffold layers in thin-film perovskite solar cells. *J Mater Chem A*. 2014;2(39):16429-16433.

4. Ahangharnejhad RH, Song Z, Mariam T, et al. Protecting perovskite solar cells against moisture-induced degradation with sputtered inorganic barrier layers. *ACS Appl Energy Mater*. 2021;4(8):7571-7578.
5. Yoo GY, Azmi R, Kim C, et al. Stable and colorful perovskite solar cells using a nonperiodic SiO_2/TiO_2 multi-nanolayer filter. *ACS Nano*. 2019;13(9):10129-10139.
6. Lee S, Kim CU, Bae S, et al. Improving light absorption in a perovskite/Si tandem solar cell via light scattering and UV-down shifting by a mixture of SiO_2 nanoparticles and phosphors. *Adv Funct Mater*. 2022;32(35):2204328.
7. Wang X, Wang W, Liu J, et al. Reducing optical reflection loss for perovskite solar cells via printable mesoporous SiO_2 antireflection coatings. *Adv Funct Mater*. 2022;32(44):2203872.
8. Wang Y, Zhou X, Liang C, et al. Enhanced efficiency of perovskite solar cells by using core-ultrathin shell structure $Ag@SiO_2$ nanowires as plasmonic antennas. *Adv Electron Mater*. 2017;3(11):1700169.
9. Lee K, Yoon CM, Noh J, Jang J. Morphology-controlled mesoporous SiO_2 nanorods for efficient scaffolds in organometal halide perovskite solar cells. *Chem Commun*. 2016;52(22):4231-4234.
10. Chandrasekhar PS, Dubey A, Reza KM, et al. Higher efficiency perovskite solar cells using $Au@SiO_2$ core–shell nanoparticles. *Sustain Energy Fuels*. 2018;2(10):2260-2267.
11. Trinh CK, Lee H, So MG, Lee CL. Synthesis of chemically stable ultrathin SiO_2-coated core–shell perovskite QDs via modulation of ligand binding energy for all-solution-processed light-emitting diodes. *ACS Appl Mater Interfaces*. 2021;13(25):29798-29808.
12. Ding J, Jing L, Cheng X, et al. Design growth of $MAPbI_3$ single crystal with (220) facets exposed and its superior optoelectronic properties. *J Phys Chem Lett*. 2018;9(1):216-221.
13. Ding N, Zhou D, Sun X, et al. Highly stable and water-soluble monodisperse $CsPbX_3/SiO_2$ nanocomposites for white-LED and cells imaging. *Nanotechnology*. 2018;29(34):345703.
14. Di X, Shen L, Jiang J, et al. Efficient white LEDs with bright green-emitting $CsPbBr_3$ perovskite nanocrystal in mesoporous silica nanoparticles. *J Alloys Compd*. 2017;729:526-532.
15. Sun C, Zhang Y, Ruan C, et al. Efficient and stable white LEDs with silica-coated inorganic perovskite quantum dots. *Adv Mater*. 2016;28(45):10088-10094.
16. Xu Y, Hu X, Tang H, et al. Highly efficient silica coated perovskite nanocrystals with the assistance of ionic liquids for warm white LEDs. *Nanoscale*. 2023;15(2):631-643.
17. Li X, Ma W, Liang D, Cai W, Zhao S, Zang Z. High-performance $CsPbBr_3@Cs_4PbBr_6/SiO_2$ nanocrystals via double coating layers for white light emission and visible light communication. *eeScience*. 2022;2(6):646-654.
18. Liu A, Zhu H, Bai S, et al. High-performance inorganic metal halide perovskite transistors. *Nat Electron*. 2022;5(2):78-83.
19. Liu J, Haroldson R, Verkhogliadov G, et al. Ultrasensitive perovskite photodetector achieved when configured with a Si metal oxide semiconductor field-effect transistor. *Adv Photonics Res*. 2023;4(1):2200034.
20. Jana A, Cho S, Patil SA, et al. Perovskite: scintillators, direct detectors, and x-ray imagers. *Mater Today*. 2022;55:110-136.
21. Getachew G, Wibrianto A, Rasal AS, Direrse WB, Chang JY. Metal halide perovskite nanocrystals for biomedical engineering: recent advances, challenges, and future perspectives. *Coord Chem Rev*. 2023;482:215073.
22. Kumar P, Patel M, Park C, et al. Highly luminescent biocompatible $CsPbBr_3@SiO_2$ core–shell nanoprobes for bioimaging and drug delivery. *J Mater Chem B*. 2020;8(45):10337-10345.
23. Song W, Wang Y, Wang B, et al. Super stable $CsPbBr_3@SiO_2$ tumor imaging reagent by stress-response encapsulation. *Nano Res*. 2020;13(3):795-801.
24. Wu H, Chen Y, Zhang W, Khan MS, Chi Y. Water-dispersed perovskite nanocube@SiO_2-C_{18}-PC core–shell nanoparticles for cell imaging. *ACS Appl Nano Mater*. 2021;4(11):11791-11800.
25. Avugadda SK, Castelli A, Dhanabalan B, et al. Highly emitting perovskite nanocrystals with 2-year stability in water through an automated polymer encapsulation for bioimaging. *ACS Nano*. 2022;16(9):13657-13666.
26. Pramanik A, Patibandla S, Gao Y, Gates K, Ray PC. Water triggered synthesis of highly stable and biocompatible 1D nanowire, 2D nanoplatelet, and 3D nanocube $CsPbBr_3$ perovskites for multicolor two-photon cell imaging. *JACS Au*. 2021;1(1):53-65.
27. Zhang H, Wang X, Liao Q, et al. Embedding perovskite nanocrystals into a polymer matrix for tunable luminescence probes in cell imaging. *Adv Funct Mater*. 2017;27(7):1604382.
28. Yang Z, Xu J, Zong S, et al. Lead halide perovskite nanocrystals–phospholipid micelles and their biological applications: multiplex cellular imaging and in vitro tumor targeting. *ACS Appl Mater Interfaces*. 2019;11(51):47671-47679.
29. Lian H, Li Y, Saravanakumar S, et al. Metal halide perovskite quantum dots for amphiprotic bio-imaging. *Coord Chem Rev*. 2022;452:214313.
30. Talianov PM, Peltek OO, Masharin M, et al. Halide perovskite nanocrystals with enhanced water stability for upconversion imaging in a living cell. *J Phys Chem Lett*. 2021;12(37):8991-8998.
31. Gao J, Qian X, Wei Q, et al. Construction of core-shell cesium lead bromide-silica by precipitation coating method with applications in aqueous photocatalysis. *J Colloid Interface Sci*. 2022;623:974-984.
32. Li S, Lei D, Ren W, et al. Water-resistant perovskite nanodots enable robust two-photon lasing in aqueous environment. *Nat Commun*. 2020;11(1):1192.
33. Cherevkov S, Azizov R, Sokolova A, et al. Interface chemical modification between all-inorganic perovskite nanocrystals and porous silica microspheres for composite materials with improved emission. *Nanomaterials*. 2021;11(1):119.
34. Singh AN, Kajal S, Kim J, Jana A, Kim JY, Kim KS. Interface engineering driven stabilization of halide perovskites against moisture, heat, and light for optoelectronic applications. *Adv Energy Mater*. 2020;10(30):2000768.
35. De Roo J, Ibáñez M, Geiregat P, et al. Highly dynamic ligand binding and light absorption coefficient of cesium lead bromide perovskite nanocrystals. *ACS Nano*. 2016;10(2):2071-2081.
36. Dong X, Fang X, Lv M, et al. Improvement of the humidity stability of organic–inorganic perovskite solar cells using ultrathin Al_2O_3 layers prepared by atomic layer deposition. *J Mater Chem A*. 2015;3(10):5360-5367.

37. Yang S, Chen S, Mosconi E, et al. Stabilizing halide perovskite surfaces for solar cell operation with wide-bandgap lead oxysalts. *Science*. 2019;365(6452):473-478.
38. Jana A, Kim KS. Water-stable, fluorescent organic−inorganic hybrid and fully inorganic perovskites. *ACS Energy Lett*. 2018; 3(9):2120-2126.
39. Zhong Q, Liu J, Chen S, et al. Highly stable $CsPbX_3/PbSO_4$ core/shell nanocrystals synthesized by a simple post-treatment strategy. *Adv Opt Mater*. 2021;9(5):2001763.
40. Wang H, Wei Y, Li H, et al. Octylammonium sulfate decoration enhancing the moisture durability of quasi-2D perovskite film for light-emitting diodes. *Adv Mater Interfaces*. 2021; 8(13):2100442.
41. Liu H, Worku M, Mondal A, et al. Efficient and stable blue light emitting diodes based on $CsPbBr_3$ nanoplatelets with surface passivation by a multifunctional organic sulfate. *Adv Energy Mater*. 2023;13(33):2201605.
42. Sardar S, Maity P, Mittal M, et al. Synthesis and characterization of polypyrrole encapsulated formamidinium lead bromide crystals for fluorescence memory recovery. *J Mol Liq*. 2022;349:118485.
43. Liang S, Zhang M, Biesold GM, et al. Recent advances in synthesis, properties, and applications of metal halide perovskite nanocrystals/polymer nanocomposites. *Adv Mater*. 2021; 33(50):2005888.
44. Zhao Y, He Z, Ren F, et al. One-step preparation of blue-emitting $CsPbBr_3$ quantum dots loaded on natural mineral halloysite nanotube. *Appl Clay Sci*. 2021;208:106110.
45. Hao J, Qu X, Qiu L, et al. One-step loading on natural mineral halloysite nanotube: an effective way to enhance the stability of perovskite $CsPbX_3$ (X = Cl, Br, I) quantum dots. *Adv Opt Mater*. 2019;7(4):1801323.
46. Wang Q, Zheng X, Deng Y, Zhao J, Chen Z, Huang J. Stabilizing the α-phase of $CsPbI_3$ perovskite by sulfobetaine zwitterions in one-step spin-coating films. *Joule*. 2017;1(2): 371-382.
47. Chen Q, Yang X, Zhou Y, Song B. Zwitterions: promising interfacial/doping materials for organic/perovskite solar cells. *New J Chem*. 2021;45(34):15118-15130.
48. Krieg F, Ochsenbein ST, Yakunin S, et al. Colloidal $CsPbX_3$ (X = Cl, Br, I) nanocrystals 2.0: zwitterionic capping ligands for improved durability and stability. *ACS Energy Lett*. 2018; 3(3):641-646.
49. Mollick S, Mandal TN, Jana A, Fajal S, Desai AV, Ghosh SK. Ultrastable luminescent hybrid bromide perovskite@MOF nanocomposites for the degradation of organic pollutants in water. *ACS Appl Nano Mater*. 2019;2(3):1333-1340.
50. Zhang W, Saliba M, Stranks SD, et al. Enhancement of perovskite-based solar cells employing core-shell metal nanoparticles. *Nano Lett*. 2013;13(9):4505-4510.
51. Kulbak M, Gupta S, Kedem N, et al. Cesium enhances long-term stability of lead bromide perovskite-based solar cells. *J Phys Chem Lett*. 2016;7(1):167-172.
52. Zhang X, Lv J, Liu J, et al. Stable EMT type zeolite/$CsPbBr_3$ perovskite quantum dot nanocomposites for highly sensitive humidity sensors. *J Colloid Interface Sci*. 2022;616:921-928.
53. Fulari AV, Jana A, Han J, et al. Precursor silanization assisted synthesis and optical tuning of dual-phase perovskite nanocrystals embedded in silica matrix with high environmental stability. *J Colloid Interface Sci*. 2023;630(Pt A): 212-222.
54. Huang S, Li Z, Kong L, Zhu N, Shan A, Li L. Enhancing the stability of $CH_3NH_3PbBr_3$ quantum dots by embedding in silica spheres derived from tetramethyl orthosilicate in "waterless" toluene. *J Am Chem Soc*. 2016;138(18):5749-5752.
55. Zhong Q, Cao M, Hu H, et al. One-pot synthesis of highly stable $CsPbBr_3@SiO_2$ core–shell nanoparticles. *ACS Nano*. 2018; 12(8):8579-8587.
56. Zhu L, Wu C, Riaz S, Dai J. Stable silica coated DDAB-$CsPbX_3$ quantum dots and their application for white light-emitting diodes. *JOL*. 2021;233:117884.
57. González-Pedro V, Veldhuis SA, Begum R, et al. Recovery of shallow charge-trapping defects in CsPbX3 nanocrystals through specific binding and encapsulation with amino-functionalized silanes. *ACS Energy Lett*. 2018;3(6):1409-1414.
58. Tang X, Chen W, Liu Z, et al. Ultrathin, core–shell structured SiO_2 coated Mn^{2+}-doped perovskite quantum dots for bright white light-emitting diodes. *Small*. 2019;15(19):1900484.
59. Zhang F, Shi ZF, Ma ZZ, et al. Silica coating enhances the stability of inorganic perovskite nanocrystals for efficient and stable down-conversion in white light-emitting devices. *Nanoscale*. 2018;10(43):20131-20139.
60. Xu L, Chen J, Song J, et al. Double-protected all-inorganic perovskite nanocrystals by crystalline matrix and silica for triple-modal anti-counterfeiting codes. *ACS Appl Mater Interfaces*. 2017;9(31):26556-26564.
61. Hu Z, Liu Z, Bian Y, et al. Enhanced two-photon-pumped emission from in situ synthesized nonblinking $CsPbBr_3/SiO_2$ nanocrystals with excellent stability. *Adv Opt Mater*. 2018; 6(3):1700997.
62. Rosales BA, Schutt K, Berry JJ, Wheeler LM. Leveraging low-energy structural thermodynamics in halide perovskites. *ACS Energy Lett*. 2023;8(4):1705-1715.
63. Jin RJ, Lou YH, Wang ZK. Doping strategies for promising organic–inorganic halide perovskites. *Small*. 2023;19(16): 2206581.
64. Jana A, Meena A, Patil SA, et al. Self-assembly of perovskite nanocrystals. *Prog Mater Sci*. 2022;129:100975.
65. Li J, Han Z, Liu J, Zou Y, Xu X. Compositional gradient engineering and applications in halide perovskites. *Chem Commun*. 2023;59(35):5156-5173.
66. Otero-Martínez C, Fiuza-Maneiro N, Polavarapu L. Enhancing the intrinsic and extrinsic stability of halide perovskite nanocrystals for efficient and durable optoelectronics. *ACS Appl Mater Interfaces*. 2022;14(30):34291-34302.
67. Zheng X, Wu C, Jha SK, Li Z, Zhu K, Priya S. Improved phase stability of formamidinium lead triiodide perovskite by strain relaxation. *ACS Energy Lett*. 2016;1(5):1014-1020.
68. Kim G, Min H, Lee KS, Lee DY, Yoon SM, Il SS. Impact of strain relaxation on performance of α-formamidinium lead iodide perovskite solar cells. *Science*. 2020;370(6512):108-112.
69. Li Z, Yang M, Park JS, Wei SH, Berry JJ, Zhu K. Stabilizing perovskite structures by tuning tolerance factor: formation of formamidinium and cesium lead iodide solid-state alloys. *Chem Mater*. 2016;28(1):284-292.
70. Huang H, Bodnarchuk MI, Kershaw SV, Kovalenko MV, Rogach AL. Lead halide perovskite nanocrystals in the

research spotlight: stability and defect tolerance. *ACS Energy Lett*. 2017;2(9):2071-2083.
71. Charles B, Dillon J, Weber OJ, Islam MS, Weller MT. Understanding the stability of mixed A-cation lead iodide perovskites. *J Mater Chem A*. 2017;5(43):22495-22499.
72. Ma L, Guo D, Li M, et al. Temperature-dependent thermal decomposition pathway of organic–inorganic halide perovskite materials. *Chem Mater*. 2019;31(20):8515-8522.
73. Zhao J, Cai B, Luo Z, et al. Investigation of the hydrolysis of perovskite organometallic halide $CH_3NH_3PbI_3$ in humidity environment. *Sci Rep*. 2016;6(1):21976.
74. Huang J, Tan S, Lund PD, Zhou H. Impact of H_2O on organic–inorganic hybrid perovskite solar cells. *Energy Environ Sci*. 2017;10(11):2284-2311.
75. Leguy AMA, Hu Y, Campoy-Quiles M, et al. Reversible hydration of $CH_3NH_3PbI_3$ in films, single crystals, and solar cells. *Chem Mater*. 2015;27(9):3397-3407.
76. Askar AM, Bernard GM, Wiltshire B, Shankar K, Michaelis VK. Multinuclear magnetic resonance tracking of hydro, thermal, and hydrothermal decomposition of $CH_3NH_3PbI_3$. *J Phys Chem C*. 2017;121(2):1013-1024.
77. Zhao L, Kerner RA, Xiao Z, et al. Redox chemistry dominates the degradation and decomposition of metal halide perovskite optoelectronic devices. *ACS Energy Lett*. 2016;1(3):595-602.
78. Xiong H, Rui Y, Li Y, Zhang Q, Wang H. Hydrophobic coating over a $CH_3NH_3PbI_3$ absorbing layer towards air stable perovskite solar cells. *J Mater Chem C*. 2016;4(28):6848-6854.
79. Yu X, Wang Y, Gao P. The effect of redox reactions on the stability of perovskite solar cells. *ChemPhotoChem*. 2023;7(8): e202200311.
80. He J, Fang WH, Long R, Prezhdo OV. Why oxygen increases carrier lifetimes but accelerates degradation of $CH_3NH_3PbI_3$ under light irradiation: time-domain ab initio analysis. *J Am Chem Soc*. 2020;142(34):14664-14673.
81. Kerner RA, Xu Z, Larson BW, Rand BP. The role of halide oxidation in perovskite halide phase separation. *Joule*. 2021; 5(9):2273-2295.
82. Siegler TD, Dunlap-Shohl WA, Meng Y, et al. Water-accelerated Photooxidation of $CH_3NH_3PbI_3$ perovskite. *J Am Chem Soc*. 2022;144(12):5552-5561.
83. Lee JW, Kim SG, Yang JM, Yang Y, Park NG. Verification and mitigation of ion migration in perovskite solar cells. *APL Mater*. 2019;7(4):041111.
84. Roh T, Zhu H, Yang W, Liu A, Noh YY. Ion migration induced unusual charge transport in tin halide perovskites. *ACS Energy Lett*. 2023;8(2):957-962.
85. Mbumba MT, Malouangou DM, Tsiba JM, Bai L, Yang Y, Guli M. Degradation mechanism and addressing techniques of thermal instability in halide perovskite solar cells. *Sol Energy*. 2021;230:954-978.
86. Boyd CC, Cheacharoen R, Leijtens T, McGehee MD. Understanding degradation mechanisms and improving stability of perovskite photovoltaics. *Chem Rev*. 2019;119(5):3418-3451.
87. Ning Y, Lv L, Lu Y, et al. Investigation on thermal degradation process of polymer solar cells based on blend of PBDTTT-C and PC_{70} BM. *Int J Photoenergy*. 2014;2014:354837.
88. Kumar A, Bansode U, Ogale S, Rahman A. Understanding the thermal degradation mechanism of perovskite solar cells via dielectric and noise measurements. *Nanotechnology*. 2020; 31(36):365403.
89. Fang R, Wu S, Chen W, et al. [6,6]-Phenyl-C61-butyric acid methyl ester/cerium oxide bilayer structure as efficient and stable electron transport layer for inverted perovskite solar cells. *ACS Nano*. 2018;12(3):2403-2414.
90. Tan W, Bowring AR, Meng AC, McGehee MD, McIntyre PC. Thermal stability of mixed cation metal halide perovskites in air. *ACS Appl Mater Interfaces*. 2018;10(6):5485-5491.
91. Jeon NJ, Noh JH, Yang WS, et al. Compositional engineering of perovskite materials for high-performance solar cells. *Nature*. 2015;517(7535):476-480.
92. Saliba M, Orlandi S, Matsui T, et al. A molecularly engineered hole-transporting material for efficient perovskite solar cells. *Nat Energy*. 2016;1(2):15017.
93. Saliba M, Matsui T, Seo JY, et al. Cesium-containing triple cation perovskite solar cells: improved stability, reproducibility and high efficiency. *Energy Environ Sci*. 2016;9(6):1989-1997.
94. Abdi-Jalebi M, Dar MI, Sadhanala A, et al. Impact of monovalent cation halide additives on the structural and optoelectronic properties of $CH_3NH_3PbI_3$ perovskite. *Adv Energy Mater*. 2016;6(10):1502472.
95. Wu J, Li Y, Tan S, et al. Enhanced perovskite solar cell efficiency via the electric-field-induced approach. *ACS Appl Mater Interfaces*. 2020;12(24):27258-27267.
96. Hu J, Chen P, Luo D, et al. Tracking the evolution of materials and interfaces in perovskite solar cells under an electric field. *Commun Mater*. 2022;3(1):39.
97. Shi J, Li Y, Li Y, et al. Eliminating the electric field response in a perovskite heterojunction solar cell to improve operational stability. *Sci Bull*. 2021;66(6):536-544.
98. Nie J, Zhang Y, Li L, Zhang Y. High-performance Piezophototronic solar cells based on polarization modulation perovskite. *Adv Devices Instrum*. 2023;4:0025.
99. Mahapatra A, Prochowicz D, Tavakoli MM, Trivedi S, Kumar P, Yadav P. A review of aspects of additive engineering in perovskite solar cells. *J Mater Chem A*. 2020;8(1):27-54.
100. Deng W, Liang X, Kubiak PS, Cameron PJ. Molecular interlayers in hybrid perovskite solar cells. *Adv Energy Mater*. 2018;8(1):1701544.
101. Li L, Li B, Dong J, Zhang J. Roles of silanes and silicones in forming superhydrophobic and superoleophobic materials. *J Mater Chem A*. 2016;4(36):13677-13725.
102. Xie Y, Hill CAS, Xiao Z, Militz H, Mai C. Silane coupling agents used for natural fiber/polymer composites: a review. *Compos Part A Appl Sci Manuf*. 2010;41(7):806-819.
103. Asenath Smith E, Chen W. How to prevent the loss of surface functionality derived from Aminosilanes. *Langmuir*. 2008; 24(21):12405-12409.
104. Wang B, Li H, Dai Q, et al. Robust molecular dipole-enabled defect passivation and control of energy-level alignment for high-efficiency perovskite solar cells. *Angew Chem Int Ed*. 2021;60(32):17664-17670.
105. Dai Z, Yadavalli SK, Chen M, Abbaspourtamijani A, Qi Y, Padture NP. Interfacial toughening with self-assembled monolayers enhances perovskite solar cell reliability. *Science*. 2021; 372(6542):618-622.

106. Shi Y, Zhang H, Tong X, et al. Interfacial engineering via self-assembled thiol silane for high efficiency and stability perovskite solar cells. *Sol RRL*. 2021;5(7):2100128.
107. Liu C, Zhou X, Chen S, Zhao X, Dai S, Xu B. Hydrophobic Cu_2O quantum dots enabled by surfactant modification as top hole-transport materials for efficient perovskite solar cells. *Adv Sci*. 2019;6(7):1801169.
108. Bai Y, Dong Q, Shao Y, et al. Enhancing stability and efficiency of perovskite solar cells with crosslinkable silane-functionalized and doped fullerene. *Nat Commun*. 2016;7(1):12806.
109. Zhang Y, Hsu BYW, Ren C, Li X, Wang J. Silica-based nanocapsules: synthesis, structure control and biomedical applications. *Chem Soc Rev*. 2015;44(1):315-335.
110. Shen J, Zhu Q. Stability strategies of perovskite quantum dots and their extended applications in extreme environment: a review. *Mater Res Bull*. 2022;156:111987.
111. Duan Y, Wang D-Y, Costa RD. Recent progress on synthesis, characterization, and applications of metal halide perovskites@metal oxide. *Adv Funct Mater*. 2021;31(49):2104634.
112. Li Z, Kong L, Huang S, Li L. Highly luminescent and ultrastable $CsPbBr_3$ perovskite quantum dots incorporated into a silica/alumina monolith. *Angew Chem Int Ed*. 2017;129(28):8246-8250.
113. Gu K, Wang Y, Shen J, Zhu J, Zhu Y, Li C. Effective singlet oxygen generation in silica-coated $CsPbBr_3$ quantum dots through energy transfer for photocatalysis. *ChemSusChem*. 2020;13(4):682-687.
114. Luo B, Pu YC, Lindley SA, et al. Organolead halide perovskite nanocrystals: branched capping ligands control crystal size and stability. *Angew Chem Int Ed*. 2016;55(31):8864-8868.
115. Cheng J, Yuan S, Zhu L, et al. Room-temperature in situ synthesis of a highly efficient $CsPbBr_3/SiO_2$ sol entirely in ethanol solvent by constructing amine-functionalized silica micelles. *Langmuir*. 2020;36(21):6017-6024.
116. Zhang Q, Li Z, Liu M, et al. Bifunctional passivation strategy to achieve stable $CsPbBr_3$ nanocrystals with drastically reduced thermal-quenching. *J Phys Chem Lett*. 2020;11(3):993-999.
117. Hu H, Wu L, Tan Y, et al. Interfacial synthesis of highly stable $CsPbX_3$/oxide Janus nanoparticles. *J Am Chem Soc*. 2018;140(1):406-412.
118. Wang B, Zhang S, Liu B, Li J, Cao B, Liu Z. Stable $CsPbBr_3$:Sn@SiO_2 and Cs_4PbBr_6:Sn@SiO_2 core–shell quantum dots with tunable color emission for light-emitting diodes. *ACS Appl Nano Mater*. 2020;3(3):3019-3027.
119. Liang X, Chen M, Wang Q, Guo S, Yang H. Ethanol-precipitable, silica-passivated perovskite nanocrystals incorporated into polystyrene microspheres for long-term storage and reusage. *Angew Chem Int Ed*. 2019;131(9):2825-2829.
120. Zeng FL, Yang M, Qin JL, et al. Ultrastable luminescent organic–inorganic perovskite quantum dots via surface engineering: coordination of methylammonium bromide and covalent silica encapsulation. *ACS Appl Mater Interfaces*. 2018;10(49):42837-42843.
121. Ma X, Yang W, Ge X, et al. Design a novel multifunctional ($CsPbBr_3/Fe_3O_4$)@MPSs@SiO_2 magneto-optical microspheres for capturing circulating tumor cells. *Appl Surf Sci*. 2021;551(15):149427.
122. Zhang C, Zhang H, Wang R, et al. Exciton photoluminescence of $CsPbBr_3$@SiO_2 quantum dots and its application as a phosphor material in light-emitting devices. *Opt Mater Express*. 2020;10(4):1007.
123. Zhao H, Wei L, Zeng P, Liu M. Formation of highly uniform thinly-wrapped $CsPbX_3$@silicone nanocrystals via self-hydrolysis: suppressed anion exchange and superior stability in polar solvents. *J Mater Chem C*. 2019;7(32):9813-9819.
124. Collantes C, González Pedro V, Bañuls MJ, Maquieira Á. Monodispersed $CsPb_2Br_5$@SiO_2 core–shell nanoparticles as luminescent labels for biosensing. *ACS Appl Nano Mater*. 2021;4(2):2011-2018.
125. Tu S, Chen M, Wu L. Dual-encapsulation for highly stable all-inorganic perovskite quantum dots for long-term storage and reuse in white light-emitting diodes. *Chem Eng J*. 2021;412(15):128688.
126. Zhou Y, Yu Y, Zhang Y, et al. Highly photoluminescent $CsPbBr_3/CsPb_2Br_5$NCs@TEOS nanocomposite in light-emitting diodes. *Inorg Chem*. 2021;60(6):3814-3822.
127. Li L, Zhang Z, Chen Y, et al. Sustainable and self-enhanced electrochemiluminescent ternary suprastructures derived from $CsPbBr_3$ perovskite quantum dots. *Adv Funct Mater*. 2019;29(32):1902533.
128. He K, Shen C, Zhu Y, et al. Stable luminescent $CsPbI_3$ quantum dots passivated by (3-aminopropyl)triethoxysilane. *Langmuir*. 2020;36(34):10210-10217.
129. Liao JF, Xu YF, Wang XD, Chen HY, Kuang DB. $CsPbBr_3$ nanocrystal/MO_2 (M = Si, Ti, Sn) composites: insight into charge-carrier dynamics and photoelectrochemical applications. *ACS Appl Mater Interfaces*. 2018;10(49):42301-42309.
130. Park DH, Han JS, Kim W, Jang HS. Facile synthesis of thermally stable $CsPbBr_3$ perovskite quantum dot-inorganic SiO_2 composites and their application to white light-emitting diodes with wide color gamut. *Dye Pigment*. 2018;149:246-252.
131. Bu IY, Ke HW, Fu YS, Guo TF. Highly stable perovskite; light $CsPbBr_3$/silica composite prepared via novel electrospray injection process. *Optik (Stuttg)*. 2021;238:166690.
132. Meng C, Yang D, Wu Y, Zhang X, Zeng H, Li X. Synthesis of single $CsPbBr_3$@SiO_2 core–shell particles via surface activation. *J Mater Chem C*. 2020;8(48):17403-17409.
133. Liu Z, Hu Z, Shi T, et al. Stable and enhanced frequency upconverted lasing from $CsPbBr_3$ quantum dots embedded in silica sphere. *Opt Express*. 2019;27(7):9459-9466.
134. Gao F, Yang W, Liu X, et al. Highly stable and luminescent silica-coated perovskite quantum dots at nanoscale-particle level via nonpolar solvent synthesis. *Chem Eng J*. 2021;407(1):128001.
135. Hsu SC, Huang YM, Huang CP, et al. Improved Long-term reliability of a silica-encapsulated perovskite quantum-dot light-emitting device with an optically pumped remote film package. *ACS Omega*. 2021;6(4):2836-2845.
136. An MN, Park S, Brescia R, et al. Low-temperature molten salts synthesis: $CsPbBr_3$ nanocrystals with high photoluminescence emission buried in mesoporous SiO_2. *ACS Energy Lett*. 2021;6(3):900-907.
137. Son S, Jeon S, Chae D, et al. Colored emitters with silica-embedded perovskite nanocrystals for efficient daytime radiative cooling. *Nano Energy*. 2021;79:105461.

138. Yan D, Shi T, Zang Z, Zhao S, Du J, Leng Y. Stable and low-threshold whispering-gallery-mode lasing from modified $CsPbBr_3$ perovskite quantum dots@SiO_2 sphere. *Chem Eng J*. 2020;401(1):126066.
139. Gong XK, Zhang XS, Liu X, et al. Novel cryogenic dual-emission mechanism of lead-free double perovskite $Cs_2AgInCl_6$ and using SiO_2 to enhance their photoluminescence and photostability. *J Hazard Mater*. 2021;403(5):123821.
140. Yu X, Wu L, Yang D, et al. Hydrochromic $CsPbBr_3$ nanocrystals for anti-counterfeiting. *Angew Chem Int Ed*. 2020;59(34):14527-14532.
141. Malgras V, Tominaka S, Ryan JW, et al. Observation of quantum confinement in monodisperse methylammonium lead halide perovskite nanocrystals embedded in mesoporous silica. *J Am Chem Soc*. 2016;138(42):13874-13881.
142. Su Y, Jing Q, Xu Y, Xing X, Lu Z. Preventing anion exchange between perovskite nanocrystals by confinement in porous SiO_2 nanobeads. *ACS Omega*. 2019;4(26):22209-22213.
143. Anderson BD, Wu WC, Tracy JB. Silica overcoating of CdSe/CdS core/shell quantum dot nanorods with controlled morphologies. *Chem Mater*. 2016;28(14):4945-4952.
144. Chang KP, Wu CJ, Lo CW, Lin YS, Yen CC, Wuu DS. Synthesis of SiO_2-coated CdSe/ZnS quantum dots using various dispersants in the photoresist for color-conversion micro-LED displays. *Mater Sci Semicond Process*. 2022;148:106790.
145. Xuan TT, Liu JQ, Li HL, et al. Microwave synthesis of high luminescent aqueous CdSe/CdS/ZnS quantum dots for crystalline silicon solar cells with enhanced photovoltaic performance. *RSC Adv*. 2015;5(10):7673-7678.
146. Chen X, Liu F, Jiang Q, Sun L, Wang Q. Synthesis and properties of water-soluble silica-coated ZnSe/ZnS semiconductor quantum dots. *J Inorg Organomet Polym Mater*. 2012;22(1):6-11.
147. Lei H, Dai P, Wang X, et al. In situ defect passivation with silica oligomer for enhanced performance and stability of perovskite solar cells. *Adv Mater Interfaces*. 2020;7(3):1901716.
148. Park S, An MN, Almeida G, et al. $CsPbX_3/SiO_x$ (X = Cl, Br, I) monoliths prepared via a novel sol–gel route starting from Cs_4PbX_6 nanocrystals. *Nanoscale*. 2019;11(40):18739-18745.
149. Rossi C, Scarfiello R, Brescia R, et al. Exploiting the transformative features of metal halides for the synthesis of $CsPbBr_3$@SiO_2 core–shell nanocrystals. *Chem Mater*. 2022;34(1):405-413.
150. He Y, Yoon YJ, Harn YW, et al. Unconventional route to dual-shelled organolead halide perovskite nanocrystals with controlled dimensions, surface chemistry, and stabilities. *Sci Adv*. 2019;5(11):eaax4424.
151. Li X, Wang Y, Sun H, Zeng H. Amino-mediated anchoring perovskite quantum dots for stable and low-threshold random lasing. *Adv Mater*. 2017;29(36):1701185.
152. Yang J, Liu Z, Pi M, et al. High efficiency up-conversion random lasing from formamidinium lead bromide/amino-mediated silica spheres composites. *Adv Opt Mater*. 2020;8(12):2000290.
153. Wu SH, Mou CY, Lin HP. Synthesis of mesoporous silica nanoparticles. *Chem Soc Rev*. 2013;42(9):3862-3875.
154. Vallet-Regí M, Schüth F, Lozano D, Colilla M, Manzano M. Engineering mesoporous silica nanoparticles for drug delivery: where are we after two decades? *Chem Soc Rev*. 2022;51(13):5365-5451.
155. Paul G, Bisio C, Braschi I, et al. Combined solid-state NMR, FT-IR and computational studies on layered and porous materials. *Chem Soc Rev*. 2018;47(15):5684-5739.
156. Chipanina NN, Lazareva NF, Oznobikhina LP, Lazarev IM, Shainyan BA. The hydrolysis of (O-Si)-chelate [N-(acetamido)methyl]dimethylchlorosilanes. DFT and MP2 study, QTAIM and NBO analysis. *Comput Theor Chem*. 2015;1070:162-173.
157. Liu Y, Cai L, Xu Y, et al. In-situ passivation perovskite targeting efficient light-emitting diodes via spontaneously formed silica network. *Nano Energy*. 2020;78:105134.
158. Nassif N, Livage J. From diatoms to silica-based biohybrids. *Chem Soc Rev*. 2011;40(2):849-859.
159. Bansal P, Khan Y, Nim GK, Kar P. Surface modulation of solution processed organolead halide perovskite quantum dots to large nanocrystals integrated with silica gel G. *Chem Commun*. 2018;54(28):3508-3511.
160. Li Z, Kang Q, Chen L, Zhang B, Zou G, Shen D. Enhancing aqueous stability and radiative-charge-transfer efficiency of $CsPbBr_3$ perovskite nanocrystals via conductive silica gel coating. *Electrochim Acta*. 2020;330:135332.
161. Lee SY, Jeon S, Ahn J, et al. Highly stretchable white-light electroluminescent devices with gel-type silica-coated all-inorganic perovskite. *Appl Surf Sci*. 2021;563:150229.
162. Jana A, Bathula C, Park Y, et al. Facile synthesis and optical study of organic-inorganic lead bromide perovskite-clay (kaolinite, montmorillonite, and halloysite) composites. *Surf Interfaces*. 2022;29:101785.
163. Abdullayev E, Lvov Y. Halloysite clay nanotubes for controlled release of protective agents. *J Nanosci Nanotechnol*. 2011;11(11):10007-10026.
164. Yuan L, Zhou Y, Wang Z, Mei E, Liang X, Xiang W. Eco-friendly all-inorganic $CsPbX_3$ (X = Cl, Br, and I) perovskite nanocrystals in pyrophyllite for bright white light-emitting diodes. *Appl Clay Sci*. 2021;211:106158.
165. van Wijk J, Heunis T, Harmzen E, Dicks LMT, Meuldijk J, Klumperman B. Compartmentalization of bacteria in microcapsules. *Chem Commun*. 2014;50(97):15427-15430.
166. Kataoka S, Banerjee S, Kawai A, et al. Layered hybrid perovskites with micropores created by alkylammonium functional silsesquioxane interlayers. *J Am Chem Soc*. 2015;137(12):4158-4163.
167. Lin D, Xu X, Wang J, et al. Construction of an iodine diffusion barrier using network structure silicone resin for stable perovskite solar cells. *ACS Appl Mater Interfaces*. 2021;13(7):8138-8146.
168. Wang H, Lin H, Piao X, et al. Organometal halide perovskite nanocrystals embedded in silicone resins with bright luminescence and ultrastability. *J Mater Chem C*. 2017;5(46):12044-12049.
169. Wang Y, Dong Y, Liu Q, Guo X, Zhang M, Li Y. In-situ stabilization strategy for $CsPbX_3$-silicone resin composite with enhanced luminescence and stability. *Nano Energy*. 2020;78:105150.
170. Duan Y, He K, Yang L, Xu J, Zhao W, Liu Z. 24.20%-efficiency MA-free perovskite solar cells enabled by siloxane derivative Interface engineering. *Small*. 2022;18(48):2204733.

171. Wang X, Xu Z, Zhuo S, et al. Strain modulation for high brightness blue luminescence of Pr^{3+}-doped perovskite nanocrystals via siloxane passivation. *ACS Appl Electron Mater*. 2021;3(9):3815-3823.
172. Matsushima T, Nasu R, Takekuma K, et al. Efficient perovskite light-emitting diodes with a siloxane-blended organic hole transport layer. *Adv Photonics Res*. 2022;3(10):2200003.
173. Li F, Gong C, Fan B, et al. 3D network-assisted crystallization for fully printed perovskite solar cells with superior irradiation stability. *Adv Funct Mater*. 2022;32(39):2206412.
174. Kim W, Park JB, Kim H, et al. Enhanced long-term stability of perovskite solar cells by passivating grain boundary with polydimethylsiloxane (PDMS). *J Mater Chem A*. 2019;7(36):20832-20839.
175. Jeong J, Kim M, Seo J, et al. Pseudo-halide anion engineering for α-$FAPbI_3$ perovskite solar cells. *Nature*. 2021;592(7854):381-385.
176. Choi EY, Kim JH, Kim BJ, Jang JH, Kim J, Park N. Development of moisture-proof polydimethylsiloxane/aluminum oxide film and stability improvement of perovskite solar cells using the film. *RSC Adv*. 2019;9(21):11737-11744.
177. Shi B, Lü J, Liu Y, Xiao Y, Lü C. Ultra-stable water-dispersive perovskite QDs encapsulated by triple siloxane coupling agent system with different hydrophilic/hydrophobic properties. *Mater Chem Front*. 2021;5(11):4343-4354.
178. Yoon HC, Do YR. Stable and efficient green perovskite nanocrystal–polysilazane films for white LEDs using an electrospray deposition process. *ACS Appl Mater Interfaces*. 2019;11(25):22510-22520.
179. Zou G, Li Z, Chen Z, Chu L, Yip H, Cao Y. Color-stable deep-blue perovskite light-emitting diodes based on organotrichlorosilane post-treatment. *Adv Funct Mater*. 2021;31(46):2103219.
180. Zhao S, Qin M, Xiang Y, et al. Bifunctional effects of trichloro(octyl)silane modification on the performance and stability of a perovskite solar cell via microscopic characterization techniques. *ACS Appl Energy Mater*. 2020;3(4):3302-3309.
181. Hu Y, Kareem S, Dong H, et al. $CsPbBr_3$ @SiO_2 core–shell nanoparticle films for superhydrophobic coatings. *ACS Appl Nano Mater*. 2021;4(6):6306-6315.
182. Hu Y, Fan L, Hui H, Wen H, Yang D, Feng G. Monodisperse bismuth-halide double perovskite nanocrystals confined in mesoporous silica templates. *Inorg Chem*. 2019;58(13):8500-8505.
183. Yuan S, Chen D, Li X, Zhong J, Xu X. In situ crystallization synthesis of $CsPbBr_3$ perovskite quantum dot-embedded glasses with improved stability for solid-state lighting and random upconverted lasing. *ACS Appl Mater Interfaces*. 2018;10(22):18918-18926.
184. Zhenfu Z, Zhihai W, Jiong C, Liang J, Yafei H. Nanocomposites of perovskite quantum dots embedded in magnesium silicate hollow spheres for multicolor display. *J Phys Chem C*. 2018;122(29):16887-16893.
185. Pan A, Li Y, Wu Y, et al. Stable luminous nanocomposites of $CsPbX_3$ perovskite nanocrystals anchored on silica for multicolor anti-counterfeit ink and white-LEDs. *Mater Chem Front*. 2019;3(3):414-419.
186. Li Z, Guo J, Li Z, et al. Incorporating self-assembled silane-crosslinked carbon dots into perovskite solar cells to improve efficiency and stability. *J Mater Chem A*. 2020;8(11):5629-5637.
187. Wang Q, Dong Q, Li T, Gruverman A, Huang J. Thin insulating tunneling contacts for efficient and water-resistant perovskite solar cells. *Adv Mater*. 2016;28(31):6734-6739.
188. Kim J, Khang DY, Kim JH, Lee HH. The surface engineering of top electrode in inverted polymer bulk-heterojunction solar cells. *Appl Phys Lett*. 2008;92(13):133307.
189. Wang J, Xiang X, Yao X, Xiao WJ, Lin J, Li WS. Efficient perovskite solar cells using trichlorosilanes as perovskite/PCBM interface modifiers. *Org Electron*. 2016;39:1-9.
190. Yang G, Wang C, Lei H, et al. Interface engineering in planar perovskite solar cells: energy level alignment, perovskite morphology control and high performance achievement. *J Mater Chem A*. 2017;5(4):1658-1666.
191. Zhang J, Hu Z, Huang L, et al. Bifunctional alkyl chain barriers for efficient perovskite solar cells. *Chem Commun*. 2015;51(32):7047-7050.
192. Liu L, Mei A, Liu T, et al. Fully printable mesoscopic perovskite solar cells with organic silane self-assembled monolayer. *J Am Chem Soc*. 2015;137(5):1790-1793.
193. Zhang CC, Yuan S, Lou YH, et al. Perovskite films with reduced interfacial strains via a molecular-level flexible interlayer for photovoltaic application. *Adv Mater*. 2020;32(38):2001479.
194. Wang W, Yang Z, Ding J, Kong J, Li X. Improving water-resistance of inverted flexible perovskite solar cells via tailoring the top electron-selective layers. *Sol Energy Mater Sol Cells*. 2022;238:111609.
195. Zheng R, Zhao S, Zhang H, et al. Defect passivation grain boundaries using 3-aminopropyltrimethoxysilane for highly efficient and stable perovskite solar cells. *Sol Energy*. 2021;224:472-479.
196. Xia J, Sohail M, Nazeeruddin MK. Efficient and stable perovskite solar cells by tailoring of interfaces. *Adv Mater*. 2023;35(31):2211324.
197. Kanda H, Usiobo OJ, Momblona C, et al. Light stability enhancement of perovskite solar cells using 1H,1H,2H,2H-perfluorooctyltriethoxysilane passivation. *Sol RRL*. 2021;5(3):2000650.
198. Dkhili M, Lucarelli G, De Rossi F, et al. Attributes of high-performance electron transport layers for perovskite solar cells on flexible PET versus on glass. *ACS Appl Energy Mater*. 2022;5(4):4096-4107.
199. Liu M, Li M, Li Y, et al. Defect-passivating and stable benzothiophene-based self-assembled monolayer for high-performance inverted perovskite solar cells. *Adv Energy Mater*. 2024;2303742(12):2303742.
200. Roose B, Wang Q, Abate A. The role of charge selective contacts in perovskite solar cell stability. *Adv Energy Mater*. 2019;9(5):1803140.
201. Prince KJ, Nardone M, Dunfield SP, et al. Complementary interface formation toward high-efficiency all-back-contact perovskite solar cells. *Cell Reports Phys Sci*. 2021;2(3):100363.
202. Zhang J, Sun Y, Yu H. Reducing energy loss via adjusting the anode work function and perovskite layer morphology for the efficient and stable hole transporting layer-free perovskite solar cells. *Chem Eng J*. 2022;431(P1):133948.

203. Chiba T, Hayashi Y, Ebe H, et al. Anion-exchange red perovskite quantum dots with ammonium iodine salts for highly efficient light-emitting devices. *Nat Photonics*. 2018;12(11):681-687.
204. Lin K, Xing J, Quan LN, et al. Perovskite light-emitting diodes with external quantum efficiency exceeding 20 per cent. *Nature*. 2018;562(7726):245-248.
205. Quan LN, García de Arquer FP, Sabatini RP, Sargent EH. Perovskites for light emission. *Adv Mater*. 2018;30(45):1801996.
206. Kirakosyan A, Jeon MG, Li L, Choi J. Suppressed phase and structural evolution of $CH_3NH_3PbBr_3$ microwires to $(CH_3)_2NH_2PbBr_3$ by addition of hydrazine bromide. *Appl Surf Sci*. 2021;566:150691.
207. Kirakosyan A, Chinh ND, Sihn MR, et al. Mechanistic insight into surface defect control in perovskite nanocrystals: ligands terminate the valence transition from Pb^{2+} to metallic Pb^0. *J Phys Chem Lett*. 2019;10(15):4222-4228.
208. Qiu L, Yang H, Dai Z, et al. Highly efficient and stable $CsPbBr_3$ perovskite quantum dots by encapsulation in dual-shell hollow silica spheres for WLEDs. *Inorg Chem Front*. 2020;7(10):2060-2071.
209. Wang HC, Lin SY, Tang AC, et al. Mesoporous silica particles integrated with all-inorganic $CsPbBr_3$ perovskite quantum-dot nanocomposites (MP-PQDs) with high stability and wide color gamut used for backlight display. *Angew Chem Int Ed*. 2016;55(28):7924-7929.
210. Zhang Q, Zheng W, Wan Q, et al. Confined synthesis of stable and uniform $CsPbBr_3$ nanocrystals with high quantum yield up to 90% by high temperature solid-state reaction. *Adv Opt Mater*. 2021;9(11):2002130.
211. Pan A, Wu Y, Yan K, et al. Stable luminous nanocomposites of confined Mn^{2+}-doped lead halide perovskite nanocrystals in mesoporous silica nanospheres as orange fluorophores. *Inorg Chem*. 2019;58(6):3950-3958.
212. Huang Y, Li F, Qiu L, et al. Enhancing the stability of $CH_3NH_3PbBr_3$ nanoparticles using double hydrophobic shells of SiO_2 and poly(vinylidene fluoride). *ACS Appl Mater Interfaces*. 2019;11(29):26384-26391.
213. Li X, Cai W, Guan H, et al. Highly stable $CsPbBr_3$ quantum dots by silica-coating and ligand modification for white light-emitting diodes and visible light communication. *Chem Eng J*. 2021;419:129551.
214. He M, Cheng Y, Shen L, et al. Mn-doped $CsPbCl_3$ perovskite quantum dots (PQDs) incorporated into silica/alumina particles used for WLEDs. *Appl Surf Sci*. 2018;448:400-406.
215. Liu H, Tan Y, Cao M, et al. Fabricating $CsPbX_3$-based type I and type II heterostructures by tuning the halide composition of Janus $CsPbX_3/ZrO_2$ nanocrystals. *ACS Nano*. 2019;13(5):5366-5374.
216. Loiudice A, Saris S, Oveisi E, Alexander DTL, Buonsanti R. $CsPbBr_3$ QD/AlOx inorganic nanocomposites with exceptional stability in water, light, and heat. *Angew Chem Int Ed*. 2017;56(36):10696-10701.
217. Paul S, Samanta A. N-Bromosuccinimide as bromide precursor for direct synthesis of stable and highly luminescent green-emitting perovskite nanocrystals. *ACS Energy Lett*. 2020;5(1):64-69.
218. Bao Z, Chiu HD, Wang W, et al. Highly luminescent $CsPbBr_3@Cs_4PbBr_6$ nanocrystals and their application in electroluminescent emitters. *J Phys Chem Lett*. 2020;11(23):10196-10202.
219. Shi J, Ge W, Zhu J, Saruyama M, Teranishi T. Core–shell $CsPbBr_3$@CdS quantum dots with enhanced stability and photoluminescence quantum yields for optoelectronic devices. *ACS Appl Nano Mater*. 2020;3(8):7563-7571.
220. Chen W, Hao J, Hu W, et al. Enhanced stability and tunable photoluminescence in perovskite $CsPbX_3$/ZnS quantum dot heterostructure. *Small*. 2017;13(21):1604085.
221. Li M, Zhang X, Yang P. Controlling the growth of a SiO_2 coating on hydrophobic $CsPbBr_3$ nanocrystals towards aqueous transfer and high luminescence. *Nanoscale*. 2021;13(6):3860-3867.
222. Dutta A, Behera RK, Pal P, Baitalik S, Pradhan N. Near-unity photoluminescence quantum efficiency for all $CsPbX_3$ (X = Cl, Br, and I) perovskite nanocrystals: a generic synthesis approach. *Angew Chem Int Ed*. 2019;58(17):5552-5556.
223. Grisorio R, Fasulo F, Muñoz-García AB, et al. In situ formation of zwitterionic ligands: changing the passivation paradigms of $CsPbBr_3$ nanocrystals. *Nano Lett*. 2022;22(11):4437-4444.
224. Su M, Fan B, Li H, Wang K, Luo Z. Hydroxyl terminated mesoporous silica-assisted dispersion of ligand-free $CsPbBr_3/Cs_4PbBr_6$ nanocrystals in polymer for stable white LED. *Nanoscale*. 2019;11(3):1335-1342.
225. Lal M, Levy L, Kim KS, et al. Silica nanobubbles containing an organic dye in a multilayered organic/inorganic heterostructure with enhanced luminescence. *Chem Mater*. 2000;12(9):2632-2639.
226. Philipse AP, Van Bruggen MPB, Pathmamanoharan C. Magnetic silica dispersions: preparation and stability of surface-modified silica particles with a magnetic core. *Langmuir*. 1994;10(1):92-99.
227. Liu Y, Zhang L, Long X, Jiang P, Geng C, Xu S. Ultra-stable $CsPbBr_3$ nanocrystals with lead-carboxylate/SiO_2 encapsulation for LED applications. *J Mater Chem C*. 2021;9(37):12581-12589.
228. Jeon MG, Kabir RM, Kim S, et al. Highly processable and stable PMMA-grafted $CsPbBr_3$–SiO_2 nanoparticles for down-conversion photoluminescence. *Compos Part B Eng*. 2022;239:109956.
229. Liu Z, Sinatra L, Lutfullin M, et al. One hundred-nanometer-sized $CsPbBr_3$/m-SiO_2 composites prepared via molten-salts synthesis are optimal green phosphors for LCD display devices. *Adv Energy Mater*. 2022;12(38):2201948.
230. Yang W, Fei L, Gao F, et al. Thermal polymerization synthesis of $CsPbBr_3$ perovskite-quantum-dots@copolymer composite: towards long-term stability and optical phosphor application. *Chem Eng J*. 2020;387:124180.
231. Yang W, Gao F, Qiu Y, et al. $CsPbBr_3$-quantum-dots/polystyrene@silica hybrid microsphere structures with significantly improved stability for white LEDs. *Adv Opt Mater*. 2019;7(13):1900546.
232. Erol E, Kıbrıslı O, Çelikbilek Ersundu M, Ersundu AE. Size-controlled emission of long-time durable $CsPbBr_3$ perovskite quantum dots embedded tellurite glass nanocomposites. *Chem Eng J*. 2020;401:126053.

233. Zhao C, Li Y, Ye W, et al. Ligand-free $CsPbBr_3$ perovskite quantum dots in silica-aerogel composites with enhanced stability for w-LED and display by substituting Pb^{2+} with Pr^{3+} or Gd^{3+} ions. *Adv Opt Mater*. 2022;10(10):2102200.
234. Fan M, Huang J, Turyanska L, et al. Efficient all-perovskite white light-emitting diodes made of in situ grown perovskite-mesoporous silica nanocomposites. *Adv Funct Mater*. 2023;33:2215032.
235. Zang J, Cai L, Zou Y, et al. Self-healing perovskite films enabled by fluorinated cross-linked network targeting flexible light-emitting diode. *Adv Opt Mater*. 2022;10(16):2200566.
236. Li Q, Shen D, Luo C, et al. Ultra-thermostability of spatially confined and fully protected perovskite nanocrystals by in situ crystallization. *Small*. 2022;18(15):2107452.
237. Hou J, Cao S, Wu Y, et al. Inorganic colloidal perovskite quantum dots for robust solar CO_2 reduction. *Chem A Eur J*. 2017;23(40):9481-9485.
238. Qian X, Chen Z, Yang X, et al. Perovskite cesium lead bromide quantum dots: a new efficient photocatalyst for degrading antibiotic residues in organic system. *J Clean Prod*. 2020;249:119335.
239. Wang Y, Huang H, Zhang Z, et al. Lead-free perovskite $Cs_2AgBiBr_6$@g-C_3N_4 Z-scheme system for improving CH_4 production in photocatalytic CO_2 reduction. *Appl Catal Environ*. 2021;282:119570.
240. Jiang Y, Liao JF, Chen HY, et al. All-solid-state Z-scheme α-Fe_2O_3/amine-RGO/$CsPbBr_3$ hybrids for visible-light-driven photocatalytic CO_2 reduction. *Chem*. 2020;6(3):766-780.
241. Wan S, Ou M, Zhong Q, Wang X. Perovskite-type $CsPbBr_3$ quantum dots/UiO-66(NH_2) nanojunction as efficient visible-light-driven photocatalyst for CO_2 reduction. *Chem Eng J*. 2019;358:1287-1295.
242. Huo B, Yang J, Bian Y, et al. Amino-mediated anchoring of $FAPbBr_3$ perovskite quantum dots on silica spheres for efficient visible light photocatalytic NO removal. *Chem Eng J*. 2021;406:126740.
243. Carulli F, He M, Cova F, Erroi A, Li L, Brovelli S. Silica-encapsulated perovskite nanocrystals for X-ray-activated singlet oxygen production and radiotherapy application. *ACS Energy Lett*. 2023;8(4):1795-1802.
244. Kar MR, Kumar S, Acharya TK, Goswami C, Bhaumik S. Highly water-stable, luminescent, and monodisperse polymer-coated $CsPbBr_3$ nanocrystals for imaging in living cells with better sensitivity. *RSC Adv*. 2023;13(9):5946-5956.
245. Zhong CY, Xiao L, Zhou J, et al. Two-photon photoluminescence and bio-imaging application of monodispersed perovskite-in-silica nanocrystals with high biocompatibility. *Chem Eng J*. 2022;431(P3):134110.
246. Chan KK, Giovanni D, He H, Sum TC, Yong KT. Water-stable all-inorganic perovskite nanocrystals with nonlinear optical properties for targeted multiphoton bioimaging. *ACS Appl Nano Mater*. 2021;4(9):9022-9033.
247. Song W, Wang D, Tian J, et al. Encapsulation of dual-passivated perovskite quantum dots for bio-imaging. *Small*. 2022;18(42):2204763.
248. Hao D, Zou J, Huang J. Recent developments in flexible photodetectors based on metal halide perovskite. *InfoMat*. 2020;2(1):139-169.
249. Sutherland BR, Johnston AK, Ip AH, et al. Sensitive, fast, and stable perovskite photodetectors exploiting interface engineering. *ACS Photonics*. 2015;2(8):1117-1123.
250. Li G, Wang Y, Huang L, Sun W. Research progress of high-sensitivity perovskite photodetectors: a review of photodetectors: noise, structure, and materials. *ACS Appl Electron Mater*. 2022;4(4):1485-1505.
251. Ai B, Fan Z, Wong ZJ. Plasmonic–perovskite solar cells, light emitters, and sensors. *Microsyst Nanoeng*. 2022;8(1):5.
252. Wang Q, Zhang G, Zhang H, Duan Y, Yin Z, Huang Y. High-resolution, flexible, and full-color perovskite image photodetector via electrohydrodynamic printing of ionic-liquid-based ink. *Adv Funct Mater*. 2021;31(28):2100857.
253. Mandal A, Ghosh A, Ghosh D, Bhattacharyya S. Photodetectors with high responsivity by thickness tunable mixed halide perovskite nanosheets. *ACS Appl Mater Interfaces*. 2021;13(36):43104-43114.
254. Wang T, Fang T, Li X, Xu L, Song J. Controllable transient photocurrent in photodetectors based on perovskite nanocrystals via doping and interfacial engineering. *J Phys Chem C*. 2021;125(10):5475-5484.
255. Lu X, Li J, Zhang Y, et al. Recent progress on perovskite photodetectors for narrowband detection. *Adv Photonics Res*. 2022;3(5):2100335.
256. Wei W, Zhang Y, Xu Q, et al. Monolithic integration of hybrid perovskite single crystals with heterogenous substrate for highly sensitive x-ray imaging. *Nat Photonics*. 2017;11(5):315-321.
257. Geng X, Wang F, Tian H, et al. Ultrafast photodetector by integrating perovskite directly on silicon wafer. *ACS Nano*. 2020;14(3):2860-2868.
258. Ye H, Jing H, Shih WY, Shih WH. Stabilization of methylammonium lead iodide via SiO_2 coating for photodetectors. *J Mater Res*. 2023;38(7):1941-1951.
259. Moseley ODI, Roose B, Zelewski SJ, Kahmann S, Dey K, Stranks SD. Tunable multiband halide perovskite tandem photodetectors with switchable response. *ACS Photonics*. 2022;9(12):3958-3966.
260. Martínez-Goyeneche L, Gil-Escrig L, Susic I, Tordera D, Bolink HJ, Sessolo M. Narrowband monolithic perovskite–perovskite tandem photodetectors. *Adv Opt Mater*. 2022;10(22):2201047.
261. John RA, Shah N, Vishwanath SK, et al. Halide perovskite memristors as flexible and reconfigurable physical unclonable functions. *Nat Commun*. 2021;12(1):3681.
262. Xiao X, Hu J, Tang S, et al. Recent advances in halide perovskite memristors: materials, structures, mechanisms, and applications. *Adv Mater Technol*. 2020;5(6):1900914.
263. Nguyen DA, Jo Y, Tran TU, Jeong MS, Kim H, Im H. Electrically and optically controllable p-n junction memtransistor based on an Al_2O_3 encapsulated 2D Te/ReS_2 van der Waals heterostructure. *Small Methods*. 2021;5(12):e2101303.
264. Nguyen DA, Cho S, Park S, et al. Tunable negative photoconductivity in encapsulated ambipolar tellurene for functional optoelectronic device applications. *Nano Energy*. 2023;113:108552.
265. Bach TPA, Cho S, Kim H, Nguyen DA, Im H. 2D van der Waals heterostructure with tellurene floating-gate for wide

range and multi-bit optoelectronic memory. *ACS Nano*. 2024; 18(5):4131-4139.
266. Nguyen DA, Park DY, Duong NT, et al. Large-area MoS_2 via colloidal nanosheet ink for integrated memtransistor. *Small Methods*. 2021;5(11):2100558.
267. Yin L, Huang W, Xiao R, et al. Optically stimulated synaptic devices based on the hybrid structure of silicon nanomembrane and perovskite. *Nano Lett*. 2020;20(5):3378-3387.
268. Liu M, Cao Z, Wang X, et al. Perovskite material-based memristors for applications in information processing and artificial intelligence. *J Mater Chem C*. 2023;11(39):13167-13188.
269. Kumari S, Dhar BB, Panda C, Meena A, Sen GS. Fe-TAML encapsulated inside mesoporous silica nanoparticles as peroxidase mimic: femtomolar protein detection. *ACS Appl Mater Interfaces*. 2014;6(16):13866-13873.

AUTHOR BIOGRAPHIES

Atanu Jana received his PhD from the University of Calcutta in India and pursued postdoctoral fellowships at Indiana University-Purdue University Indianapolis in the USA and the Indian Institute of Technology Delhi in India. He later worked as a Research Scientist at Ulsan National Institute of Science and Technology in South Korea. Currently, he holds the position of Assistant Professor at the Division of System Semiconductor at Dongguk University in South Korea, where his research is focused on synthesizing circularly polarized luminescent single crystals and nanomaterials tailored for various optoelectronic applications, including light-emitting diodes, display, and x-ray scintillators.

Sangeun Cho received her PhD degree in Department of Semiconductor Science from Dongguk University, South Korea in 2020. She is currently a Research Professor in the Division of System Semiconductor at Dongguk University. Her research interests include the synthesis of luminescent materials and related device applications, such as x-ray scintillators and photonic devices.

Hyunsik Im received his DPhil degree in Physics at the University of Oxford (1999). He was a research professor at the Institute of Industrial Science (IIS) at the University of Tokyo (2000–2001), and invited researcher at RIKEN, Japan (2002–present). Currently, he is a professor in Division of System Semiconductor, Dongguk University, South Korea (2001–present). His research interests include nanomaterial, nanodevices, and low-temperature physics.

How to cite this article: Jana A, Cho S, Meena A, et al. Stabilization of halide perovskites with silicon compounds for optoelectronic, catalytic, and bioimaging applications. *InfoMat*. 2024;6(12):e12559. doi:10.1002/inf2.12559